

---

---

# A New Power Control Strategy for Grid-Friendly Single-Phase Photovoltaic Systems

---

---

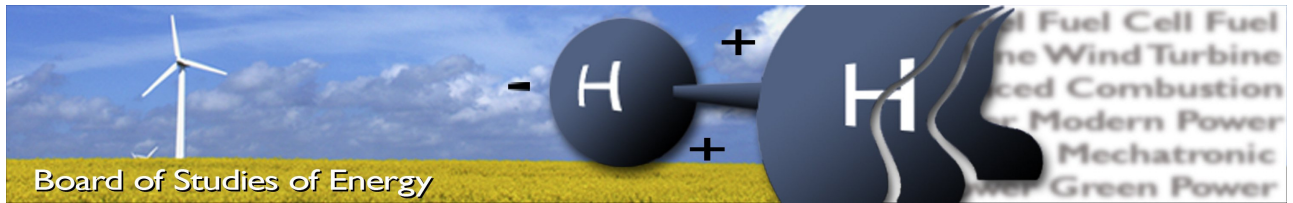
Master's Thesis  
Ariya Sangwongwanich

Aalborg University  
Department of Energy Technology  
Pontoppidanstræde 101  
DK-9220 Aalborg



**DEPARTMENT OF ENERGY TECHNOLOGY**  
AALBORG UNIVERSITY





**Title:** A New Power Control Strategy for Grid-Friendly Single-Phase Photovoltaic Systems  
**Semester:** 9th Semester  
**Semester theme:** Master's Thesis  
**Project period:** 01.09.14 to 27.05.15  
**ECTS:** 50  
**Supervisor:** Frede Blaabjerg, Yongheng Yang  
**Project group:** PED3-941

---

Ariya Sangwongwanich

Copies: 3  
 Pages, total: 84  
 Appendix: 4

**SYNOPSIS:**

With an increase of the grid-connected PV systems, an overloading in the grid may occur during the peak PV power production. In order to further enable more PV installations, the control algorithms of PV systems have to be flexible and feasible of regulating the active power in order to provide enough power capacity. This project presents one cost-effective solution by limiting the maximum feed-in power from the PV systems to a certain level by means of a Constant Power Generation (CPG) control. There are several possibilities to achieve a CPG operation, e.g. using a power/current limiter (P-/I-CPG), or modifying MPPT methods. However, the operational mode changes may challenge the system performance. Thus, a benchmarking of the CPG algorithms is provided as well as a design guideline of the most suitable high-performance algorithm to realize the constant power generation control practically.

**By signing this document, each member of the group confirms that all participated in the project work and thereby all members are collectively liable for the content of the report.**



# Contents

<b>Preface</b>	<b>v</b>
<b>Abstract</b>	<b>vi</b>
<b>1 Introduction</b>	<b>1</b>
1.1 Background . . . . .	1
1.1.1 Overview of Grid-Connected PV systems . . . . .	3
1.2 Motivation . . . . .	5
1.3 Problem Statements and Project Objectives . . . . .	7
1.4 Problem Solutions . . . . .	7
1.5 Project Limitations . . . . .	8
1.6 Thesis outline . . . . .	9
<b>2 Modeling of Grid-Connected Single-Phase PV systems</b>	<b>10</b>
2.1 Modeling of PV Cells . . . . .	10
2.2 Modeling of Boost Converters . . . . .	12
2.3 Modeling of PV inverters . . . . .	16
2.4 Modeling of Control systems . . . . .	18
2.4.1 Grid-Side Power Controllers . . . . .	18
2.4.2 Grid-Side Current Controllers . . . . .	19
2.4.3 Grid Synchronizations . . . . .	21
2.5 Performance of the Two-Stage Single-Phase PV System . . . . .	23
2.5.1 Boost Converter Control . . . . .	24
2.5.2 PV inverter Control . . . . .	24
2.6 Summary . . . . .	27
<b>3 Maximum Power Point Tracking</b>	<b>28</b>
3.1 Overview of Maximum Power Point Tracking . . . . .	28
3.2 Perturb and Observe MPPT Control . . . . .	29
3.3 MPPT Controllers . . . . .	31
3.3.1 Design consideration of MPPT controllers . . . . .	34
3.4 Performance of the MPPT controllers . . . . .	35
3.5 Summary . . . . .	41

<b>4</b>	<b>Constant Power Generation Operation</b>	<b>42</b>
4.1	Background of Active Power Control Strategies . . . . .	42
4.2	Overview of Constant Power Generations . . . . .	43
4.3	Literature Review of Constant Power Generation . . . . .	45
4.4	Analysis of Constant Power Generation Strategies . . . . .	47
4.4.1	CPG based on the Power Control (P-CPG) . . . . .	49
4.4.2	CPG based on the Current Limit (I-CPG) . . . . .	50
4.4.3	CPG based on the P&O Algorithm (P&O-CPG) . . . . .	51
4.5	Performance of the CPG Controllers . . . . .	53
4.5.1	Simulation results . . . . .	53
4.5.2	Experimental results . . . . .	55
4.6	Benchmarking of CPG methods . . . . .	63
4.7	Summary . . . . .	65
<b>5</b>	<b>Design for High Performances P&amp;O CPG Algorithm</b>	<b>66</b>
5.1	Issues of the P&O CPG Method . . . . .	66
5.1.1	Dynamic Behavior of the Conventional P&O-CPG Algorithm . . . . .	67
5.2	Design for High Performance P&O CPG Method . . . . .	68
5.2.1	Minimizing Overshoots during the MPPT to CPG Transition . . . . .	69
5.2.2	Minimizing Power Losses during the CPG to MPPT Transition . . . . .	71
5.2.3	Design Guideline and the Performance of the Modified P&O-CPG algorithm . . . . .	73
5.3	Summary . . . . .	76
<b>6</b>	<b>Conclusion</b>	<b>77</b>
	<b>Bibliography</b>	<b>80</b>
<b>A</b>	<b>Hardware Implementation of LabVIEW-FPGA</b>	<b>85</b>
A.1	Control Structure of Two-Stage Single-Phase PV System in GPIC . . . . .	86
A.2	Controller Design in LabVIEW-FPGA Environment . . . . .	87
A.2.1	Proportional Integral (PI) controller . . . . .	87
A.2.2	Proportional Resonant (PR) and Repetitive Controller (RC) . . . . .	88

# Preface

This Master's Thesis *A New Power Control Strategy for Grid-Friendly Single-Phase Photovoltaic Systems* was conducted at the Department of Energy Technology, Aalborg University during the 9th-10th semester of the Master program entitled "Power Electronics and Drives".

## Instruction for reading

The references are made according to the Institute of Electrical and Electronics Engineers (IEEE) citation style and can be found at the end of the report. Figures, tables and equations are referred to as Fig, Table, and Eq, respectively (e.g., Fig. X.Y refers to a figure Y in a chapter X). All the units used in this report are based on the SI units.

## Acknowledgments

The author would like to thank his supervisors Frede Blaabjerg, professor at Aalborg University, and Yongheng Yang, postdoctoral fellow at Aalborg University, for their kindness, patience, and valuable guidance during the study. Further, the author also appreciates the help of Huai Wang, assistant professor at Aalborg University, and Walter Neumayr during the laboratory works. In addition, the author would also like to thank his colleagues in the department for their enlightening discussions.

Finally, the author would like to express his deepest gratitude to his family for their support and encouragement.

Aalborg University, May 26, 2015

---

Ariya Sangwongwanich  
<asangw13@student.aau.dk>

# Abstract

Photovoltaics (PV) have shown a high growth rate during the last several years and are expected to play an even more significant role in the future power production. In the currently active grid codes for most countries, a maximum power point tracking (MPPT) is mandatory for grid-connected single-phase PV systems. With an increase of grid-connected PV system installation, the Distribution System Operators (DSO) may face challenges regarding overloading of the grid during PV peak production periods.

Increasing the grid capacity and integrating energy storage systems are two possibilities to solve this issue, yet requiring more investments. Therefore, this thesis proposes a cost-effective solution through an active power control strategy for single-phase PV systems. The proposed solution can contribute to prevent overloading of the distribution grid by operating the PV inverter in a Constant Power Generation (CPG) mode (i.e., limiting the maximum feed-in power of PV systems) during the peak production. This is achieved through the modification of the MPPT algorithm at the individual PV inverter level. Therefore, the possible MPPT control structures in the two-stage single-phase PV system are first investigated. Then, three selected algorithms to achieve the CPG operation are presented and their performances are examined experimentally under several test conditions, e.g., slow changing, fast changing, clear, and cloudy irradiance conditions. A benchmarking of the CPG algorithms is carried out, where it is revealed that the CPG based on the power control and the current limit can achieve fast dynamics. Nevertheless, the CPG based on the Perturb and Observe (P&O) attains the highest robustness and is considered to be the most suitable algorithm to realize the CPG control practically.

Although the P&O-CPG algorithm can ensure a stable operation regardless of the irradiance conditions, the dynamic performance is limited due to the perturbation behavior of the algorithm. Modifications in the algorithm are required in order to achieve high performances CPG operation. Thus, a design guideline for high performances P&O-CPG algorithm is provided. According to the experimental results, the dynamic performance of the P&O-CPG algorithm have been improved significantly by employing an adaptive step size and a constant voltage strategy.

# Chapter 1

## Introduction

In this chapter, the background and motivation of the project are presented. The development of the PV systems is discussed. An overview of the grid-connected PV systems is also provided where the focus is on the single-phase system configuration. Then, a challenge due to the expected wide-scaled grid-connected PV systems is pointed out. Problem statements and project objectives are presented as well as the project limitations. The thesis outline is also provided at the end of this chapter to explain the flow of the thesis.

### 1.1 Background

Due to environmental and  $CO_2$  emission concerns, Renewable Energy Sources (RESs) have gained more and more attention worldwide. Several countries have set an ambitious goal for energy production capacity concerning RESs. As a main market share of renewable energy (RE), the European Council targets 30 % of renewable by the end of 2030 [1]. With the same milestone, Germany plans to achieve 18 % of RE for gross energy consumption [2]. Denmark also sets a goal to be independent of fossil fuel by 2050 [3]. With these motivations, it can be predicted that the installed capacity of RESs will reach a much higher penetration level soon.

Among other RESs, photovoltaics (PV) have been witnessed at the highest growth rate during the last several years and are expected to play an even more significant role in the future power production [4], [5]. The world cumulative PV installed capacity during 2000-2013 is shown in Fig. 1.1. It can be seen that more than 23 GW of PV capacity was installed globally at the end of 2009. One year later, the installed capacity was almost doubled, being 40.3 GW [1]. In 2013, the total global installed capacity of PV systems reached 138.8 GW. Considering the worldwide installed capacity, Germany is a leading country with 26 % of the total PV capacity, followed by China (13 %), Italy (12 %) and Japan (10 %) as shown in Fig. 1.2 [1]. The total energy production from PV systems in Germany is 29.7 TWh, which contributes to 5.7 % of electricity consumption in 2013 [5].

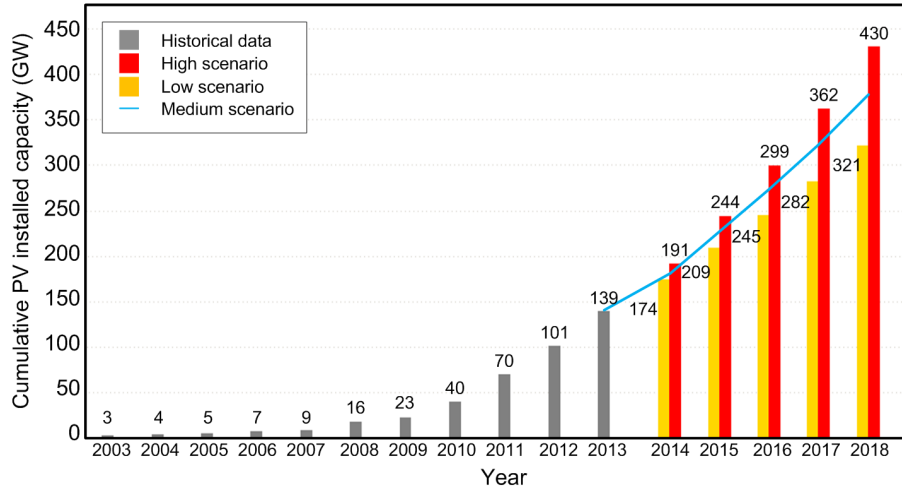


**Figure 1.1:** World cumulative PV installed capacity during 2003 - 2013 and forecast during 2014 - 2018 [1].

The conventional grid will become more decentralized in terms of production, when a high penetration level of PV systems is reached. This is mainly due to the still decreasing price of PV modules during the last several years and the interest of green power generation from PV systems. It is reported that the cost of PV power generation reduces around 20 % every time when the production capacity is doubled [6]. Since about 60 % of the overall system cost comes from PV panels, the cost reduction together with supporting policies, e.g. feed-in-tariff, are the main driving forces in PV systems investment. Although the trend of PV systems in the future is difficult to be predicted due to a number of uncertainties, for example, economics and policies, it can be expected that the global PV cumulative installed capacity will still increase and exceed 200 GW in 2015 even in the low growth scenario [1]. This cumulative PV installation forecast is also shown in Fig. 1.1.

Notably, behind this thriving increase of RESs, a drawback of RESs that the power generated by RESs (e.g. wind and solar power systems) is fluctuated depending on the weather condition remains. This could rise challenges for Distribution System Operators (DSOs) in a wide-scale PV system scenario. An overloading can occur during the peak production. This could introduce over-voltage and line frequency instability to the system, and probably damage the connected equipment [7]. Recently, grid support functions are partially required for single-phase PV systems since the focus is on maximizing the power harvesting and also islanding protection [8]. However, attentions have been brought in some countries and the demands of the next generation PV system have been discussed in [9], [10], [11], and [12]. For instance, reactive power control (voltage support) and active power control (frequency support) are expected to be required features of PV systems in the near future. Dynamic grid support like Low Voltage Ride-Through (LVRT) capability and reactive

## 1.1. Background

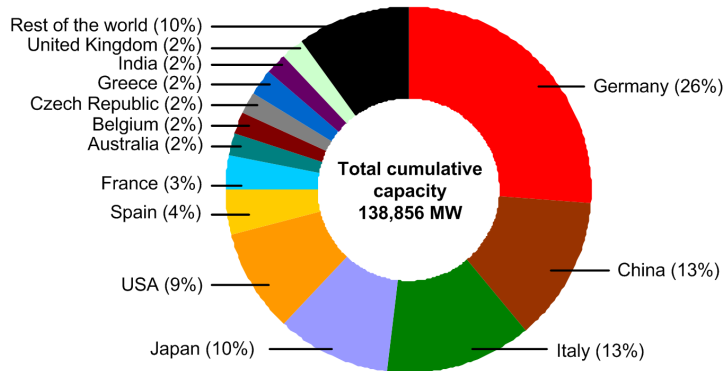


**Figure 1.2:** Total cumulative installed capacity of PV systems in 2013 [1].

current injection during the fault will also be essential in a wide-scale PV system scenario. In addition, high efficiency and reliability are also vital for the next generation PV system since they can reduce the system cost and make PV more competitive with other energy sources [9], [13]. Accordingly, a more advanced control for the PV system is desired in order to fulfill these requirements [12].

### 1.1.1 Overview of Grid-Connected PV systems

One benefit of PV systems is that the peak power production normally occurs close to the peak demand period. The peak load demand, PV power production, and electricity price during the day are shown in Fig. 1.3. Covering the peak load by PV energy production, instead of running an expensive power plant (e.g. gas turbine, diesel generator), results in a better economical solution.

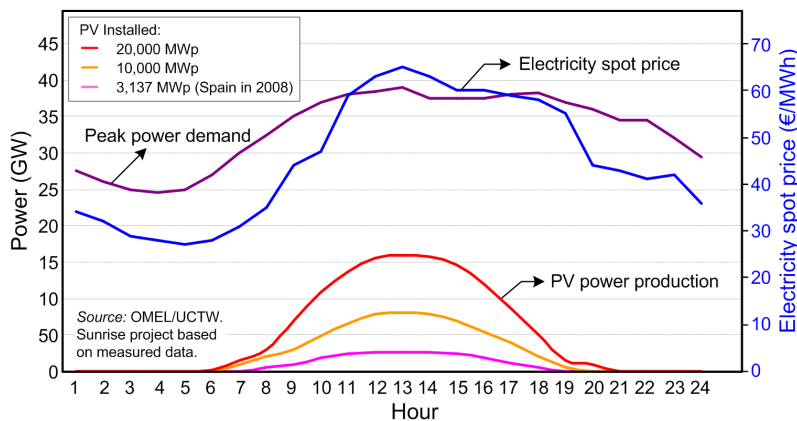


**Figure 1.3:** Daily peak power demand, PV power production, and electricity price [6].

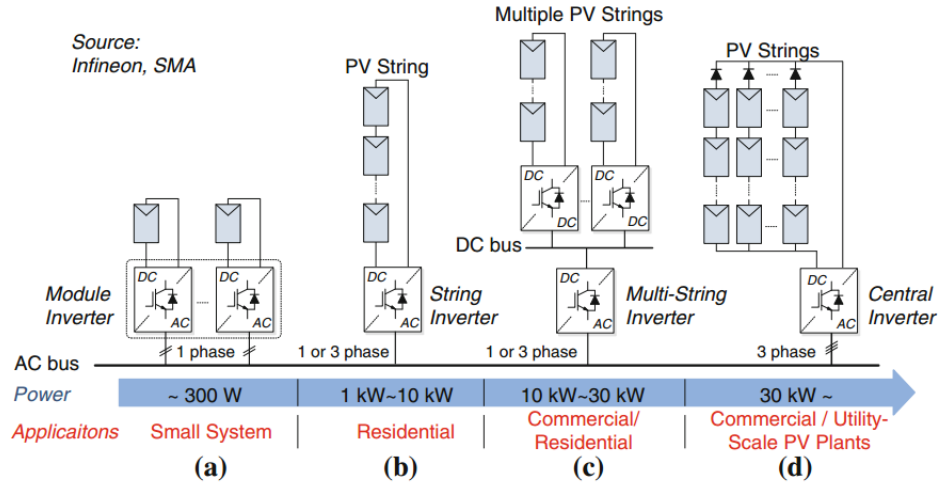


**Figure 1.4:** Grid-connected PV system configurations [8].

Another strong point of PV systems is that they are easy to be installed compared to other types of RE. This is because of the simple system configuration. Grid-connected PV systems can have different configurations mainly depending on the power rating as shown in Fig. 1.4. PV arrays may consist of a number of PV modules connected in series and/or parallel in order to satisfy output voltage and/or current level. Regarding the system configuration, central inverters are normally used in large-scale PV plants due to its low construction cost. However, there are several disadvantages such as the power losses due to common Maximum Power Point Tracking (MPPT) and in case of module mismatch. High-voltage DC cables are also required for connecting PV panels to the inverter [14]. String inverters have a better efficiency compared to central inverters since each string of PV panels is equipped with its own DC-DC converter to perform separate MPPT. Several strings can also share a common DC-AC inverter and, in this case, is referred to as multi-string inverters. Both string and multi-string inverters are usually used in residential applications. In the case of the module inverter, each PV module has its own DC-DC and DC-AC inverters which enables optimal MPPT. However, module inverters have the highest cost due to separated power converters for each module.

The control structure of grid-connected PV systems is shown in Fig. 1.5. With an absence of the transformer, the efficiency of the PV inverter is increased by approximately 2 % and the size is also reduced [14]. However, the lack of galvanic isolations from the transformer can lead to 1) a considerable leakage current from common-mode voltage and 2) the saturation of magnetic components due to DC current injection in distribution transformer [14]. As shown in the control structure, an active power is generated by the PV arrays and converted to the grid. Power electronic technology is a key to control PV systems. In most single-phase PV systems, two power electronic converters, so-called two-stage PV system, are used. A

## 1.2. Motivation

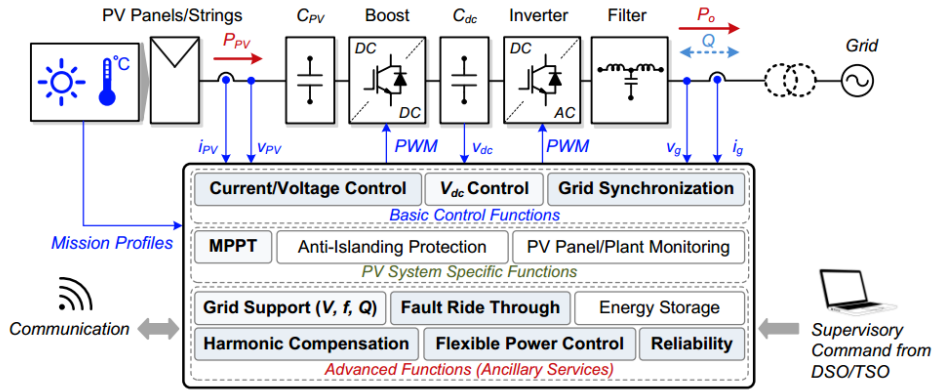


**Figure 1.5:** A two-stage single-phase grid-connected PV system control structure [8].

DC-DC boost converter is used for stepping up the DC-link voltage since the output voltage generated by the PV arrays is usually limited. The boost converter also plays an important role in extracting power from the PV arrays. An MPPT algorithm is implemented in the DC-DC converter in order to maximize the energy harvesting from the PV arrays. An active power is then transferred to the AC grid through the control of the grid-side converter. Grid-side converters, which are also referred to as PV inverters, can have several different topologies. Many industrial companies have proposed and manufactured high-efficiency transformerless PV inverters such as High Efficient and Reliable Inverter Concept (HERIC) from Sunways and H5 from SMA. Nevertheless, the most commonly used topology for single-phase PV inverter is a Full-Bridge inverter. The primary objective of PV inverters is to inject the active power to the grid with an acceptable power quality. Regarding the power quality, filters are commonly used to limit harmonics in the current injected to the grid. Passive filters with different combinations such as  $L$ ,  $LC$  or  $LCL$  filter can be inserted between the output terminal of the inverter and the grid. The design of the filter should be based on the desired attenuation of the frequency range since it depends on the filter type [8], [15]. PV inverters can also provide ancillary functions such as harmonics compensation, fault-ride-through, and flexible power control [8]. This could be considered as important supporting functions in the high penetration of PV systems scenario.

## 1.2 Motivation

Unlike wind turbine power systems, PV systems are more commonly used in residential and/or remote-area applications of lower power ratings (e.g. 3 kW to 5 kW). For example, more than 80 % of PV systems in Germany are connected to the low voltage grid, which is mainly single-phase [5]. In the currently active grid codes for most countries, a maximum power point tracking is mandatory for grid-connected

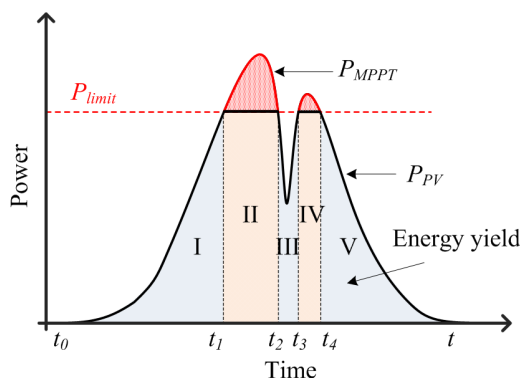


**Figure 1.6:** Constant Power Generation concept based on modifying the MPPT. The PV systems is operated in: 1) MPPT mode during I, III, V, and 2) Constant Power Generation mode during II, IV [8].

single-phase PV systems. With an increase of grid-connected PV system installation, the DSOs may face a challenge regarding an overloading of the grid during a PV peak production period [10]. For example, there is a case study in the Northern Ireland’s electricity grid where the grid was overloaded by an increased of PV installation in the local area as reported by BBC news in 2013. A new PV installation capacity was limited until the Utility Regulator upgrades their local grid and substations [16].

In order to enable more PV installations, apart from reducing the PV installation or expanding grid infrastructures, which is an expensive solution, the control algorithms of PV systems have to be flexible and feasible of regulating the active power in order to provide enough power capacity. One solution is to limit the maximum feed-in power from the PV systems to a certain level by means of a Constant Power Generation (CPG) control [8]. Actually, it is required in the German Federal Law: Renewable Energy Sources Act that the newly installed PV systems with the rated power below 30 kWp in Germany have to be able to limit the maximum feed-in power (e.g. 70 % of the rated power) unless it can be remotely controlled by the utility [11], [12]. There are several ways to implement this CPG concept as is proposed in [7]. Nevertheless, a cost-effective approach to achieve the CPG operation is by modifying MPPT control algorithm at the PV inverter level [17]. By setting a proper limit of an active power extraction from PV arrays, the PV inverter is operated under: 1) MPPT operation when the available active power is below the limit, or 2) CPG operation when the available active power reaches the power limit, which results in a constant active power injected to the grid as illustrated in Fig. 1.6. In addition to reduce the peak power production injected to the grid, another benefit of modifying the MPPT algorithm is an increase in the utilization factor of PV inverters. This is because the rated power of PV inverter, in CPG operation, is decided by the power limit, not the peak power production as usual [8]. Therefore, the focus of this project is to study a new control strategy for single-phase PV systems to unload the distribution grid, while at the same time to further increase the PV penetration.

## 1.3 Problem Statements and Project Objectives

From the motivation discussed above, the problem statement of the project is

- *Can we solve an overloading issue for the PV systems at high penetration level in a cost-effective way by proposing a new power control strategy to limit the maximum feed-in power?*

Accordingly, several key questions need to be answered.

- *How to realize the constant power generation in single-phase PV systems?*
- *Which is the most suitable MPPT control structure for implementing the CPG operation?*
- *How can we implement the new power control strategy in single-phase PV systems?*
- *What are the benefits and disadvantages of different CPG algorithms?*
- *Which is the most suitable CPG algorithm to realize the CPG operation?*
- *How to design for high performances CPG controller?*

With the purpose to solve these problems, the main aim of this project is to develop a new power control strategy for grid-friendly single-phase PV systems. The first step is studying and modeling single-phase grid-connected PV systems. Then, the new power control strategy will be carried out. The designed control strategy will be implemented in the laboratory and the performances will be analyzed. Based on this, several project tasks will be done.

## 1.4 Problem Solutions

### *Modeling single-phase PV systems*

Before designing a new power control strategy, an accurate model of single-phase PV system is required. With the aim to control the power extracted from PV arrays, the main characteristics of PV arrays such as voltage, current, and power will be described. All control systems will be implemented in power electronic converters. Therefore, the operation of both DC-DC boost converter and DC-AC Full-Bridge inverter will be analyzed using small-signal models.

### *New power control strategy for single-phase PV systems*

To enable more installation of grid-connected PV system, a new power control strategy for grid-friendly single-phase PV systems will be carried out. A control algorithm which combines CPG with MPPT operation, depending on the available active power,

will be designed. The performance of the designed power control strategy may be varied for different CPG algorithms. Thus, a benchmarking of the developed control strategy with different CPG algorithms will be provided. The designed control strategy will be implemented in the laboratory and the results will be analyzed.

### *Design for high performances CPG controller*

In order to realize the CPG operation practically, the high performances CPG controllers are demanded. A stable operation is one of the most important aspects when designing a controller. Thus, the design considerations to ensure a robust CPG operation will be discussed. In addition, the developed control strategy should also have a fast dynamic performance as well as an accurate power regulation in the steady-state. All these design considerations will be taken into account and provided as a design guideline for high performances CPG controllers.

## **1.5 Project Limitations**

In this project, the main focus is on the development of a power control strategy for single-phase PV systems. Nevertheless, the concept may also be adopted in three-phase PV systems as well. During the design process, there are several PV inverter topologies available for grid-connected single-phase PV systems as aforementioned. However, only the Full-Bridge topology is considered. The Pulse Width Modulation (PWM) technique is bipolar modulation since it has a low leakage current compared to other modulation techniques which is important in transformerless PV inverters. Considering the grid-connected application, the available synchronization and current control techniques will be used since they are not the main focuses of the project. When implementing the system in the laboratory, the PV panels are realized by using a programmable DC power supply. In summary, several limitations of the project can be listed as

- PV arrays production characteristics will be simulated by a programmable DC power supply.
- PV inverters used in this project only consider a single-phase Full-Bridge topology. A bipolar modulation technique is employed.
- The grid-side converter is not a main focus on this project. Therefore, the available model for single-phase grid synchronization and an existing current controller will be used.
- This project only considers a single-phase PV system. However, the concept may also be adopted in three-phase PV systems.

## 1.6 Thesis outline

The report consists of six main chapters and one appendix. A summary of each chapter is provided in the following.

### **Introduction**

In Chapter 1, the introduction of the project is presented. Challenges and demands for the next generation grid-connected PV systems are pointed out. This chapter also includes problem statements, project objectives, problem solutions, and project limitations.

### **Modeling of Grid-Connected Single-Phase PV systems**

Chapter 2 focuses on modeling of the system. A model of the two-stage grid-connected single-phase PV system and its control systems are presented in this chapter.

### **Maximum Power Point Tracking**

The details and analysis of MPPT algorithms are described in Chapter 3. The control structures of the MPPT controller and their design considerations are discussed.

### **Constant Power Generation Operation**

In Chapter 4, the main content of the project is provided where a new power control strategy is designed. The concept and the analysis of the CPG operation are discussed. Then, three selected algorithms to realize the CPG control are presented. Performances of the PV system with different CPG algorithms are examined and benchmarked.

### **Design for High Performances P&O CPG Algorithm**

A design guideline for high performances CPG algorithm is analyzed in Chapter 5. The required modifications to improve the performances of the P&O-CPG algorithm are addressed.

### **Conclusion**

The conclusion of the project and future works are provided in this chapter.

### **Appendix A. Hardware Implementation of LabVIEW-FPGA**

The implementation of the PV system in the LabVIEW-FPGA environment is discussed. A development platform and the controller design are provided.

## Chapter 2

# Modeling of Grid-Connected Single-Phase PV systems

This chapter focuses on the modeling of the grid-connected single-phase PV system. According to the system diagram shown in Fig. 2.1, the grid-connected single-phase PV systems consist of three main parts from the hardware point of view. The PV cells or arrays are the power source of the system, which will be modeled and represented by an equivalent circuit. Then, two power converters are employed in order to control 1) the power extraction from the PV arrays, and 2) the power delivery to the AC grid with an acceptable power quality. Small-signal models will be used to model a boost converter and a PV inverter. Then, the control systems are also presented for both the boost converter and the PV inverter. The performance of the PV system controller is validated and the results are provided at the end of the chapter.

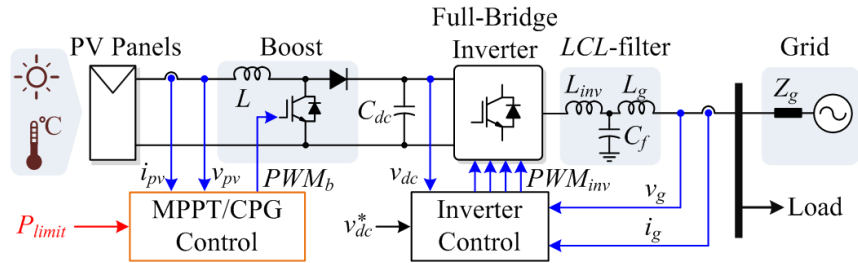


**Figure 2.1:** System diagram and control structure of a two-stage grid-connected single-phase PV system.

### 2.1 Modeling of PV Cells

As a power source of the system, a PV array is considered as one of the most important component. A PV array consists of several PV modules, and a PV module itself consists of a number of PV cells to satisfy current and/or voltage requirements

## 2.1. Modeling of PV Cells

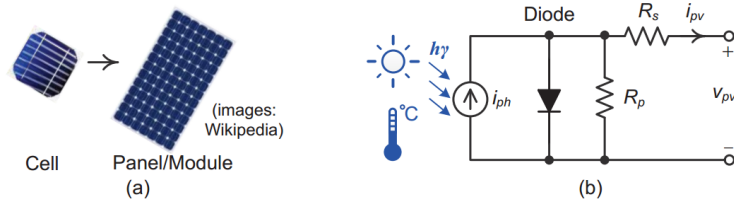


**Figure 2.2:** A PV module: (a) physical model (b) equivalent circuit of the module [8].

as shown in Fig. 2.2(a). A PV cell is a basic structure with a high modularity. Therefore, the model of PV cell is sufficient to describe the characteristic of both PV array and PV module.

A PV cell is actually a p-n junction. Thus, it has similar characteristics with a diode [18]. The junction absorbs photon energy from the light, and the charge carriers are excited and separated at the junction. This creates an electric field across the junction causing electric current to flow, thereby, converting solar energy to electricity [18]. A PV cell can be modeled by using an equivalent electrical circuit as shown in Fig. 2.2(b). This is called a five-parameter model (also single diode model), which is commonly used due to its precision and simplicity. From this model, the characteristic of PV cell can also be described by

$$i_{pv} = i_{ph} - i_o \left[ \exp\left(\frac{v_{pv} + i_{pv}R_s}{nk_B T/q}\right) - 1 \right] - \frac{v_{pv} + i_{pv}R_s}{R_p} \quad (2.1)$$

where  $i_{pv}$  and  $v_{pv}$  are the output current and voltage generated by a PV cell.  $i_{ph}$  is the photo-generated current which is mainly the current from absorbing photon energy. The photo-generated current is proportional to the solar irradiance level [8].  $i_o$  is a diode saturation current, which represents the characteristic of a diode.  $q$  is a charge of an electron,  $n$  is an ideality factor,  $k_B$  is a Boltzmann constant,  $T$  is the cell temperature in degree Kelvin [8].  $R_p$  is a shunt resistance which refers to the cell leakage currents across the junction and within the cell [19].  $R_s$  is a series resistance that represents losses from the interconnections. Other two important parameters, which are commonly used to characterize the PV cell, are short-circuit current  $i_{SC}$ , and open-circuit voltage  $v_{OC}$ . They refer to maximum current and voltage that a PV cell can generate.

**Table 2.1:** Parameters of PV arrays at the standard test condition used in this project [20].

Parameter	Value
Rated power (25°C, 1000 W/m <sup>2</sup> )	$P_{mp} = 65 \text{ W}$
Voltage at the maximum power point	$V_{mp} = 17.6 \text{ V}$
Current at the maximum power point	$I_{mp} = 3.69 \text{ A}$
Open circuit voltage	$v_{OC} = 21.7 \text{ V}$
Short circuit current	$i_{SC} = 3.99 \text{ A}$

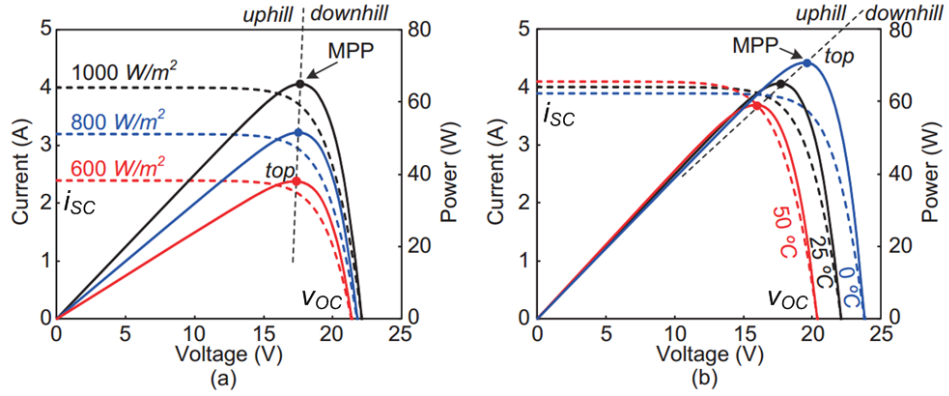


**Figure 2.3:** PV characteristic with (a) different solar irradiance levels at 25°C and (b) different ambient temperature at 1000 W/m<sup>2</sup> [8].

The PV cell characteristics are usually described by using an output current and voltage (I-V) curve. This can be obtained by solving Eq. (2.1) for a given operating condition. For example, Fig. 2.3 shows the I-V curve using the PV cell parameters from Table 2.1. When operating a PV cell, one of the most important measured value is the power production. By multiplying the output current and voltage from the I-V curve, the output power can be calculated as is also shown in the same figure. The PV cell has a characteristic of a voltage source on the right side of the I-V curve where the output voltage is almost constant. In contrast, the current source behavior is observed on the left hand of the I-V curve. There is an operating point where the output power is maximized. This point is called a Maximum Power Point (MPP). Due to the limited efficiency of the PV cell ( $< 25\%$  at present), PV systems are required always to operate close to the MPP in order to gain the maximum energy harvesting [8]. As can be seen in Figs. 2.3(a) and (b) the performances of PV cells can easily be affected by environmental conditions. The short-circuit current depends linearly on the solar irradiance level while the open-circuit voltage shows a strong dependence of the cell temperature [19]. Besides, a partial shading introduced by a passing cloud can also affect the characteristics of the PV cell. As a consequence, the operating point which satisfies the MPP condition also varies with the environmental conditions. Thus, it is essential to have a Maximum Power Point Tracking (MPPT), which is a control algorithm that can track the MPP continuously during the operation in order to maximize the power production of the PV systems. More discussions and detailed analysis of the MPPT will be provided in the next chapter.

## 2.2 Modeling of Boost Converters

Boost converters are often used in grid-connected PV systems to match the voltage level by stepping up the output voltage of PV arrays to a required DC-link voltage

## 2.2. Modeling of Boost Converters

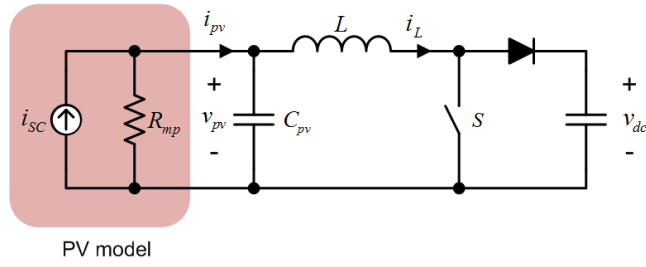


**Figure 2.4:** Equivalent circuit of PV arrays connected to a boost converter.

[21]. They also provide the control of power extraction in PV systems, for instance, by implementing MPPTs. The configuration of the PV array connected to the boost converter is shown in Fig. 2.4. In this case, the model of a PV array is obtained by using a small-signal model, where a Norton model is adopted.  $R_{mp}$  represents the corresponding resistance at the MPP. The input current source of the Norton model is equal to the short-circuit current  $i_{sc}$ , which varies with the irradiance level. The output of the boost converter is then connected to a DC-link with an expected constant voltage. This is based on an assumption that the PV inverter transfers all the extracted power to the grid, and thereby keeping the DC-link voltage constant.

The aim of the boost converter is to control the transferred DC power by controlling the duty cycle  $d$ , which refers to the subinterval when the switch is turned on. When the switch is turned on, the DC input power is transferred to an inductor. An equivalent circuit during this period is shown in Fig. 2.5(a). The inductor voltage and capacitor current can be expressed as

$$\left. \begin{aligned} L \frac{di_L}{dt} &= v_{pv} \\ C_{pv} \frac{dv_{pv}}{dt} &= i_{sc} - \frac{v_{pv}}{R_{mp}} - i_L \end{aligned} \right\}, \quad 0 \leq t < dT_{sw}$$

When the switch is turned off, the equivalent circuit is shown in Fig. 2.5(b) and the

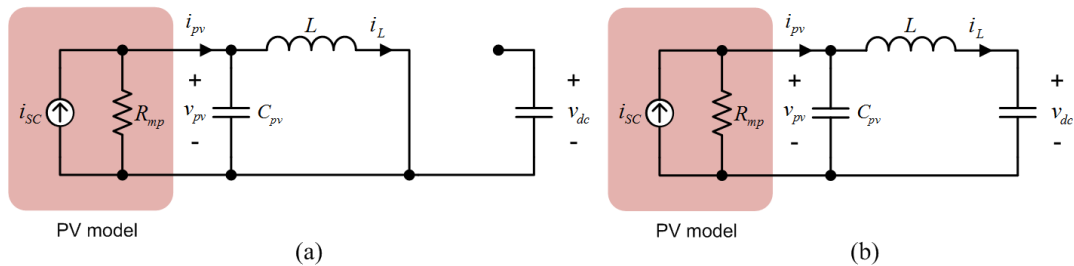


**Figure 2.5:** Equivalent circuits of the boost converter when (a) switch is on and (b) switch is off.

inductor voltage and capacitor current can be expressed as

$$\left. \begin{aligned} L \frac{di_L}{dt} &= v_{pv} - v_{dc} \\ C_{pv} \frac{dv_{pv}}{dt} &= i_{SC} - \frac{v_{pv}}{R_{mp}} - i_L \end{aligned} \right\}, \quad dT_{sw} \leq t < T_{sw}$$

The average values of the inductor voltage and capacitor current over one switching period can be obtained as

$$L \frac{d\langle i_L \rangle}{dt} = \langle v_{pv} \rangle - (1-d)\langle v_{dc} \rangle \quad (2.2)$$

$$C_{pv} \frac{d\langle v_{pv} \rangle}{dt} = \langle i_{SC} \rangle - \frac{\langle v_{pv} \rangle}{R_{mp}} - \langle i_L \rangle \quad (2.3)$$

Another important variable is the output current of the PV arrays, which can be derived as

$$\begin{aligned} i_{pv} &= i_{SC} - \frac{v_{pv}}{R_{mp}} \\ \langle i_{pv} \rangle &= \langle i_{SC} \rangle - \frac{\langle v_{pv} \rangle}{R_{mp}} \end{aligned} \quad (2.4)$$

In order to vary the duty cycle of the boost converter to control the transferred power, e.g. MPPT, a transfer function in the frequency domain of the duty cycle and the PV output current or voltage is required [22]. Because the converter equation is non-linear, a small-signal model is adopted for linearizing the converter model. The variables in Eqs. (2.2), (2.3) and (2.4) can be replaced by introducing small signals as described below [22]

$$\hat{i}_L(s) = \frac{1}{Ls} \hat{v}_{pv}(s) + \frac{(D-1)}{Ls} \hat{v}_{dc}(s) + \frac{V_{dc}}{Ls} \hat{d}(s) \quad (2.5)$$

$$\hat{v}_{pv}(s) = \frac{1}{C_{pv}s} \hat{i}_{SC}(s) - \frac{1}{R_{mp}C_{pv}s} \hat{v}_{pv}(s) - \frac{1}{C_{pv}s} \hat{i}_L(s) \quad (2.6)$$

$$\hat{i}_{pv}(s) = \hat{i}_{SC}(s) - \frac{1}{R_{mp}} \hat{v}_{pv}(s) \quad (2.7)$$

where " $\hat{\cdot}$ " refers to the small variation term. From Eqs. (2.5), (2.6) and (2.7) the transfer functions, which represent the relationship between the duty cycle of the boost converter and the PV voltage and current, can be obtained as

$$G_v(s) = \frac{\hat{v}_{pv}}{\hat{d}} = \frac{-V_{dc}R_{mp}}{LC_{pv}R_{mp}s^2 + Ls + R_{mp}} \quad (2.8)$$

$$G_i(s) = \frac{\hat{i}_{pv}}{\hat{d}} = \frac{V_{dc}}{LC_{pv}R_{mp}s^2 + Ls + R_{mp}} \quad (2.9)$$

## 2.2. Modeling of Boost Converters

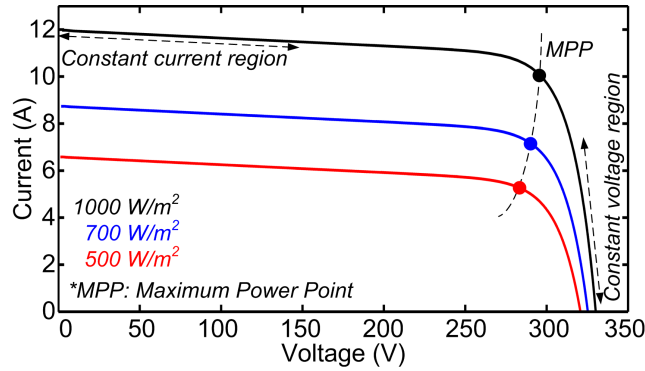


**Figure 2.6:** Current-voltage characteristic curve of the PV arrays.

Actually, it is also possible to control the boost converter from the PV array output power  $P_{pv}$ . Considering the transfer functions in Eqs. (2.8) and (2.9), the transfer functions of the  $v_{pv}$  and  $i_{pv}$  are decoupled. If it is assumed that the input DC power source has a characteristic of a constant output current  $I_{pv}$ , the relationship between the duty cycle of the boost converter and the PV array output power can be written as shown in Eq. (2.10). On the other hand, if the input power source has a characteristic of a constant output voltage  $V_{pv}$ , the transfer function of the PV arrays output power can also be derived as given in Eq. (2.11).

$$G_{p,v}(s) = \frac{\hat{v}_{pv} I_{pv}}{\hat{d}} = \frac{-V_{dc} R_{mp} I_{pv}}{LC_{pv} R_{mp} s^2 + Ls + R_{mp}} \quad (2.10)$$

$$G_{p,i}(s) = \frac{\hat{i}_{pv} V_{pv}}{\hat{d}} = \frac{V_{dc} V_{pv}}{LC_{pv} R_{mp} s^2 + Ls + R_{mp}} \quad (2.11)$$

In PV system applications, it is well known that the PV array has almost constant output current or voltage characteristic in some operating regions as shown in Fig. 2.6. Thus, it is possible to apply the control of the boost input power, as derived in Eqs. (2.10) and (2.11), with the grid-connected PV systems in this project, especially when the power control strategy is employed.

However, it is worth mentioning that the accuracy of the PV cell based on the Norton model in Fig. 2.4 decreases as the operating point moves away from the MPP, which is where the linearization takes place. This leads to two cautions when applying the control of the boost converter: 1) the transfer functions in Eqs. (2.8) and (2.9) may not be accurate when the operating point is far away from the MPP, and 2) the assumption in Eqs. (2.10) and (2.11) may not be true when the operating point is close to the MPP, since the PV array has neither constant current or voltage characteristic at the MPP. In order to have a very precise model of the boost converter with the PV arrays in the wide-range operation, a further investigation is required. Nevertheless, an error from the linearization can be considered as a disturbance of the system and can be compensated by using a feedback control system [23].

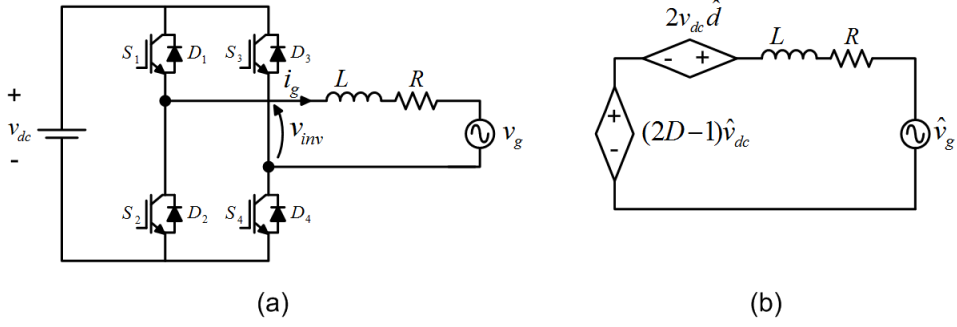


**Figure 2.7:** (a) Single-phase FB inverter with an  $L$ -filter and (b) small-signal model [8].

## 2.3 Modeling of PV inverters

PV inverters, or grid-side converters, have a main objective to transfer all the power extracted from the boost stage to the grid by controlling the DC-link voltage [15]. Fig. 2.7 shows a configuration of a grid-connected PV inverter. In this case, a Full-Bridge (FB) inverter is connected to the grid through an  $L$ -filter for simplicity.

Similar to the boost converter, the PV inverter is controlled by adjusting the duty cycle to generate an output voltage. There are several PWM techniques that can be employed in FB inverters. Nevertheless, a bipolar modulation is chosen due to its low leakage current, which is preferable in transformerless PV systems [15]. There are two switching states in the bipolar modulation: 1)  $S_1 S_4$  are on and  $S_2 S_3$  are off, and 2)  $S_1 S_4$  are off and  $S_2 S_3$  are on. This can be expressed by the following equation

$$\begin{cases} L \frac{di_g}{dt} = v_{dc} - Ri_g - v_g, & 0 \leq t < dT_{sw} \\ L \frac{di_g}{dt} = -v_{dc} - Ri_g - v_g, & dT_{sw} \leq t < T_{sw} \end{cases}$$

where  $L$  and  $R$  are the inductance and resistance of the  $L$ -filter respectively.  $v_{inv}$  is an inverter output voltage.  $v_{dc}$  is an input DC voltage from the boost stage,  $v_g$  and  $i_g$  are grid voltage and current, respectively, and  $d$  is the duty cycle.

In order to design a controller, the transfer function of the PV inverter in the frequency domain is required. Again, a small-signal model is adopted for linearizing the non-linear characteristic of the switches. The average value of the inductor voltage can be calculated as shown in Eq. (2.12). Then, the small signals are introduced. By using Eq. (2.13), the transfer function of the system can be obtained and used to design a controller for the PV inverter.

$$L \frac{d\langle i_g \rangle}{dt} = (2d - 1)\langle v_{dc} \rangle - R\langle i_g \rangle - \langle v_g \rangle \quad (2.12)$$

$$\hat{i}_g(s) = \frac{2D - 1}{Ls + R} \hat{v}_{dc}(s) + \frac{2V_{dc}}{Ls + R} \hat{d}(s) - \frac{1}{Ls + R} \hat{v}_g(s) \quad (2.13)$$

### 2.3. Modeling of PV inverters

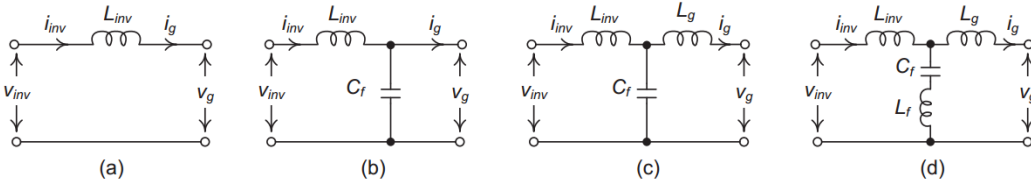


**Figure 2.8:** Different grid filter configurations of PV inverters (a)  $L$ -filter, (b)  $LC$ -filter, (c)  $LCL$ -filter, and (d)  $LLCL$ -filter [8].

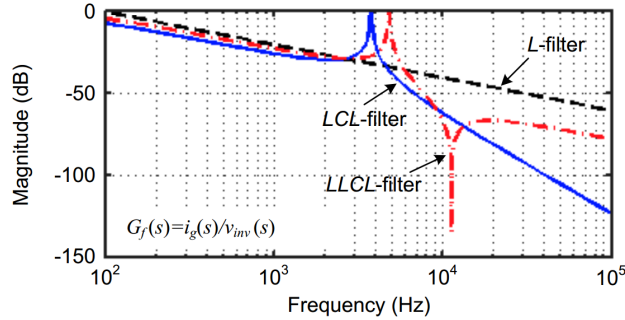


**Figure 2.9:** Frequency response of different filter configurations shown in Fig. 2.8 [8].

Considering grid-connected applications, one main consideration is the Total Harmonic Distortion (THD) in the grid current, which is introduced by the PWM switching behavior of the inverter. In order to satisfy the THD requirement of the grid interconnection standards (e.g. grid codes) [8], [15], the grid filters are employed. The main roles of the grid filters are to attenuate the harmonics in the injected current which can be divided into two aspects: 1) suppressing the high switching noise and 2) smoothing the injected current [8], [24]. Various configurations of the grid filter can be used. The  $L$ -filter shown in Fig. 2.7 is the simplest configuration. However, a high value of inductance is required to reduce the current harmonics at the switching frequency around 2-15 kHz [25]. In some cases,  $L$ -filter is not suitable due to its poor high-order harmonics attenuation performance [8]. In order to have a better harmonics attenuation, high-order filters, which is a combination of inductor and capacitor, are usually employed. Figs. 2.8 and 2.9 show different possible configurations of high-order filters and their frequency response, respectively. According to the frequency response in Fig. 2.9,  $LCL$ -filter has a better rejection at the higher (e.g. double switching) frequency harmonics compared to the other configurations. Therefore, it will be used in this project.

The  $LCL$ -filter shown in Fig. 2.8(c) offers a satisfactory attenuation performance as discussed previously. However, the combination of  $L$  and  $C$  can cause a resonance problem, which may lead to instability of the controller [15]. Thus, a damping resistor is often used in the  $LCL$ -filter as shown in Fig. 2.10, where  $L_{inv}$  and  $L_g$  are the input and grid inductors,  $C_f$  is the filter capacitor and  $R_d$  is the damping resistor.

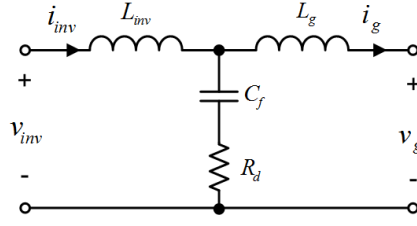


Figure 2.10: An  $LCL$ -filter with a damping resistor.

## 2.4 Modeling of Control systems

In a two-stage grid-connected PV system, the power control is done by two converters. The boost converter controls the power extracted from PV arrays while the PV inverter controls the power injected to the grid. The control structure of the system is shown in Fig. 2.11. The main focus of the project is on the power control of the boost converter, which will be discussed in details in Chapter 3 and 4. Nevertheless, it is also necessary to describe the control and operation of the PV inverter since it is vital in grid-connected PV systems. Therefore, a brief discussion about the control of single-phase PV inverters and their grid synchronization techniques is provided in this section.

### 2.4.1 Grid-Side Power Controllers

In the grid-connected converter, two cascaded control loops are usually employed [21]. The outer loop controls the power injected to the grid by means of the DC-link voltage management. The inner loop is the current controller which handles the power quality issue and needs to response faster than the outer power loop [21].

Actually, there are various control structures for the outer power loop, depending on the application. However, one commonly used control structure is the DC-link voltage controller shown in Fig. 2.12. The DC-link voltage should be kept constant in order to balance the power flow between the DC and AC sides [21]. This can be

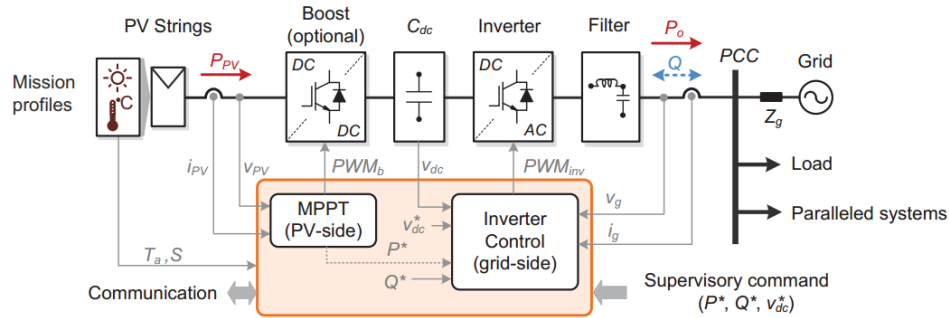
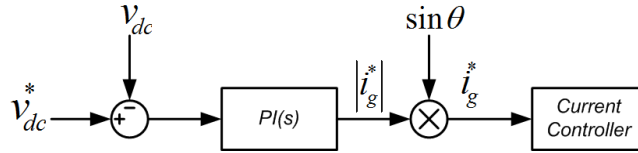


Figure 2.11: Control structure of two-stage grid-connected PV systems [8].

## 2.4. Modeling of Control systems

done by using a Proportional-Integral (PI) controller to regulate the DC-link voltage. By doing so, the output of the outer loop will give a required amplitude of the grid current  $|i_g^*|$ , according to the difference between the reference and the measured DC-link voltage. Then, the reference grid current  $i_g^*$  can be obtained by multiplying  $|i_g^*|$  with  $\sin \theta$ , where  $\theta$  is the phase angle of the grid voltage provided by a Phase Locked Loop (PLL).



**Figure 2.12:** Control structure of the DC-link controller.

### 2.4.2 Grid-Side Current Controllers

The control diagram of the inner current loop is given in Fig. 2.13. In the current controller, a Proportional-Resonant (PR) controller is used [15] since it can track a sinusoidal reference signal without a steady-state error at the resonant frequency. This is due to the fact that PR controllers have a high gain around the resonant frequency as can be seen in Fig. 2.14(a) [15], [21]. For example, this resonant frequency should be chosen at around 50 Hz, which is the grid frequency (in Europe). However, the grid frequency can be deviated in a small range, e.g., 49.5-50.5 Hz. The ideal PR controller in Fig. 2.14(a) will not be able to track any other frequency component than the 50 Hz. To solve this problem, a non-idea PR controller, which has the frequency response as shown in Fig. 2.14(b), is practically used in order to improve the tracking performance of the current controller. In addition, the grid frequency obtained from the PLL should be used as a resonant frequency, instead of a fixed 50 Hz, in order to adjust the resonant frequency of the current controller.

The transfer function of the inverter is realized by a delay introduced from the PWM generation and the sampling [15]. Then, the difference between the inverter

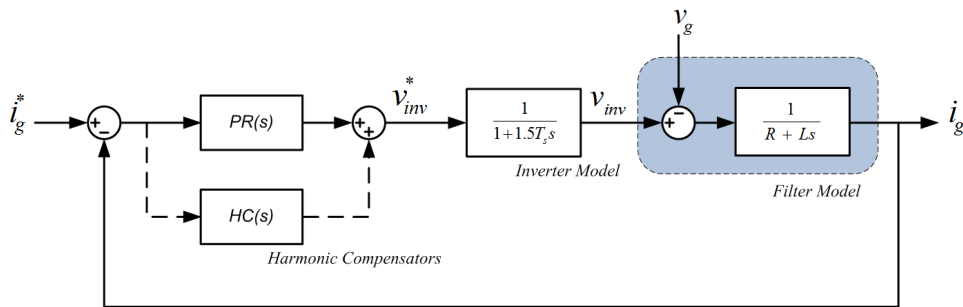


**Figure 2.13:** Current control structure with harmonic compensators [8].

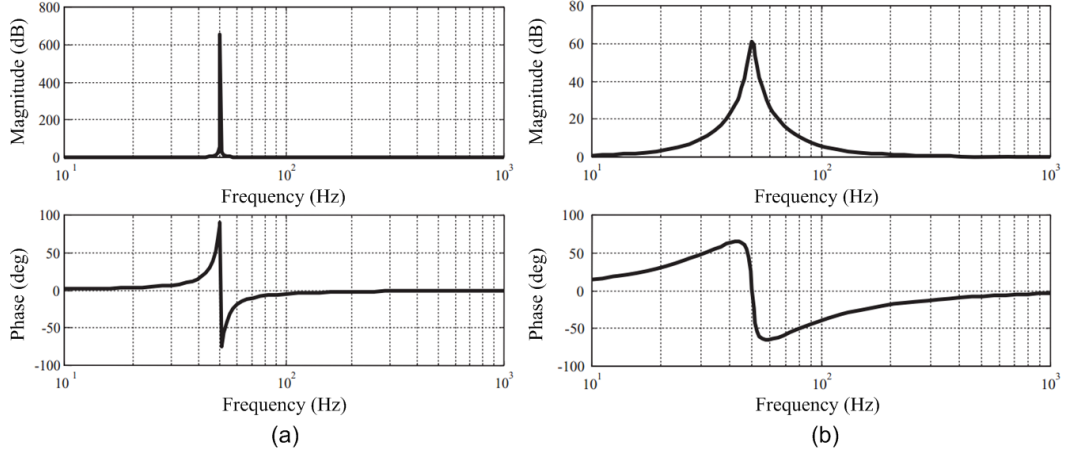


**Figure 2.14:** Bode plots of (a) ideal and (b) non-ideal PR compensator [15].

output voltage and the grid voltage is fed to the grid filter transfer function resulting in the grid current fed back to the PR controller.

### Harmonic Compensations

Harmonic compensators can be added in parallel with the current controller to suppress harmonics appearing in the grid current due to, e.g., dead time and background distortions in the grid.

A harmonics compensator by means of a Repetitive Controller (RC) as shown in Fig. 2.15 was presented in [26], [27], [28]. The main idea is to use delays and feedback loop to generate a periodic signal resulting in a satisfactory performance in tracking a periodic signal, which is the case for the presented harmonics in the grid-connected system. The transfer function of the RC in Eq. (2.14) has poles at the multiples of the fundamental frequency. This enables the controller to compensate the harmonic components in a wide frequency range. It is also suitable to be implemented in digital controllers with a limited resource, i.e., Field-Programmable Gate Array (FPGA), due to its simple control structure.

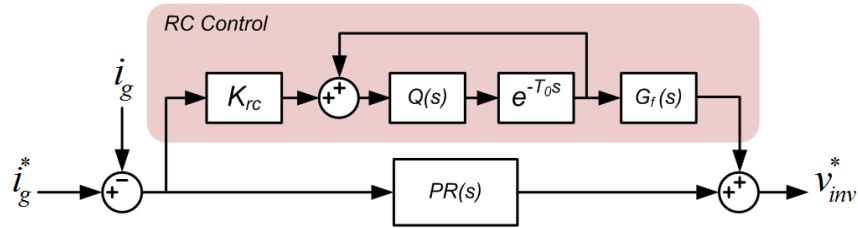


**Figure 2.15:** Control structure of the Repetitive Controller (RC) added in parallel with the Proportional-Resonant (PR) Controller [26], [27], [28].

## 2.4. Modeling of Control systems

$$G_{RC}(z) = \frac{K_{rc}z^{-N}Q(z)}{1 - z^{-N}Q(z)}G_f(z) \quad (2.14)$$

where  $N = f_s/f_g$  with  $f_s$  being the sampling frequency and  $f_g$  being the grid fundamental frequency.  $K_{rc}$  is the controller gain,  $Q(z)$  is a low-pass filter, and  $G_f(z)$  is a phase-lead compensator.

Nevertheless, the RC controller has a slower response compared to other methods (e.g. selective harmonic compensation) since the controller uses the same gain  $K_{rc}$  to compensate all the frequency components. The frequency range of the attenuation is also usually limited, by employing a low-pass filter, in practical implementation due to the stability issues [27]. Besides, the controller is also sensitive to the variation in the grid frequency since the design of the controller relies on a fixed number of the sampling delay corresponding to the fundamental frequency of the AC grid and the sampling frequency of the controller [26], [29].

### 2.4.3 Grid Synchronizations

In grid-connected PV applications, an accurate grid monitoring method and stable synchronization system are crucial [15]. Grid information such as the grid voltage and its phase angle are required parameters for the controller. Among other synchronization techniques, the PLL based methods are popular [30].

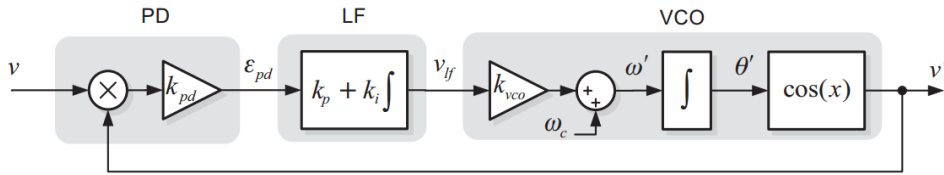


**Figure 2.16:** Basic structure of PLLs [15].

A basic of PLL consists of three main parts as shown in Fig. 2.16. A Phase Detector (PD) generates an error between the input signal and the output signal from the internal oscillator [15]. A Loop Filter (LF) is the second part which has a function to filter the high-frequency AC components. It can be realized by using a PI controller. Then, the output AC signal and the phase angle are generated by a Voltage-Controlled Oscillator (VCO) [15], [31]. There are several ways to implement PLL-based synchronization techniques, e.g., the T/4 Delay PLL, the Enhanced PLL (EPLL), the Second Order Generalized Integrator (SOGI) based PLL. Actually, the main difference between all these techniques is the PD part as shown in Fig. 2.17. To choose the most suitable synchronization technique, a brief overview of each PLL is discussed and their performances are compared.

The idea of T/4 Delay PLL is that the input signal is shifted by 90 degrees (at the fundamental frequency), which corresponds to a quarter of the total sampling period of the controller, to generate an orthogonal signal [15]. After applying a Park Transformation, one of the  $dq$ -component signals is used for extracting the amplitude,

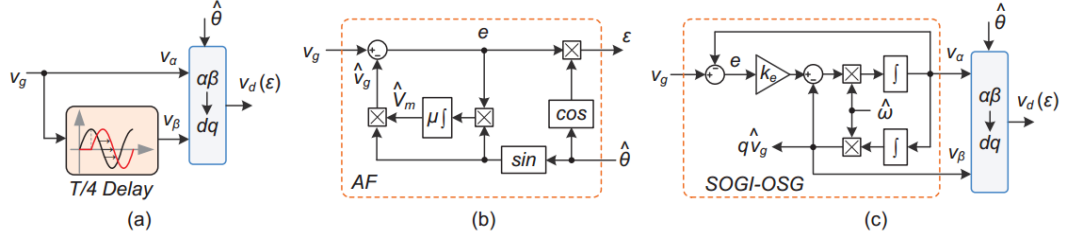


**Figure 2.17:** Phase Detector structure of different PLL systems (a) T/4 Delay PLL, (b) EPLL, and (c) SOGI-PLL [8].

while the other one goes directly to LF and VCO to extract the phase angle. T/4 Delay PLL is considered as one of the easiest technique to extract the phase angle in a single-phase system. However, it shows a poor performance under grid frequency variations and harmonics [30]. The EPLL technique tracks both amplitude and phase angle of the grid by using an adaptive filter [15]. It has a slow dynamic performance under disturbances [30]. Another candidate for PLL based on the adaptive filter is the SOGI PLL. Unlike the EPLL, the SOGI PLL has two-weight adaptive filters, which results in a performance similar to a sinusoidal integrator [30]. The SOGI PLL shows a better tracking performance, especially during the frequency variations, compared with the others [8], [30]. A benchmarking of these three PLL techniques under different disturbances is given in Table 2.2 [8].

Considering the hardware implementation platform, the utilization of the available resources in the FPGA controller is crucial as is discussed in Appendix A. The EPLL offers a satisfactory performance while requiring less complexity and computation burden mainly due to the absence of the reference frame transformation. Therefore, it will be used in the implementation.

**Table 2.2:** Benchmarking of the selected PLL techniques [8].

PLL technique		T/4 Delay PLL	EPLL	SOGI-OSG PLL
<b>Voltage sag (0.45 p.u.)</b>	settling time (ms)	4.7	7.8	8
	frequency error (Hz)	0.26	0.91	0.62
<b>Phase jump (+90 °)</b>	settling time (ms)	75	120	72
	frequency error (Hz)	16.1	16	19.1
<b>Freq. jump (+1 Hz)</b>	settling time (ms)	Oscillate	186	111
	frequency error (Hz)	(-1.2, 1.2)	8.4	10.4
<b>Harmonic immunity</b>		NO	★★	★★★
<b>OSG mechanism (easy for power calculation)</b>		YES	NO	YES
<b>Implementation complexity</b>		★	★★	★★★

Notes: the more ★, the better the harmonic rejection ability or the more complicated the PLL is.

## 2.5 Performance of the Two-Stage Single-Phase PV System

To verify the analysis of the two-stage single-phase PV system and its control in the above sections, experimental tests have been carried out by using the laboratory setup in Fig. 2.18. The PV arrays with the rated power of 3 kW are realized by using a PV simulator which can emulate the behavior of the PV arrays according to the PV cell parameters and the irradiance profile. The parameters of the two-stage single-phase PV system and its control system can be found in Table 2.3 and 2.4, respectively. The digital controller is developed in the FPGA platform, where further detailed discussions are provided in Appendix A. The main goal of this section is to illustrate the controllability of the two-stage single-phase PV system.

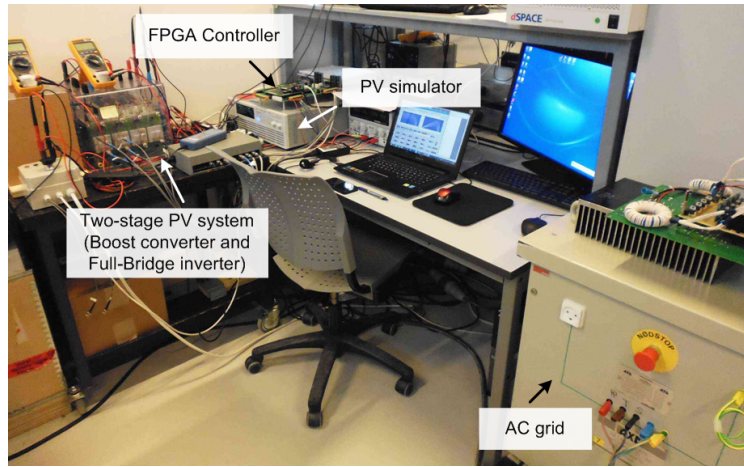


**Figure 2.18:** Laboratory setup of the Two-Stage Single-Phase PV System used in the experiment.

**Table 2.3:** Parameters of the Two-Stage Single-Phase PV System.

Boost converter inductor	$L = 1.8 \text{ mH}$
PV-side capacitor	$C_{pv} = 1000 \text{ } \mu\text{H}$
DC-link capacitor	$C_{dc} = 1100 \text{ } \mu\text{H}$
$LCL$ -filter	Inverter-side inductor: $L_{inv} = 4.8 \text{ mH}$ , Grid-side inductor: $L_g = 4 \text{ mH}$ , Capacitor: $C_f = 4.3 \text{ } \mu\text{F}$
Switching frequency	Boost converter: $f_b = 16 \text{ kHz}$ , Full-Bridge inverter: $f_{inv} = 8 \text{ kHz}$
DC-link voltage	$V_{dc} = 450 \text{ V}$
Grid nominal voltage (RMS)	$V_g = 230 \text{ V}$
Grid nominal frequency	$\omega_0 = 2\pi \times 50 \text{ rad/s}$

**Table 2.4:** Control System Parameters.

Boost converter (PI)	Voltage controller: $k_p = 5, k_i = 0.01$ Current controller: $k_p = 10, k_i = 1$ Power controller: $k_p = 0.1, k_i = 0.0001$
DC-link (PI) controller	$k_p = 0.05, k_i = 10$
Current (PR) controller	$k_p =, k_i =$
Harmonic compensation (RC) controller	$k_{rc} = 1, m = 3, \alpha_1 = 0.5$
Sampling frequency of the digital controller	$T_s = 20$ kHz

### 2.5.1 Boost Converter Control

The performance of three different controllers for the boost converter, where the control parameters are  $v_{pv}^*$ ,  $i_{pv}^*$ , and  $P_{pv}^*$ , is investigated. The focus of this part is only on the boost converter side by assuming that the DC-link voltage is properly regulated by the PV inverter, which will be analyzed later.

The experimental results of the boost converter when the reference  $v_{pv}^*$ ,  $i_{pv}^*$ , and  $P_{pv}^*$  experiences a step change of  $v_{pv}^* = 370$  V to 400 V,  $i_{pv}^* = 5$  A to 7 A, and  $P_{pv}^* = 1700$  W to 2100 W are shown in Figs. 2.19(a), 2.19(b), and 2.19(c) respectively. It can be seen from the results that the controller of the boost converter can follow the reference shortly after the step change is introduced for all three cases. It is also observed that the setting time of the boost controller is less than 0.05 s. This can ensure that the designed controllers are capable of implementing power control strategies of the PV system (e.g. MPPT) where the reference value is typically updated in the period of 0.05 - 2 s [32], [33], [34].

### 2.5.2 PV inverter Control

There are three main parts in the control of the PV inverter: 1) Grid synchronization, 2) Current controller, and 3) Power controller. The synchronization is done through the PLL, where the extracted phase of the grid voltage is shown together with the grid voltage  $v_g$  and the grid current  $i_g$  in Fig. 2.20(a).

It can be seen that the phase angle generated by the PLL corresponds to the measured grid voltage  $v_g$ . Moreover, the PV inverter is at a unity power factor, according to the control diagram in Fig. 2.12. The measured grid frequency of the PLL is 50 Hz with a very small deviation.

The performance of the current controller is tested by introducing a step change in the grid current amplitude  $|i_g^*|$ . As it can be seen in Fig. 2.20(b), the measured grid current  $i_g$  can follow the reference  $i_g^*$  when a step change from 15 A to 18 A is introduced. As aforementioned, the DC-link voltage should be regulated in order to properly transfer the extracted power from the PV arrays to the AC grid. The DC-link controller can be tested by introducing a step change in the input power. By

## 2.5. Performance of the Two-Stage Single-Phase PV System

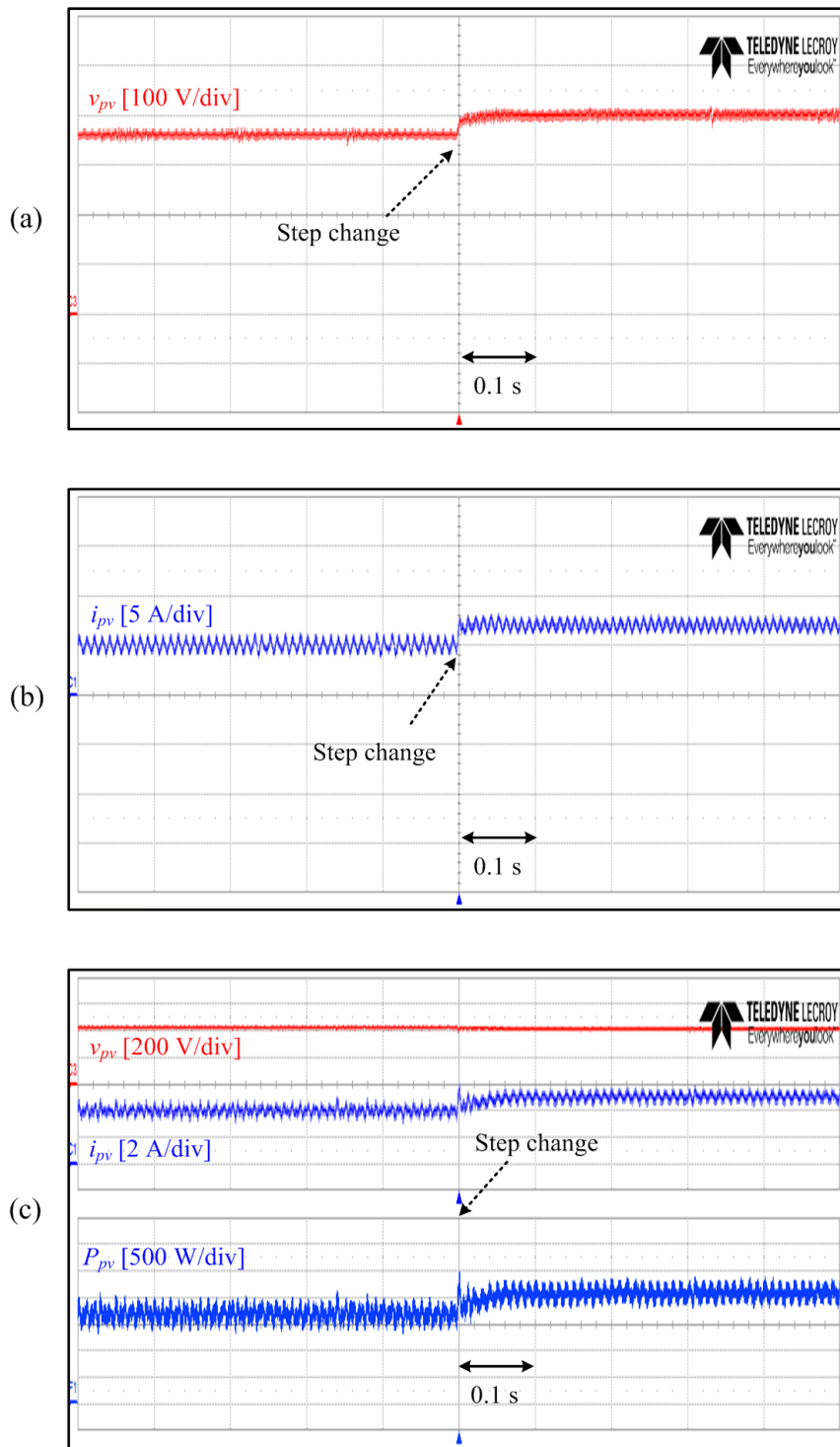


**Figure 2.19:** Experimental results of the boost converter when the input (a) voltage  $v_{pv}$ , (b) current  $i_{pv}$ , and (c) power  $P_{pv}$  is controlled. The reference input experiences a step change from (a)  $v_{pv}^* = 370$  V to 400 V, (b)  $i_{pv}^* = 5$  A to 7 A, and (c)  $P_{pv}^* = 1700$  W to 2100 W.

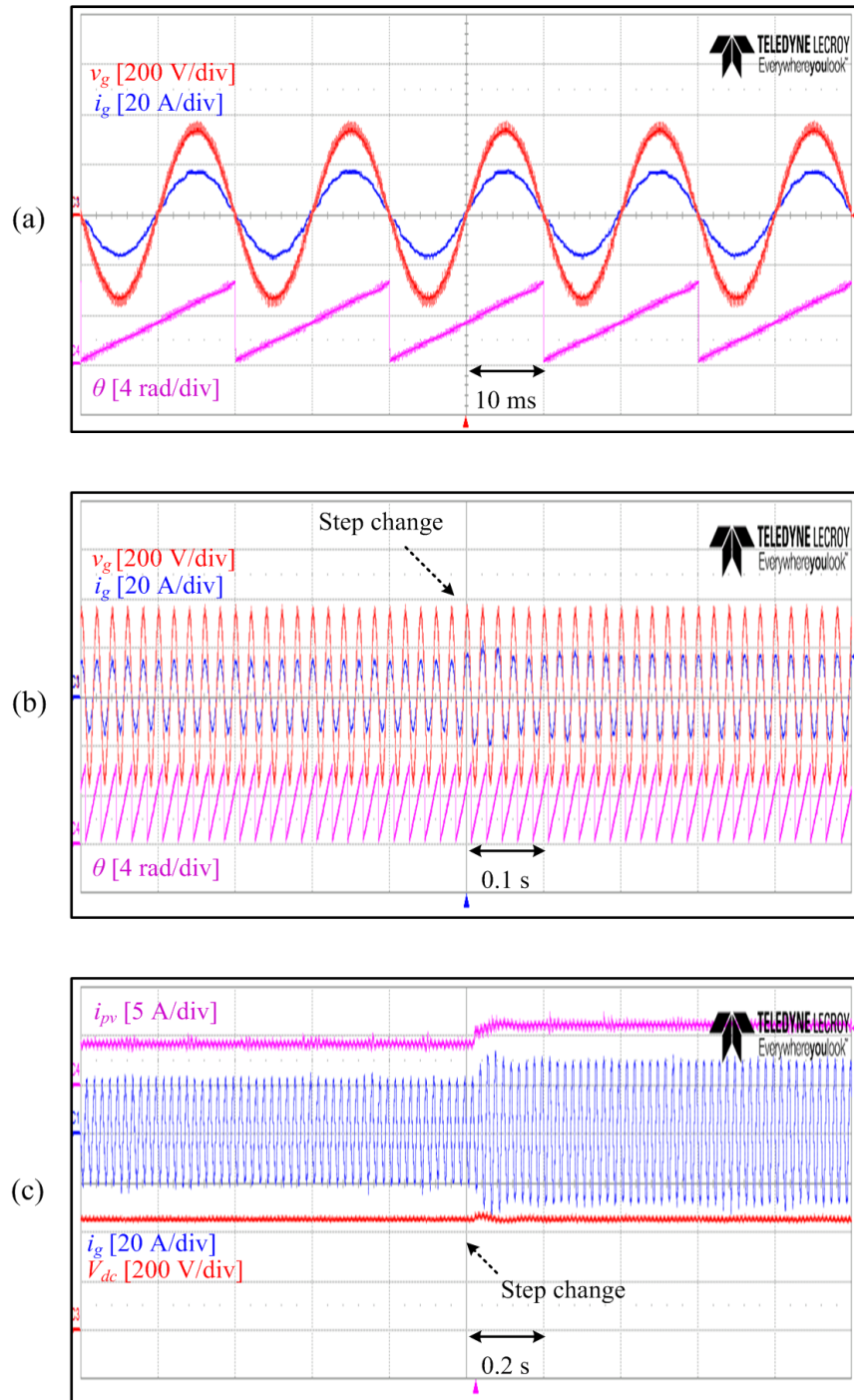


**Figure 2.20:** Experimental results of (a) the PLL where the extracted phase angle of the grid voltage is shown together with the grid voltage and current, (b) the current controller where the proportional resonant (PR) controller is employed together with the harmonic compensator by means of the repetitive controller, where the reference experiences a step change from  $|i_g^*| = 15$  A to 18 A, and (c) the DC-link voltage controller when the controller experiences a step change in the input power, where the reference value of the DC-link voltage is chosen at 450 V.

## 2.6. Summary

doing so, the DC-link voltage will be increased due to the excess energy in the DC-link. As a consequence, the DC-link voltage controller should increase the reference amplitude of the grid current  $|i_g^*|$  in order to deliver more power to the grid and, thereby, keep the DC-link voltage to a reference value. Fig. 2.20(c) shows the experimental results where the DC-link voltage reference is chosen to be 450 V. It can be observed that the DC-link voltage increases when the power injecting from the PV arrays is increased, through the change in the  $i_{pv}$ . However, the DC-link voltage can be regulated, through the PI controller, at 450 V after a short time period. It can also be seen in Fig. 2.20(c) that the grid current  $i_g$  also changes accordingly.

According to the above results, it can be concluded that the controller of the two-stage PV system is properly designed. The boost converter can track the reference input signal, according to the controller type, while the PV inverter illustrates the capability of transferring the extracted DC power to the AC grid.

## 2.6 Summary

In this chapter, the components in the two-stage single-phase PV systems have been modeled. The characteristic of the PV cells has been analyzed and modeled with an equivalent circuit. Both the boost converter and the PV inverter have been modeled using small-signal models. The control systems of the two-stage single-phase PV systems are also taken into consideration, where the focus is mainly on the grid side. The main aim of the controller in the inverter stage is to deliver the extracted DC power from the PV arrays to the AC grid. This power delivery can be ensured by employing a cascade control loop, which consists of a DC-link controller and a current controller. The DC-link controller regulates the DC-link voltage to a constant value by generating a corresponding reference grid current for the current controller. Then, the objective of the current controller, which acts as an inner loop, is to regulate the grid current. The PR controller is employed in the current controller due to its superior performance at tracking a sinusoidal reference signal. Harmonic compensation is an additional functionality which can be provided by adding the RC in parallel with the PR controller. The performances of the two-stage single-phase PV system are verified experimentally.

## Chapter 3

# Maximum Power Point Tracking

Maximum Power Point Tracking (MPPT) control is the main focus of this chapter. Perturb and Observe (P&O) which is one of the most commonly used MPPT algorithms is presented. Different possible MPPT controller structures are also discussed and analyzed. The design considerations of the MPPT controller are given and the performance verification in the laboratory under the several test conditions is provided at the end of the chapter.

### 3.1 Overview of Maximum Power Point Tracking

In PV systems, one main consideration is the efficiency of the power production of the system [15]. It is desirable that the PV systems deliver the maximum available power to the grid all the time due to the fact that PV modules have low conversion efficiency and also a high initial cost [35], [36], [37]. Therefore, in most cases, it is required for PV systems to operate at the Maximum Power Point (MPP). As discussed in Fig. 2.3, the MPP of the PV arrays varies with the environmental conditions. In order to maximize the power production of PV systems, Maximum Power Point Tracking (MPPT) algorithm, which continuously tracks the MPP during operation, is essential. In general, the demands of the MPPT algorithm can be divided into three main aspects [38], [39]:

- Fast dynamic response - It is desirable that the MPPT algorithm can keep the PV system operates at the MPP under the changing environmental conditions. In order to do so, a fast tracking algorithm which can follow the change in the MPP is required.
- High accuracy under the steady-state condition - During the steady-state condition, the MPPT algorithm should keep the PV system to operate at the MPP with a minimum deviation. An accurate tracking performance of the MPPT algorithm is essential since it can effectively reduce energy losses of the PV systems. This will increase the overall efficiency of the PV system.

### 3.2. Perturb and Observe MPPT Control

- Robustness to disturbances - Instability can be introduced by the fast changing irradiance condition and noise from the measurements. Therefore, robustness is one of the most important design consideration of the MPPT algorithm.

Accordingly, several MPPT algorithms have been proposed, among which the Perturb and Observe (P&O) algorithm is the most widely used method. [38], [40], [41]. In this chapter, the P&O MPPT algorithm, also known as a hill-climbing method, will be discussed.

## 3.2 Perturb and Observe MPPT Control

In terms of complexity, the P&O MPPT is the simplest one, which makes it widely used in PV systems [35], [40], [42]. The operation principle of the P&O MPPT is shown in Fig. 3.1. The operating voltage of the PV arrays  $v_{pv}$  is “perturbed” intentionally and then the corresponding change in the output power of the PV arrays is “observed” in order to determine the direction of the next perturbation. If a perturbation of  $v_{pv}$  leads to an increase of the PV output power  $P_{pv}$ , the next perturbation should be continued in the same direction (i.e.,  $a \rightarrow b \rightarrow c$ ). Otherwise, if the change of the  $v_{pv}$  results in a decrease of the  $P_{pv}$  (i.e.,  $c \rightarrow d$ ), the perturbation should reverse the direction [39], [41].

A flow chart of the P&O MPPT algorithm is shown in Fig. 3.2, where  $V_{pv,n}$  and  $I_{pv,n}$  are the measured voltage and current of the present sampling, which can be multiplied to obtain the PV output power  $P_{pv,n}$ . Similarly,  $V_{pv,n-1}$  and  $I_{pv,n-1}$  are the measured voltage and current of the previous sampling and  $P_{pv,n-1}$  is the PV output power of the previous sampling. *STEP* is the step size of the perturbation and  $v_{pv}^*$  is the reference PV voltage for the boost converter. It should be noted that the P&O method can also be applied with the perturbation of the operating current of the PV arrays  $i_{pv}$  instead of the voltage. The control algorithms are identical.

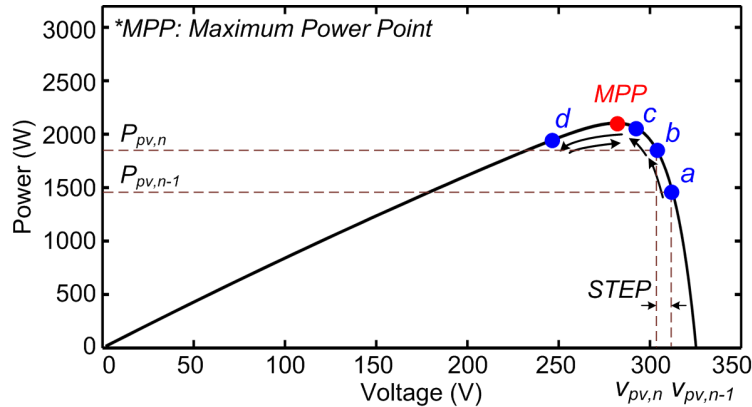


**Figure 3.1:** Concept of the Perturb and Observe (P&O) MPPT algorithm.

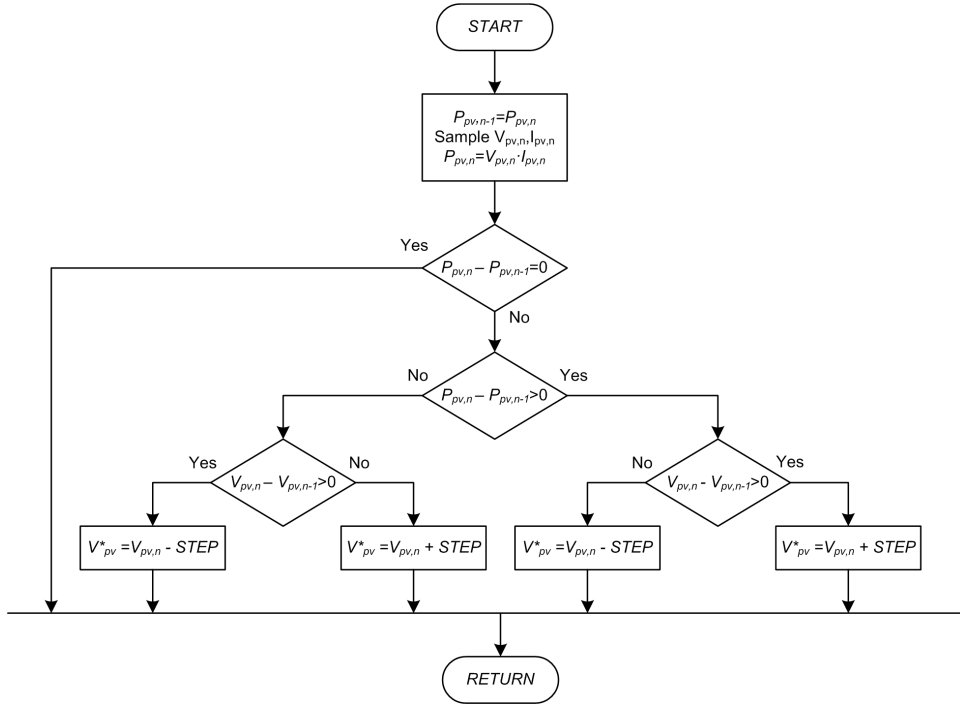


**Figure 3.2:** Flow chart of the Perturb and Observe (P&O) MPPT algorithm [35].

Once the MPP is reached, the PV output power will oscillate around the MPP [38], [41]. This unavoidable oscillation results in power losses of the PV systems, which is one main drawback of the P&O MPPT algorithm [42]. In order to reduce the oscillation, a small step size should be chosen. However, there is a trade-off between the reduction in the oscillation and the tracking speed, since a smaller step size will slow down the MPPT control [41]. Another disadvantage of the P&O MPPT is the poor tracking performance in a rapid changing irradiance condition [41], [42]. When the irradiance level changes very fast, (e.g., PV arrays are shaded by a moving cloud), the P&O MPPT algorithm may track the MPP in the wrong direction as illustrated in Fig. 3.3.

It can be seen in Fig. 3.3 that without the change in the irradiance, the P&O MPPT should see a lower  $P_{pv}$  in the next perturbation (point b). However, because the  $P_{pv}$  increases due to the irradiance change, the  $P_{pv}$  measured in the next perturbation (point c) is higher than the present PV output power (point a). As a result, the perturbation continues in the wrong direction by decreasing the  $v_{pv}$  and moves away from the real MPP. This problem can be alleviated if the step size is large enough to ensure that the change in the  $P_{pv}$  is due to the perturbation, not the increased irradiance. However, a large step size will result in more power losses in the steady-state operation [43]. Another solution is to increase the sampling rate of the MPPTs. Nevertheless, in practice, the sampling rate of MPPT is limited by the dynamic performance of the converter.

### 3.3. MPPT Controllers

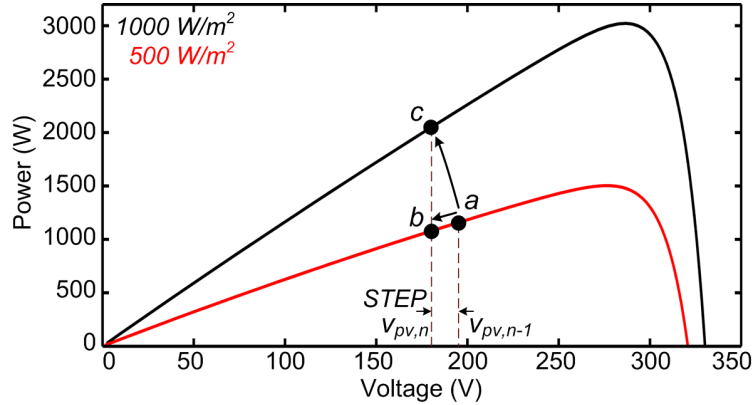


**Figure 3.3:** Performance of the Perturb and Observe (P&O) MPPT algorithm under a fast changing irradiance condition [41].

Notably, although the P&O MPPT algorithm is simple, there are two main drawbacks - power oscillations around the MPP and poor tracking performance under rapid change environmental conditions. Several methods to enhance the P&O MPPT algorithm have been proposed. For example, in [38] and [39], a variable step size of the P&O MPPT is used. In [44], an extra measurement point between each perturbation is used to eliminate the error of the  $P_{pv}$  under a fast-changing environmental condition. Nevertheless, these solutions may introduce more complexity of the algorithm and can give smaller robustness.

### 3.3 MPPT Controllers

In the previous section, the MPPT algorithm has been discussed. Typically, the P&O MPPT algorithm can give either PV output voltage  $v_{pv}^*$  or current  $i_{pv}^*$  as the reference. Therefore, in most cases, the boost converter controls are realized by using a closed-loop control, where either the  $v_{pv}^*$  or  $i_{pv}^*$  is directly used as the reference, which is shown in Fig. 3.4. A Proportional-Integral (PI) controller is employed in the close-loop control to adjust the duty cycle of the boost converter according to an error between the reference and the measured value. It should be pointed out that the subtraction between the reference and measured value of voltage- and current-based controller has an opposite sign. This is due to the fact that the transfer function of  $\frac{v_{pv}}{d}$  has a negative resistance term as derived in Eq. (2.8).

These two control structures are very suitable for the normal MPPT operation where the MPP needs to be tracked continuously. Although the controllers do not directly control the PV output power  $P_{pv}$ , the MPP can be tracked by controlling the boost converter input voltage  $v_{pv}$  or current  $i_{pv}$ . However, these two control structures might not be considered as the most suitable control structure for implementing a power control strategy. In other power control strategies apart from the MPPT, the control over  $i_{pv}$  or  $v_{pv}$  may not ensure the control over  $P_{pv}$ , especially, when the

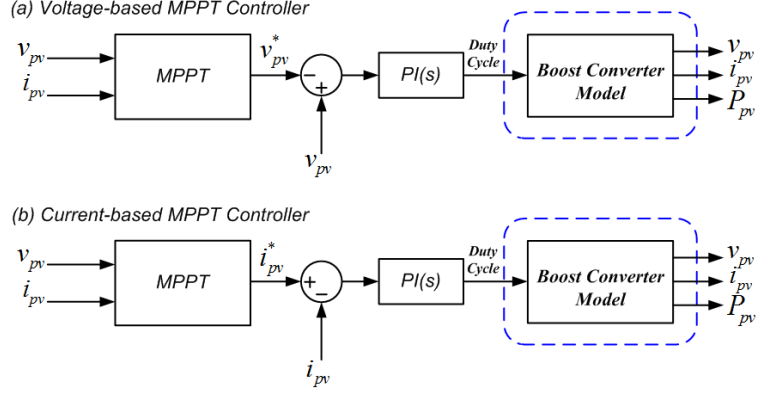


**Figure 3.4:** MPPT control structures based on (a) voltage and (b) current control.

irradiance is changing. Therefore, another MPPT control structure, which gives the  $P_{pv}^*$  as the reference will also be taken into consideration. As can be seen in Fig. 3.5, the MPPT controller can also be realized by using a power control structure. This control structure is actually a modification of the voltage- and current-based MPPT controller, but an additional calculation is required in order to obtain the power reference  $P_{pv}^*$ , as discussed in Section 2.2. The power reference  $P_{pv}^*$  is then compared with the measured PV power  $P_{pv}$ . Similarly to other MPPT control structures, a PI controller can be employed to regulate the PV output power by adjusting the duty cycle of the boost converter, as is shown in Fig. 3.5.

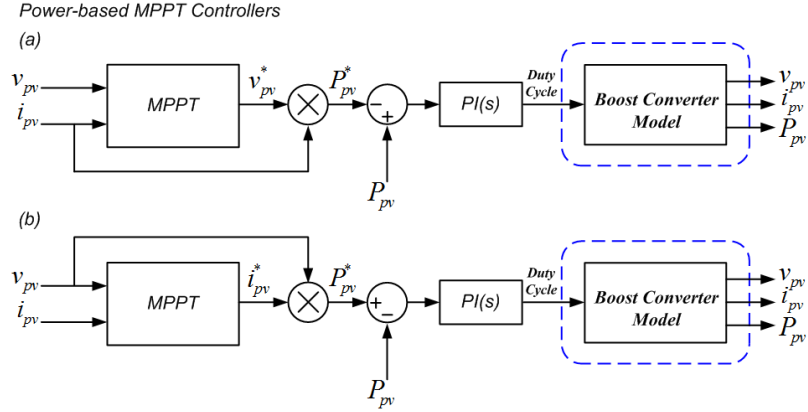


**Figure 3.5:** MPPT control structures based on power control where (a) the reference  $v_{pv}^*$  is multiplied with the measured  $i_{pv}$  and (b) the reference  $i_{pv}^*$  is multiplied with the measured  $v_{pv}$ .

It is worth mentioning that the power-based MPPT controller in Fig. 3.5(a) is based on the assumption that the measured  $i_{pv}$  is almost constant as it was derived in Eq. (2.10). Similarly, it is required that the measured PV voltage  $v_{pv}$  is almost constant when applying the power-based MPPT controller in Fig. 3.5(b). If these

### 3.3. MPPT Controllers

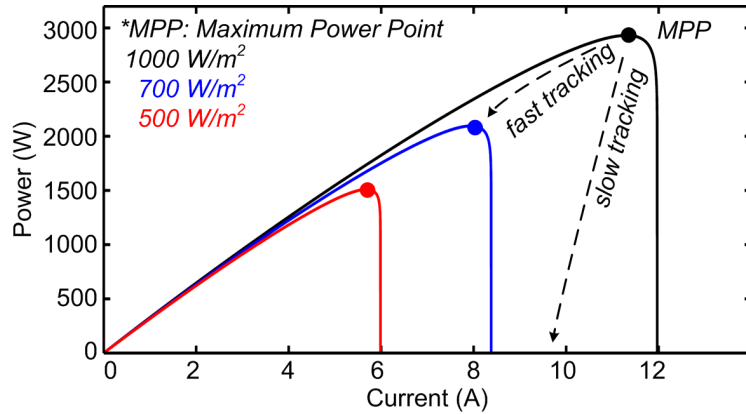


**Figure 3.6:** Power-current characteristic curve of the PV arrays at different irradiance levels.

conditions are violated, the system will be unstable. In fact, the operating point of the PV system always starts from an open-circuit voltage, where the  $v_{pv}$  is almost constant. As a consequence, it is not possible to use the power-based MPPT controller in Fig. 3.5(a) in the practical implementation, since the PV system will not be able to operate properly at the start-up process. In the case of the power-based MPPT controller in Fig. 3.5(b), the operating point will never go into a constant current region in normal operation. Therefore, it is only possible to use the controller in Fig. 3.5(b) in a practical implementation.

On one hand, an advantage of this control structure is that the power extracted from the PV arrays is controlled directly. There is a possibility to implement the power control strategy by modifying the power reference, which will be discussed in details in Chapter 4. On the other hand, noise and variation of the measured PV voltage  $v_{pv}$  will appear in the power reference  $P_{pv}^*$  due to the multiplication, which is a main drawback of this power-based MPPT controller.

It should also be noted that the stability issues may appear, when the current-based MPPT controller is employed. Considering the power-current (P-I) curve of the PV arrays shown in Fig. 3.6, it can be noticed that the P-I curve has a very steep slope on the right side of the MPP. There is a chance that the operating point of the PV system may go to the short-circuit condition under the decreasing irradiance condition as is stated in [34] and [45]. Assuming that the irradiance level is  $1000 \text{ W/m}^2$  and the PV system is operating at the MPP, the irradiance level suddenly decreases to  $700 \text{ W/m}^2$ . It can be seen from Fig. 3.6 that the operating point of the system may "fall off the hill" if the MPPT algorithm cannot track fast enough. The situation could become even worse if the irradiance level in Fig. 3.6 suddenly drops e.g. from  $1000 \text{ W/m}^2$  to  $500 \text{ W/m}^2$ . This incident can also affect the stability of the power-based MPPT controller to some extent, since the PV current  $i_{pv}$  is also used for calculating the power reference  $P_{pv}^*$ .

### 3.3.1 Design consideration of MPPT controllers

The efficiency is one of the most important issues in the PV systems. This is due to the limited energy conversion efficiency of the PV arrays. It is defined in *EN50530* standard that the overall efficiency of the PV system ( $\eta_{total}$ ) can be calculated as [47]

$$\eta_{total} = \eta_{CONV} \cdot \eta_{MPPT} \quad (3.1)$$

where  $\eta_{MPPT}$  is the MPPT efficiency, which is a ratio between the extracted DC power and the available power of the PV arrays.  $\eta_{CONV}$  is a conversion efficiency, which is mainly related to the losses in power converters. These losses are, in most cases, related to the hardware limitations (e.g. power-semiconductor technology). In order to maintain a high efficiency of the overall PV system, it is very crucial to design an MPPT controller that can achieve a very high efficiency ( $\eta_{MPPT} > 95\%$ ) [45].

The P&O MPPT algorithm relies very much on the two design parameters: 1) the step size of the perturbation and 2) the sampling (updated) frequency of the MPPT algorithm. Considering the step size of the perturbation, there is a trade-off between the dynamic and the steady-state performance. A large step size will result in a faster tracking speed, especially, under a fast changing irradiance condition. Nevertheless, the amplitude of the oscillation in the steady-state condition is directly proportional to the step size. This means the energy losses due to the dynamic performance of the MPPT algorithm can be reduced by using a large step size but the energy losses in the steady-state condition will be increased at the same time. In practice, the step size should also be large enough to prevent undesired effects, which could lead to a wrong tracking decision, due to the noise from the measurements.

The sampling frequency of the MPPT algorithm is another design parameter that can significantly affect the performance of the MPPT controller. Actually, the dynamic performance of the MPPT controller (e.g., under a fast irradiance change) can be improved by increasing the sampling frequency. However, the sampling frequency of the MPPT algorithm is restricted by the dynamics of the boost converter. In

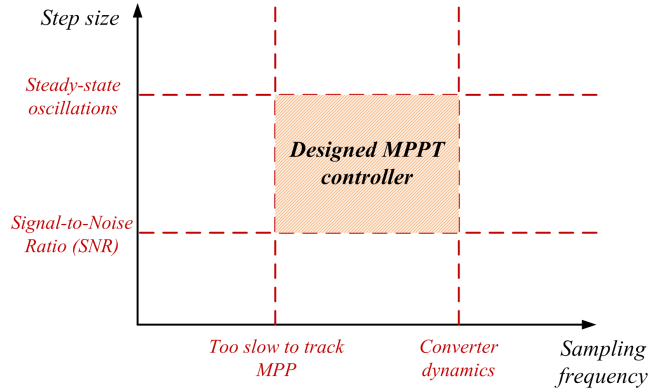


**Figure 3.7:** Design constrains and considerations of the MPPT controllers [32], [46].

### 3.4. Performance of the MPPT controllers

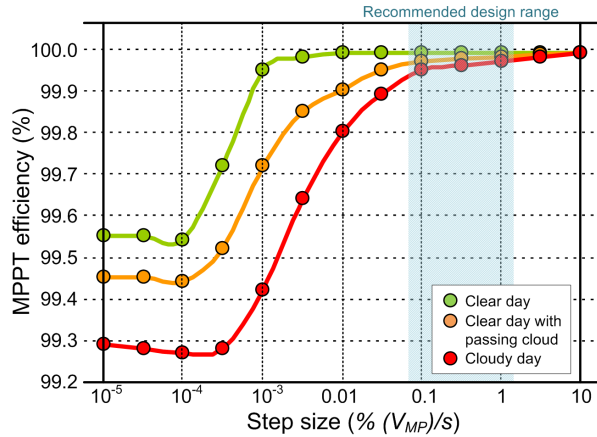


**Figure 3.8:** Tracking efficiency as a function of the step size of the MPPT controllers [48].

other words, the boost converter controller needs to reach the steady-state condition before the reference value from the MPPT controller (i.e.,  $i_{pv}^*$ ,  $v_{pv}^*$  or  $P_{pv}^*$ ) is updated [33]. Typically, the sampling frequency of the MPPT algorithm is in the range of 0.5 - 20 Hz [32], [33], [34].

The relation between the step size, sampling frequency, and the performance of the MPPT controller is summarized in Fig. 3.7. In order to find the suitable design parameters, the step size,  $STEP$ , sampling frequency of the MPPT controller,  $f_{MPPT}$ , and also the power level of the PV systems should be considered together [32], [33], [46]. According to the design guideline in [48], the step size of the voltage-based MPPT controller as a function of the sampling frequency of the MPPT algorithm should be within a range of

$$\frac{0.1}{100} V_{mp} \cdot f_{MPPT} < STEP < \frac{1}{100} V_{mp} \cdot f_{MPPT} \quad (3.2)$$

which is shown in Fig. 3.8.

### 3.4 Performance of the MPPT controllers

Three MPPT controllers (e.g., voltage-, current-, and power-based) have been designed with the P&O MPPT algorithm, using the system configuration shown in Fig. 2.11. The parameters of the controllers are given in Table 3.1. The sampling frequency of the MPPT is designed considering the dynamic of the boost converter. More precisely, the sampling frequency should not exceed 20 Hz, which corresponds to the settling time period of the boost converter controller. In fact, the presence of the double-line frequency variation in the voltage and/or current of the PV arrays due to the mismatch between DC and AC power can have a negative impact to the performance of the MPPT controller [49]. In order to alleviate the affect of this 100 Hz variation, the sampling period of the MPPT algorithm should be chosen as a

**Table 3.1:** Designed Parameters of MPPT Controllers.

<b>Design parameter:</b>	<i>Voltage-based MPPT controller</i>	<i>Current-based MPPT controller</i>	<i>Power-based MPPT controller</i>
<b>Step size</b>	2 V	0.15 A	0.15 A (simulation), 0.2 A (experiment)
<b>Sampling rate (simulation)</b>	10 Hz		
<b>Sampling rate (experiment)</b>	200 Hz		

multiple of 0.01 s (corresponded to 100 Hz), which can reduce the influence of the 100 Hz variation in the measurements. According to these criterions, the sampling frequency of the MPPT algorithm is chosen as 10 Hz. Regarding the step size of the perturbation, it is chosen based on the guideline in [48], which was also discussed in Section 3.3, as well as a practical tuning in order to prevent undesired effects due to the presence of noise from the measurements. It should be noted that the step size of the power-based MPPT controller in the experiment is slightly larger than the value in the simulation due to the presence of the sensing noise.

#### A. Dynamic performances of the MPPT controllers

Two irradiance profiles are used in the simulation model. The ramp irradiance condition is used to emulate the slow changing irradiance condition, e.g., during a clear day. In fact, the irradiance level can also change rapidly when the PV arrays experience a cloudy environmental condition. Therefore, a trapezoidal irradiance profile with a fast changing in the slope is also used to test the MPPT controllers. It should be mentioned that the change in the irradiance used in the simulation is relatively fast compared to a typical irradiance profile in the real measured data. This is due to the limited simulation time and the available memory. However, the sampling rate of the MPPT algorithm is also increased to 200 Hz, which is higher than the typical sampling rate of 0.5 - 20 Hz [32], [46], in order to have a more realistic simulation model. An alternative solution is to use a simplified model which is not considered in this project.

The dynamic performances of the voltage-, current-, power-based MPPT controllers in the simulation are shown in Figs. 3.9, 3.10, and 3.11. It can be seen that all the MPPT controllers have similar tracking performances under the ramp irradiance condition. A small variation in the PV output power can be seen in Fig. 3.11(a) when the power-based MPPT controller is employed. The performances of the MPPT controllers are deviated when the fast changing irradiance profile is used. Both the current- and power-based MPPT controllers have a poor dynamic performance under a rapid decrease in the irradiance level, resulting in large power losses as can be seen in Figs. 3.10(b) and 3.11(b).

### 3.4. Performance of the MPPT controllers

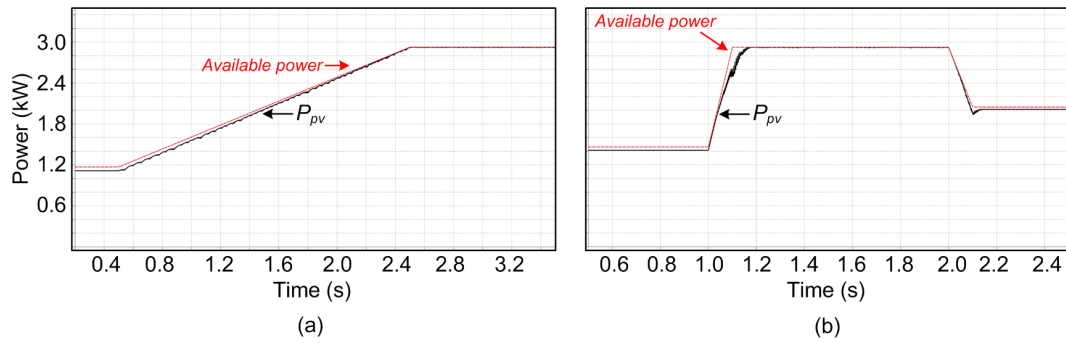


**Figure 3.9:** Simulation dynamic performances of the voltage-based MPPT controller: (a) ramp irradiance and (b) fast changing irradiance.

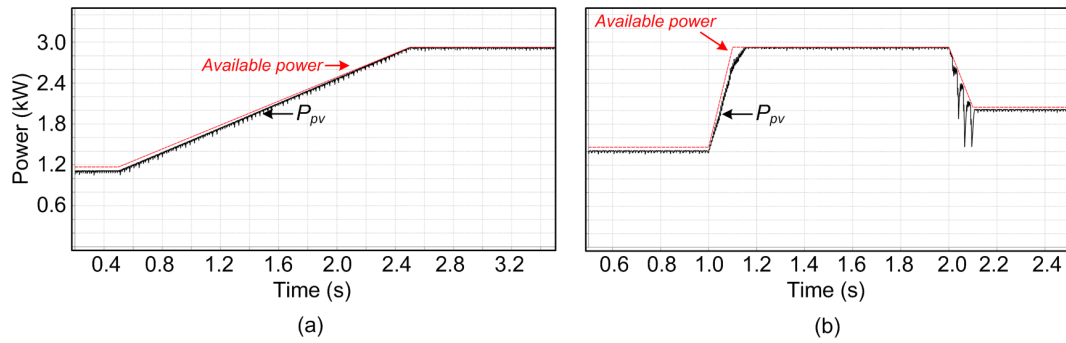


**Figure 3.10:** Simulation dynamic performances of the current-based MPPT controller: (a) ramp irradiance and (b) fast changing irradiance.

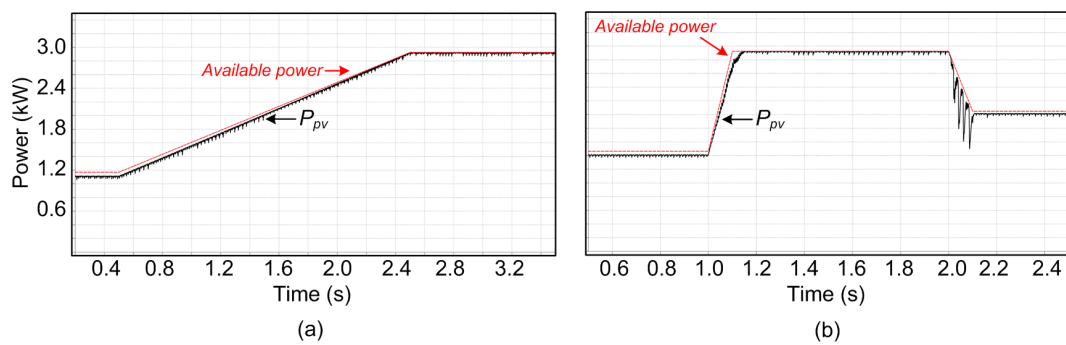


**Figure 3.11:** Simulation dynamic performances of the power-based MPPT controller: (a) ramp irradiance and (b) fast changing irradiance.

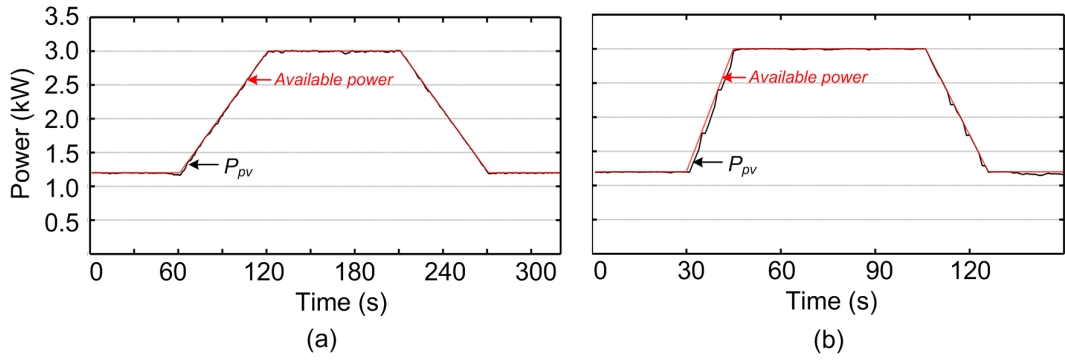


**Figure 3.12:** Experiment dynamic performances of the voltage-based MPPT controller: (a) normal irradiance and (b) fast changing irradiance.

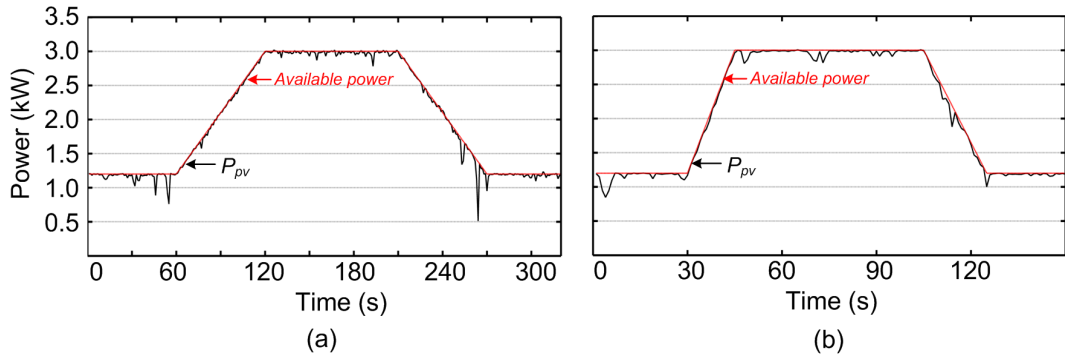


**Figure 3.13:** Experiment dynamic performances of the current-based MPPT controller: (a) normal irradiance and (b) fast changing irradiance.

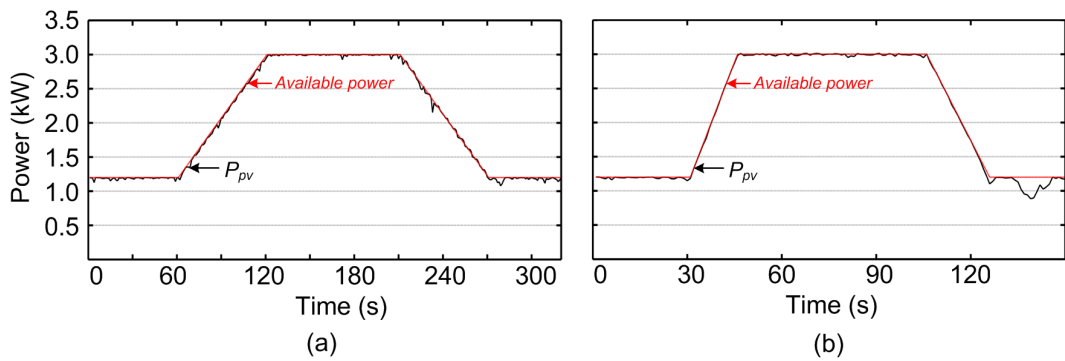


**Figure 3.14:** Experiment dynamic performances of the power-based MPPT controller: (a) normal irradiance and (b) fast changing irradiance.

### 3.4. Performance of the MPPT controllers

Furthermore, experiments have been carried out under solar irradiance change conditions. Two trapezoidal irradiance profiles with different slopes are used to emulate the normal and fast changing irradiance conditions. The experimental results of the MPPT controllers are shown in Figs. 3.12, 3.13, and 3.14. As can be seen from the experimental results, the voltage-based MPPT controller has the most robust operation where the oscillation under the steady-state condition is minimized compared to the other MPPT controllers. A large variation in the  $P_{pv}$  is observed in the current-based MPPT controller. Moreover, the loss of power production under the decreasing irradiance is the main drawback of this type of MPPT controller as can be seen in Fig. 3.13. Considering the dynamic performance under a fast increasing irradiance condition, the power-based MPPT controller has the fastest response, while the power losses are significant for the voltage-based MPPT controller.

#### B. Performances of MPPT controllers under real irradiance profiles

In order to observe the performance of the MPPT controllers in the real operation, the PV simulator has been programmed by using the two recorded irradiance and temperature profiles in Fig. 3.15. The time scale of the recorded profiles is scaled down in order to accelerate the testing time from 24 hours to 24 minutes. By using these two irradiance profiles, it is possible to emulate the environmental conditions of a clear and a cloudy day conditions in the experimental setup.

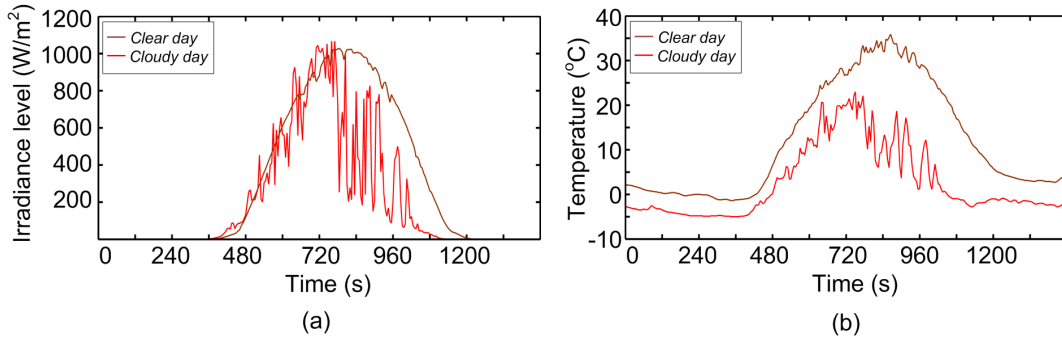


**Figure 3.15:** Recorded (a) daily irradiance and (b) daily PV arrays temperature profiles, after scaling the time to 24 minutes.

The experimental results of different MPPT controllers are shown in Figs. 3.16, 3.17, and 3.18. It has been revealed that the voltage-based MPPT controller has an excellent performance under both clear and cloudy conditions. A poor tracking performance is observed when the current-based MPPT controller is employed. The controller experiences an instability operation under the decreasing irradiance condition as can be seen from Fig. 3.17. The power-based MPPT controller has a satisfied performance under the clear day condition. However, there is a significant power losses under a decreased irradiance in the cloudy day condition and the PV system has a risk of instability operation, i.e., at  $t = 800$  s.

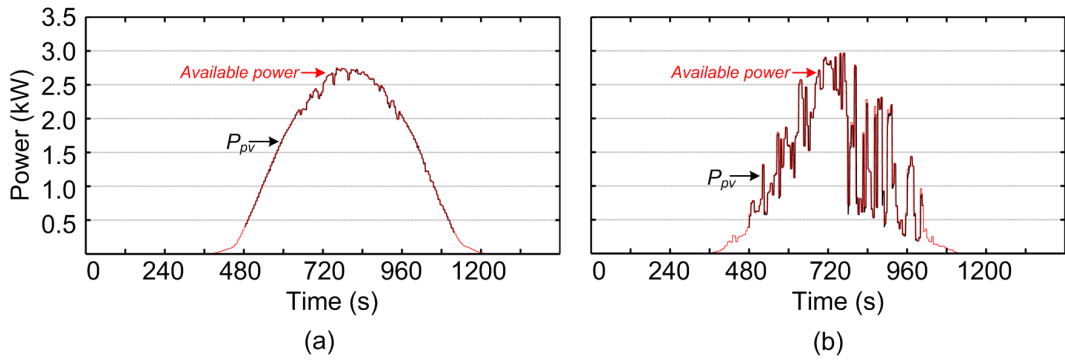


**Figure 3.16:** Experimental results of the voltage-based MPPT controller under real irradiance profiles: (a) clear day and (b) cloudy day.

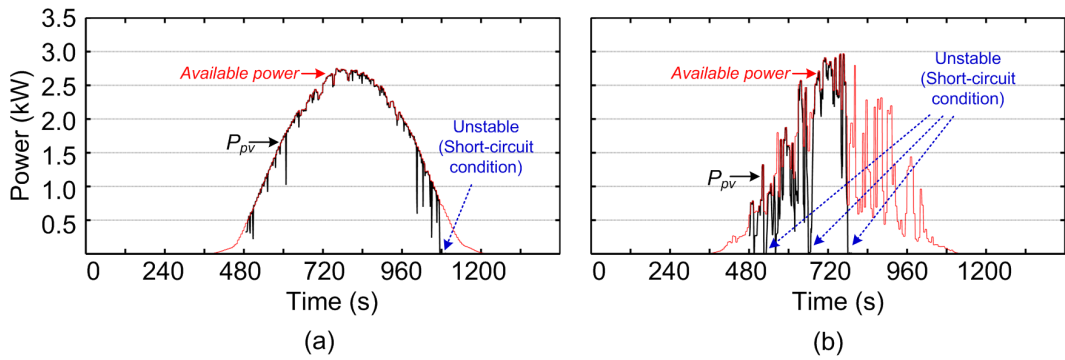


**Figure 3.17:** Experimental results of the current-based MPPT controller under real irradiance profiles: (a) clear day and (b) cloudy day.

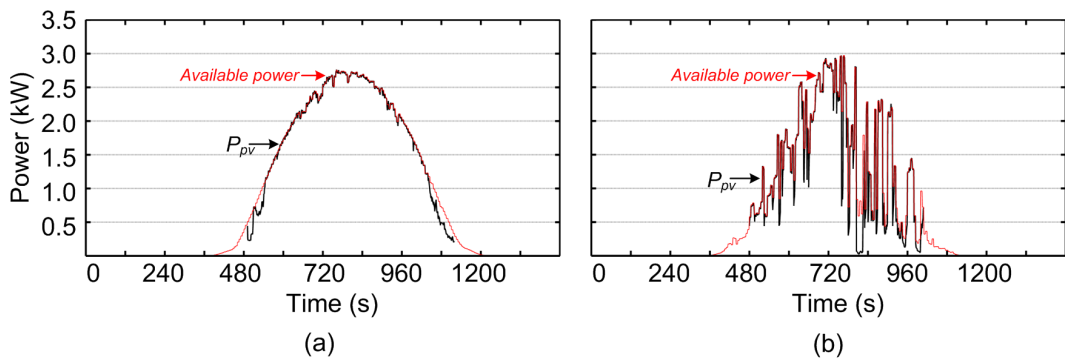


**Figure 3.18:** Experimental results of the power-based MPPT controller under real irradiance profiles: (a) clear day and (b) cloudy day.

## 3.5 Summary

MPPT control is required in order to maintain the high efficiency of the overall PV system. In terms of complexity, the P&O is one of the most commonly used MPPT algorithms and is employed in this project

The MPPT algorithm provides a reference for the boost converter controller which can be realized by several ways. Typically, the boost converter is controlled by its input voltage or current. Alternatively, it is also possible to directly control the input power of the boost converter, which may be suitable for active power control strategy implementation.

Design considerations regarding the step size and the sampling rate of the MPPT controllers have been discussed. Then, the performances of the MPPT controllers have been verified with both simulation and experiments under several irradiance conditions. It has been observed that the voltage-based MPPT controllers have a superior performance compared to the others, especially, under a decreasing irradiance condition. An instability can occur when the current-based MPPT controllers operate under a fast decreasing irradiance condition, e.g., cloudy condition. The power-based MPPT control also has such a risk of instability.

## Chapter 4

# Constant Power Generation Operation

This chapter begins with a background of active power control strategies. Then, an overview of a Constant Power Generation (CPG) in the PV systems is presented. Prior-art work regarding the active power control in the PV system is discussed. The focus of this chapter is on three selected algorithms to realize the CPG operation. Performances of the presented CPG algorithms are verified and a benchmarking of different CPG algorithms is provided at the end of the chapter

### 4.1 Background of Active Power Control Strategies

The power generated by PV systems is fluctuating dependent on the weather conditions. Typically, the peak power production occurs around a midday when the irradiance level is usually high. Conventionally in most countries, it is required that PV systems should operate in MPPT mode as presented in Chapter 3. However, in a wide-scale PV system scenario, this can lead to an overloading of the distribution sys-

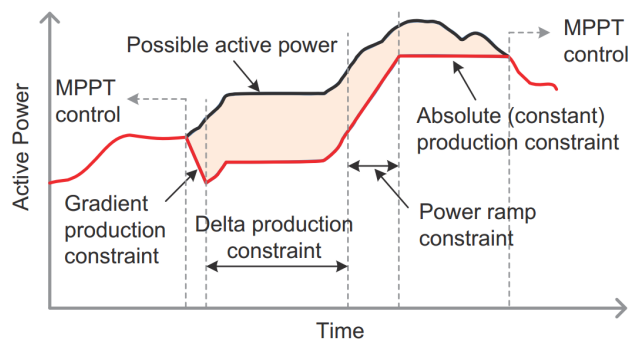


**Figure 4.1:** Active power control functions for wind turbine power systems defined in the Danish grid code [50].

## 4.2. Overview of Constant Power Generations

tem during the peak power production of the PV systems [7], [12], [51]. To solve this problem, apart from expanding the grid infrastructure or reducing the installation of PV systems, better power controllability of PV systems is required. Since most of PV systems are connected to a single-phase system, the control of active power is more effective than the reactive power due to the high R/X ratio characteristic of distribution systems [8], [12].

Active power control strategies have been successfully implemented in wind turbine power systems. In the Danish grid code, the active power control functions are defined as shown in Fig. 4.1 [50]. Considering an absolute (constant) production constraint, the output power of the wind turbine is regulated at a constant set point value. This active power control function is the main focus in this chapter and will be referred to as a CPG control.

## 4.2 Overview of Constant Power Generations

The CPG concept for PV systems was introduced in [7], [17]. The main objective of this control strategy is to prevent an overloading by limiting the maximum feed-in power of the PV systems to a certain level. Specifically, the PV system is operated in the MPPT mode, when the available active power ( $P_{pv}$ ) is below the setting maximum feed-in power ( $P_{limit}$ ). However, when the available power reaches  $P_{limit}$ , the output power of the PV system will be kept at  $P_{pv} = P_{limit}$ , and leading to a constant active power injection as shown in Eq. (4.1) and Fig. 4.2.

$$P_{pv} = \begin{cases} P_{MPPT}, & \text{when } P_{pv} \leq P_{limit} \\ P_{limit}, & \text{when } P_{pv} > P_{limit} \end{cases} \quad (4.1)$$

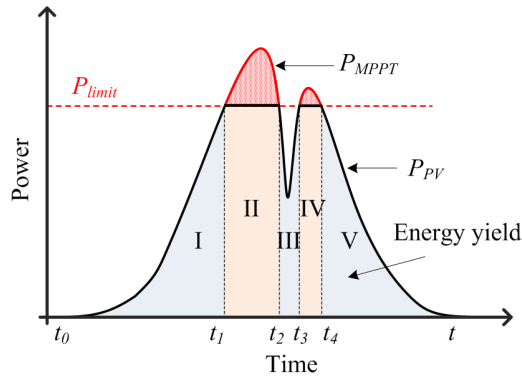


**Figure 4.2:** Constant Power Generation (CPG) concept, where the PV systems is operated in: 1) MPPT mode during I, III, V, and 2) CPG mode during II, IV [8] [17].

Obviously, the CPG operation decreases the energy harvesting by limiting the maximum power production of the PV systems, which leads to undesired energy

losses for the PV systems owner or customer. However, the peak power production usually occurs only in a short period during the day. Considering the monthly or yearly power production from the PV systems, the energy losses from the CPG operation is relatively small, while the DSO gains a significant benefit from preventing an overloading during the peak power generation as it is illustrated in Fig. 4.3 [17].

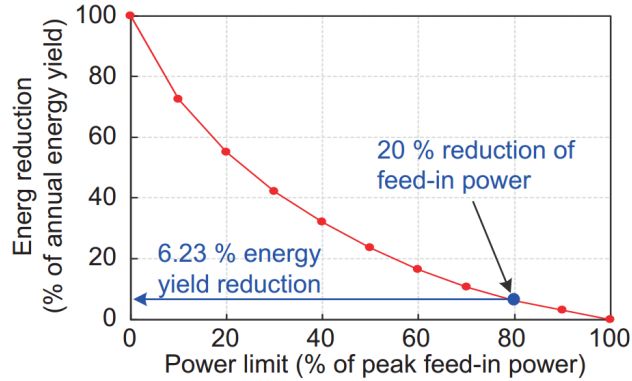


**Figure 4.3:** Energy yield reduction due to limited maximum feed-in power from a 3 kW grid-connected single-phase PV system used in Danish climate [8].

As presented in [17], the CPG control can be done by various approaches:

- Integrating more Energy Storage System (CPG-ESS) – A flexible power control of PV system can be achievable by storing the surplus energy in an energy storage system. One advantage of this method is that the PV output power can be smoothed and also free of power fluctuations. Moreover, the PV system can produce the output power higher than the nominal value by continuously discharging the stored energy. Nevertheless, the energy storage systems increase the cost of the overall system and their lifetime limit should also be taken into account.
- Power Management Control (CPG-PMC) – CPG can also be achievable from the system control level. In this case, several PV systems are controlled by the central control unit. Depending on the output power level at the point of connection, some PV systems are requested to operate in CPG mode, while the others operate in MPPT mode. By doing so, a total power production of an aggregated PV systems can be kept constant. This method requires a communication line between a central control unit and each PV system.
- Modifying MPPT Control (CPG-MPPT) – A third way to realize CPG control is by modifying the MPPT algorithm at an individual PV system level. The power limit, which is chosen as the maximum feed-in power to the grid, is used as a criterion to decide the operating mode between the MPPT and CPG. As long as the instantaneous power extracted from PV arrays is below the

### 4.3. Literature Review of Constant Power Generation

setting power limit, the PV system operates in the MPPT mode. When the power limit is reached, the PV system changes from MPPT to CPG operating mode through the modification of the MPPT algorithm. In this way, the CPG operation is achievable without any need of extra energy storage system or a central control unit, which is a strong benefit of this method.

As it can be seen, both CPG-ESS and CPG-PMC require more investment which might not be suitable for cost-effective PV systems. Hence, only CPG based on modifying MPPT method is taken into consideration in this thesis.

## 4.3 Literature Review of Constant Power Generation

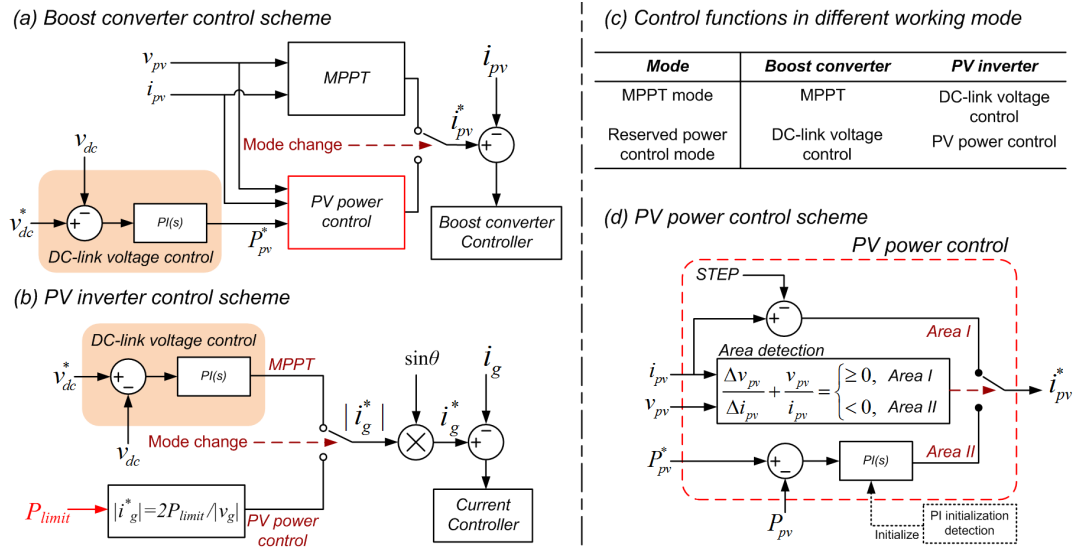


**Figure 4.4:** Control diagrams of the two-stage PV systems in MPPT and reserved power mode [34].

Actually, several publications have recently been discussing on active power control strategy similar to the CPG-MPPT operation. In [52], an absolute power control strategy for single-stage three-phase PV systems was presented. In two-stage grid-connected PV systems, a reserved power control mode was also presented in [34]. According to the control diagrams shown in Fig. 4.4(c), during the normal MPPT operation, the boost converter is controlled by the MPPT controller while the PV inverter is controlled by the DC-link voltage controller. However, when the reserve power control is activated, the active power extraction is controlled by the PV inverter, through the current controller, while the boost converter is now controlling the DC-link voltage. Unlike the power control strategy in [34], where the control of the boost converter and the PV inverter are dependent, an active power generated by PV system can also be limited by controlling only the boost converter side as

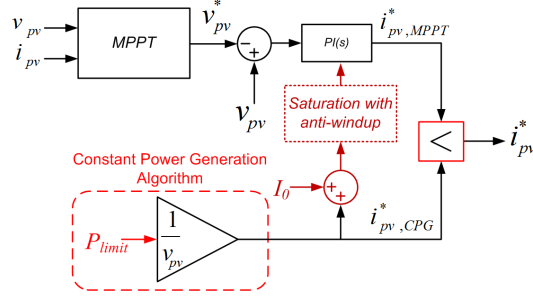


**Figure 4.5:** Control strategy for the MPPT and limited power point tracking, where  $i_{pv}^*$  is the reference PV current [53].

was discussed in [53]. Here two different controllers are employed: 1) MPPT controller, and 2) limiting power controller. The operating mode is decided by using the reference current as a criterion as is shown in Fig. 4.5. During the limiting power operation, the reference PV current  $i_{pv}^*$  is directly calculated by dividing the power limit  $P_{limit}$  with the measured PV voltage  $v_{pv}$ . However, this calculation is accurate only when the PV systems is operating in the constant voltage region in Fig. 2.6.

All the publications mentioned above share a similar idea that the PV power  $P_{pv}$  should be regulated by operating the PV system at the right side of the MPP as is shown in Fig. 4.6. Actually, a stable operation may not be ensured when operating the PV systems in this area. It was pointed out in [34] that the control of the boost converter might fail under the rapid decrease in the irradiance, which makes the operating point of the PV system go to the short-circuit condition. Fig. 4.4(d) presents the proposed solution in [34], where the operating area of the PV system is continuously monitored and the reference current of the boost converter will be forced to decrease, when the short-circuit condition is detected. In fact, the instability during the decrease irradiance condition can be avoided by choosing a proper operating area of the PV system in the CPG operation. More detailed analysis will be discussed in the following section.

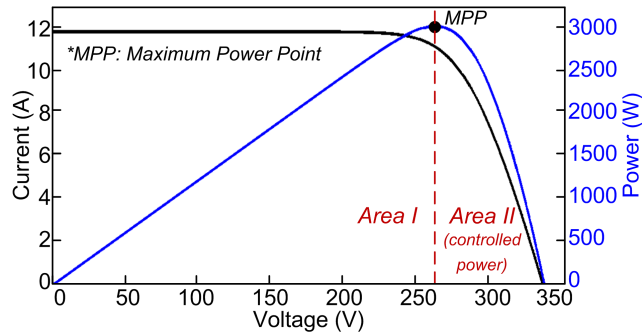


**Figure 4.6:** Power-voltage characteristic curve of the PV arrays and the operating area of the PV system in MPPT and Controlled Power mode [34].

#### 4.4. Analysis of Constant Power Generation Strategies

Another drawback of active power control strategies presented in [34] and [53] is due to the use of a condition switch to change the operating mode between the MPPT and CPG (or reserved, limiting power control). Only one of these two controllers (MPPT or CPG) is activated during the operation leading to a difficulty when a PI controller is implemented to do the control. It should be mentioned that the integral action of the PI controller relies on an accumulated error in the former sampling periods. A method to properly initialize the PI controller, when activating the CPG controller is required, leading to a more complicated control structure.

Although several approaches have been presented, improvements are still required in order to achieve a high performance and robust CPG controller. Stability of the CPG controller is another important issue, which has not yet been fully investigated. Besides, the dynamic performances should also be examined under various irradiance profiles other than just a step-change like what has been done in [34] and [52].

### 4.4 Analysis of Constant Power Generation Strategies

Although the CPG by modifying the MPPT algorithm offers a cost-effective solution to achieve the CPG operation, the design of the CPG algorithm could be a challenge. To avoid an abrupt transition between the two operating modes, it is preferable to use only one controller for both MPPT and CPG operations, and to avoid the use of the switch condition. Consequently, the controller needs to be designed with two main objectives: 1) maximizing the extracted power from the PV arrays during the MPPT operation and 2) limiting the extracted power from the PV arrays during the CPG operation. In the MPPT operating mode, when  $P_{pv} \leq P_{limit}$ , it is obvious that the controller should track the MPP similar to the typical MPPT controller as mentioned in Chapter 3. Likewise, in the CPG operating mode, the controller should operate in the same way by tracking the so-called Constant Power Point (**CPP**) which is the operating point that meets the  $P_{pv} = P_{limit}$  condition. Thus, it is vital to discuss the possible **CPPs** in the CPG operation by analyzing the characteristic of the PV arrays.

Let us consider the possible operating areas of the PV system in the CPG operation. From the P-V and I-V characteristic curves of the PV arrays as shown in Fig. 4.7, there are two possible operating points – **CPP-a** and **CPP-b**, for the CPG operating mode at a certain power level (i.e.,  $P_{limit}$ ). In two-stage grid-connected PV systems, theoretically, there is no restriction in the operating range of the PV voltage  $v_{pv}$ , since the DC-link voltage is stepped up by the boost converter and regulated by the DC-link controller of the PV inverter. This is not the case in the single-stage grid-connected PV systems where the PV voltage  $v_{pv}$  is directly corresponding to the DC-link voltage and has to be in a certain limit in order to ensure the power delivery of the PV inverter [54]. By operating the PV systems at **CPP-b**, the  $i_{pv}$  is lower than that of **CPP-a**, resulting in lower conduction losses. However, the slope of the P-V curve is much higher on the right side of the MPP. This means that it is more difficult to control the PV system at **CPP-b**, since a small change in the

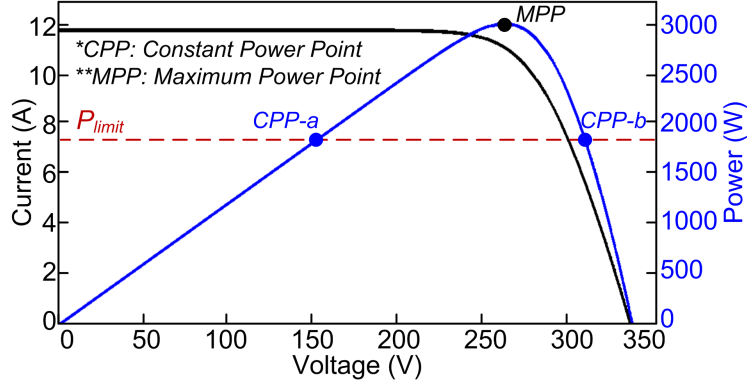


**Figure 4.7:** PV characteristic curves, where two Constant Power Points (*CPP*) for a certain  $P_{limit}$  in CPG operation are located.

PV voltage  $v_{pv}$  can result in a large variation in the output power  $P_{pv}$ . Moreover, the operating point of the PV system may go into the open-circuit condition under a fast decreasing irradiance condition, e.g., when a cloud is passing. This problem can be explained from the P-V curve shown in Fig. 4.8. It is assumed that the irradiance suddenly drops from  $1000 \text{ W/m}^2$  to  $200 \text{ W/m}^2$ . It can be noticed that the open-circuit voltage of the PV arrays reduces from  $V_{OC}$  to  $V'_{OC}$ , due to the decreased irradiance. If the PV system was operating (when the irradiance is  $1000 \text{ W/m}^2$ ) in the area above  $V'_{OC}$ , which are highlighted as the red area in Fig. 4.8, the PV system will go directly to the open-circuit condition at the instance that the irradiance level suddenly drops to  $200 \text{ W/m}^2$ . Therefore, it can be pointed out that there is a risk of instability, when the  $P_{pv}$  is regulated at the *CPP-b*, compared to *CPP-a* or the normal MPPT operation.

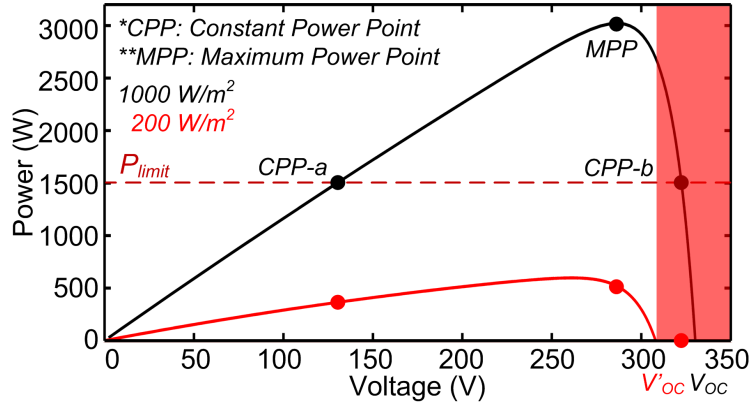


**Figure 4.8:** Instability due to the CPG operation at the *CPP-b*, where the red highlighted area refers to an unstable operation during a fast decrease of the irradiance level from  $1000 \text{ W/m}^2$  to  $200 \text{ W/m}^2$ .

#### 4.4. Analysis of Constant Power Generation Strategies

In a steady-state operation, when the irradiance level is constant, the CPG algorithms should keep the PV systems to operate at one of the **CPPs** with a minimum of oscillations. However, under a changing irradiance condition, the dynamic performance of CPG algorithms should be able to ensure a stable CPG operation regardless of the irradiance conditions. Moreover, it is observed in [17] that a change of the operating mode between CPG and MPPT may introduce instability. Based on these requirements, the demands for designing the CPG controller are:

- A smooth transition between CPG and MPPT operation.
- CPG operation should be ensured regardless of the irradiance conditions.
- Power losses during the steady-state CPG operation should be minimized.

Therefore, three CPG strategies have been investigated in this project: 1) CPG based on the power control, 2) CPG based on the current limit, and 3) CPG based on the P&O algorithm.

##### 4.4.1 CPG based on the Power Control (P-CPG)

The control structure of the boost stage in Fig. 3.5 makes it possible to directly control the input power of the boost converter (i.e., the PV output power). Actually, the idea of regulating the active power of the PV system through the power control of the boost converter was presented in [54], where the main objective of the power control method is to match the power production of the PV system with the power consumption of the household. To apply this idea with a CPG method, an input power reference from the MPPT controller  $P_{pv}^*$  is limited by using a saturation block as it is shown in Fig. 4.9. When the  $P_{pv}^*$  reaches the value of the  $P_{limit}$ , the reference of the input power of the boost converter is kept at the  $P_{limit}$  value and the PV system is entering into the CPG operating mode. Due to the fact that this control structure is based on the power-based MPPT controller, the PV system will only be able to operate at the **CPP-b** in the CPG operation, as discussed in Section 3.3.

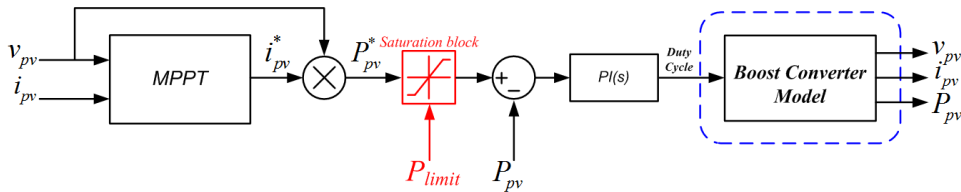


**Figure 4.9:** Control structure of the CPG based on the power control (P-CPG).

In this approach, the PV power reference  $P_{pv}^*$  will never go above  $P_{limit}$  resulting in a fast dynamic performance of the CPG controller when the operating mode changes from MPPT to CPG. This is a strong point of the P-CPG method, where the extracted power of the PV arrays is directly controlled.

#### 4.4.2 CPG based on the Current Limit (I-CPG)

This CPG method is based on the fact that the PV voltage  $v_{pv}$  is almost constant at the right side of the MPP. The control of the PV current  $i_{pv}$  in this region can effectively control the PV output power  $P_{pv}$ . Thus, a CPG operation can be realized by limiting the PV current  $i_{pv}$  according to  $P_{limit}$  as shown in Fig. 4.10. The  $P_{limit}$  level corresponds to the rectangular area under the *CPP-b*.

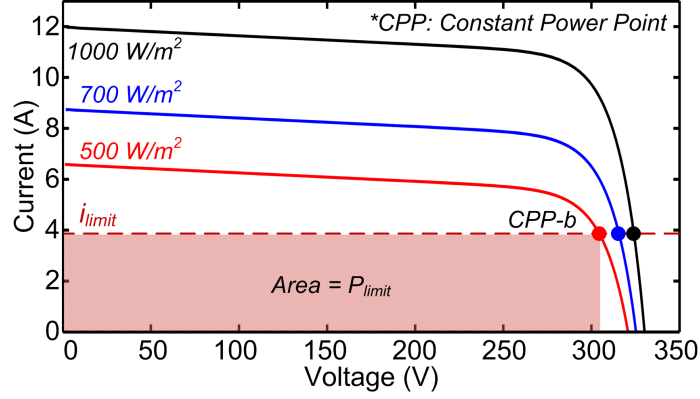


**Figure 4.10:** Operation principle of the CPG based on the current limit (I-CPG).

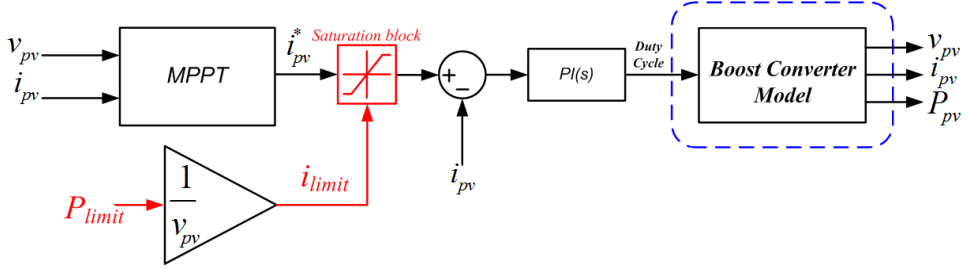


**Figure 4.11:** Control structure of the CPG based on the current limit (I-CPG).

It can be observed that the value of  $i_{limit}$  should be adapted according to the irradiance level in order to achieve the same  $P_{limit}$  under different irradiance levels (e.g. a lower value of  $i_{limit}$  should be used when the irradiance level increases). However, this online  $i_{limit}$  calculation is difficult to be implemented since it requires both the I-V characteristic of the PV array and the irradiance level measurement, which may result in a complicated control structure. An alternative solution, which offers a good approximation, was presented in [53]. By assuming that the PV voltage  $v_{pv}$  is almost constant,  $i_{limit}$  can be calculated as in Eq. (4.2).

$$i_{limit} = \frac{P_{limit}}{v_{pv}} \quad (4.2)$$

According to the CPG concept in Eq. (4.1), it is essential to ensure that the performance during the MPPT operation will not be diminished by the current limit

#### 4.4. Analysis of Constant Power Generation Strategies

when  $P_{pv} \leq P_{limit}$ . During the MPPT operation, the relationship between  $P_{pv}$  and  $P_{limit}$  can be obtained as

$$P_{pv} \leq P_{limit}$$

Thus,

$$\begin{aligned} \frac{P_{pv}}{v_{pv}} &\leq \frac{P_{limit}}{v_{pv}} \\ i_{pv} &\leq i_{limit} \end{aligned} \quad (4.3)$$

From the relationship between the PV current  $i_{pv}$  and  $i_{limit}$  during the MPPT operation expressed in Eq. (4.3), it can be concluded that the value of  $i_{limit}$  will not affect the MPPT operation as long as  $P_{pv} \leq P_{limit}$ .

The control structure of the I-CPG algorithm is shown in Fig. 4.11. This CPG algorithm is very easy to be implemented since only one current limiting block is needed. Nevertheless, this method is an approximation and the accuracy of the control decreases when the irradiance varies in a wide range.

#### 4.4.3 CPG based on the P&O Algorithm (P&O-CPG)

The CPG control can also be realized by using the P&O concept as introduced in [52]. When  $P_{pv} > P_{limit}$ , the  $v_{pv}$  is continued to be perturbed to either the left side of the MPP (**CPP-a**) or the right side of the MPP (**CPP-b**) as shown in Fig. 4.12. After a number of iterations, the operating point will reach and oscillate around the **CPP**. This oscillation occurs due to the fact that the PV system switches the operating modes between CPG and MPPT at the  $P_{limit}$ , which is a boundary of the operating mode. The control diagram and the flow chart of the P&O-CPG algorithm are given in Figs. 4.13 and 4.14, respectively.

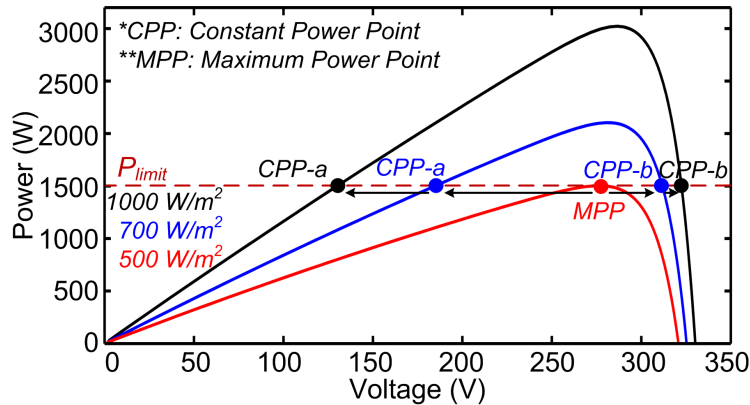


**Figure 4.12:** Operation principle of the CPG based on the perturb and observe algorithm (P&O-CPG).

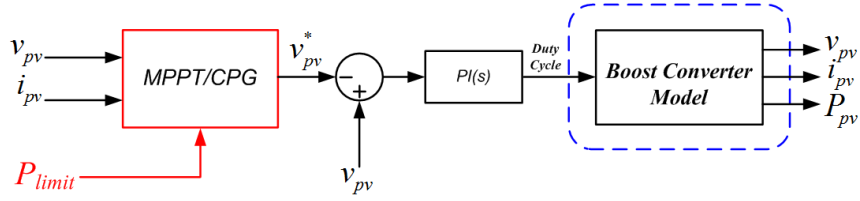


**Figure 4.13:** Control structure of the CPG based on the perturb and observe algorithm (P&O-CPG).

One advantage of the P&O-CPG algorithm is that it is possible to operate the PV system at both **CPP-a** and **CPP-b** by choosing a proper perturbation direction of the algorithm. Actually, both the dynamic and steady-state performances of the CPG controller are different when the PV system operates at different **CPPs**. Thus, the performance of the CPG operation at different **CPPs** should be compared and analyzed in order to design a proper CPG controller.

Considering the P-V curve in Fig. 4.12, the  $P_{limit}$  e.g. is chosen as  $1500\text{ W}$  which corresponds to the maximum output power of the PV arrays, when the irradiance level is  $500\text{ W/m}^2$ . When the irradiance level increases from  $500\text{ W/m}^2$  to  $1000\text{ W/m}^2$ , the PV system is entering to the CPG operation and, therefore, the P&O-CPG algorithm will perturb the voltage  $v_{pv}$  toward the **CPP** in order to achieve  $P_{pv} = P_{limit}$  condition. Due to the asymmetry of the P-V curve, the distance between the MPP at irradiance level of  $500\text{ W/m}^2$  and the target **CPP** at irradiance level of  $1000\text{ W/m}^2$  is much shorter at the right side of the MPP, compared to the left side. Consequently, with the same perturbation step size, the CPG controller requires less number of iterations in order to reach the **CPP-b** than that of the **CPP-a**. In other words, the dynamic response of the CPG controller is faster when operating at **CPP-b**. However, when the operating point of the PV system reaches the **CPP**, the power oscillations are much smaller at the **CPP-a** compared to those at the **CPP-b**. This is due to the higher slope of the P-V curve on the right side of the MPP. Besides, the slope is almost constant on the left side of the MPP, while it increases when the operating point is moving further to the right side of the MPP. As a result, the oscillations will become even larger at the low value of  $P_{limit}$ , when operating at **CPP-b**. Therefore, the steady-state performance of the CPG controller is better at the **CPP-a** than that at the **CPP-b**.

In brief, a fast dynamic performance can be achieved by operating the PV system at **CPP-b** while the power oscillations in the steady-state operation are minimized when operating at **CPP-a**. In addition, due to the perturbation behavior, both the dynamic and steady-state performances of the P&O-CPG algorithm rely on the step size of the perturbation. Actually, the influence of the step size is similar to the P&O MPPT algorithm discussed in Section 3.3.1. A large step size will increase the tracking speed but it has to be compromised with large oscillations in the steady state. In fact, the tracking speed can also be increased in the similar way as in P&O MPPT by increasing a sampling rate of the P&O-CPG algorithm.

## 4.5. Performance of the CPG Controllers

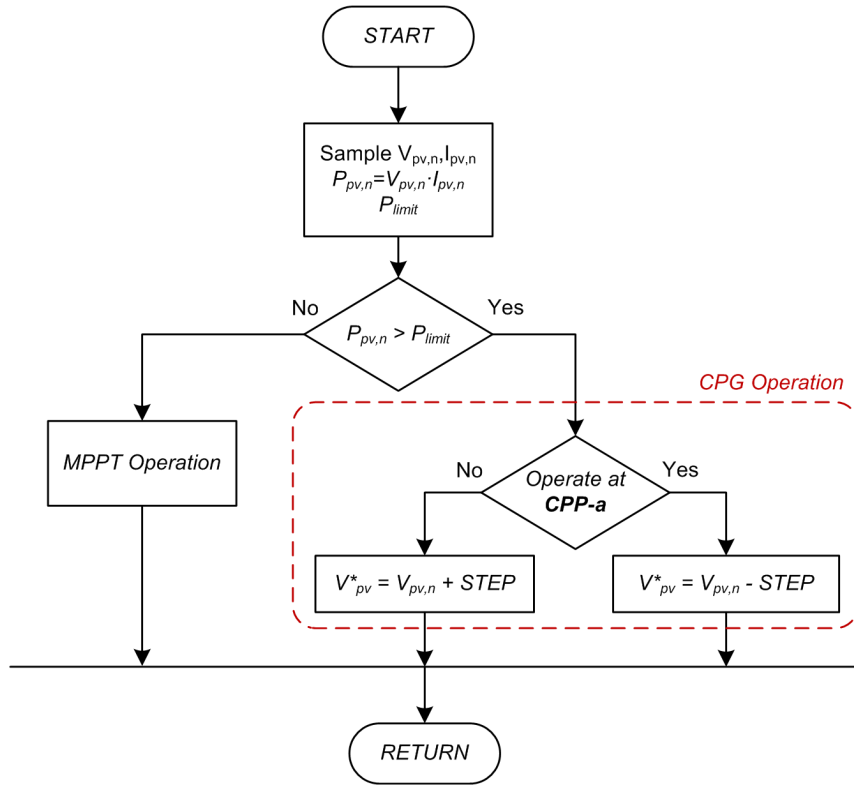


**Figure 4.14:** Flow chart of the CPG based on the perturb and observe algorithm (P&O-CPG).

## 4.5 Performance of the CPG Controllers

So far, three CPG strategies have been presented. In order to verify the feasibility of the control algorithms, simulations and the experiments have been performed. Since all three CPG algorithms are actually modified based on the MPPT controllers (P-CPG: power-based MPPT, I-CPG: current-based MPPT, P&O-CPG: voltage-based MPPT), the CPG controllers are designed with the same control system parameters as given in Tables. 2.4 and 3.1.

The PV system shown in Fig. 2.18 has been tested under various conditions. Moreover, three power limit levels  $P_{limit}$ : 20 %, 50 % and 80 % of the rated power have been chosen in the tests, which correspond to 600, 1500, and 2400 W.

### 4.5.1 Simulation results

In the simulations, two irradiance profiles are used to simulate normal and fast changing irradiance conditions. A slow ramp-changing irradiance profile is used in Fig. 4.15.

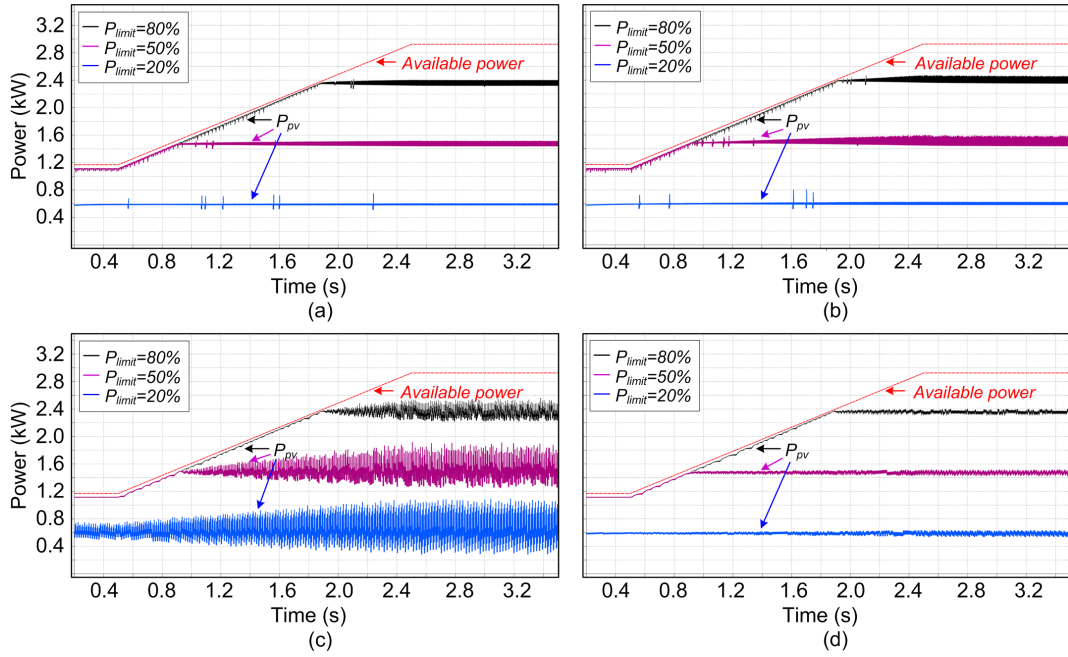


**Figure 4.15:** Simulation results of the CPG based on: (a) the power control (b) the current limit (c) the P&O at the right side of the MPP (d) the P&O at the left side of the MPP under a ramp irradiance condition.

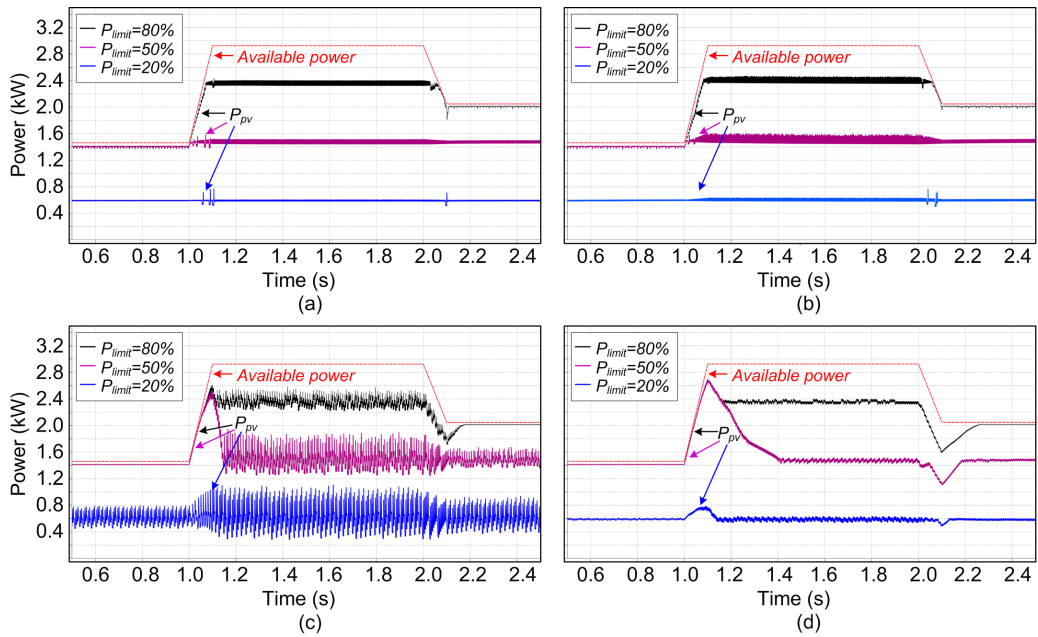


**Figure 4.16:** Simulation results of the CPG based on: (a) the power control (b) the current limit (c) the P&O at the right side of the MPP (d) the P&O at the left side of the MPP under a fast changing irradiance condition.

#### 4.5. Performance of the CPG Controllers

It can be observed in Fig. 4.15 that a smooth transition from MPPT to CPG operation can be achieved for all CPG algorithms. Considering the CPG operation, most of the CPG algorithms can limit the output power of the PV system according to  $P_{pv} = P_{limit}$  condition with a good accuracy. However, the P&O-CPG algorithm has large power oscillations when the PV system operates at the **CPP-b**. Even more, the oscillation amplitude increases at lower power limits.

The CPG algorithms are then tested with a fast-changing irradiance condition as is shown in Fig. 4.16. Under a fast-changing irradiance condition, the dynamic response of the controller is more challenged. A fast dynamic performance during the MPPT to CPG transition is attained, when the P-CPG and I-CPG algorithms are employed. P&O-CPG algorithm has a slower response resulting in an overshoot during the MPPT to CPG transition. According to the results in Figs. 4.16(c) and (d), the controller requires more numbers of iterations in order to achieve CPG operation when the P&O-CPG algorithm chooses to operate at the **CPP-a**. The slow dynamic response of the P&O-CPG algorithm also results in more power losses during the CPG to MPPT transition, e.g. when the irradiance level decreases at  $t = 2$  s.

#### 4.5.2 Experimental results

The CPG algorithms have been implemented on the system shown in Fig. 2.18. The PV simulator has been programmed to test the PV system with the CPG control in terms of: 1) steady-state performance, 2) dynamics, and 3) real irradiance profiles.

##### A. Steady-state performances of the CPG algorithms

A constant irradiance profile is used to examine the feasibility of the CPG algorithms under steady-state conditions. Here, the value of  $P_{limit}$  is varied as 100 % (MPPT operation), 80 %, 50 %, and 20 % of the rated power at  $t = 60, 120, \text{ and } 180$  s, respectively. The results shown in Fig. 4.17 demonstrate the feasibility of the CPG algorithms according to the different values of  $P_{limit}$ . It has also been confirmed that the power oscillations in the P&O-CPG algorithm increases at the low value of  $P_{limit}$  when the PV system operates at the **CPP-b**.

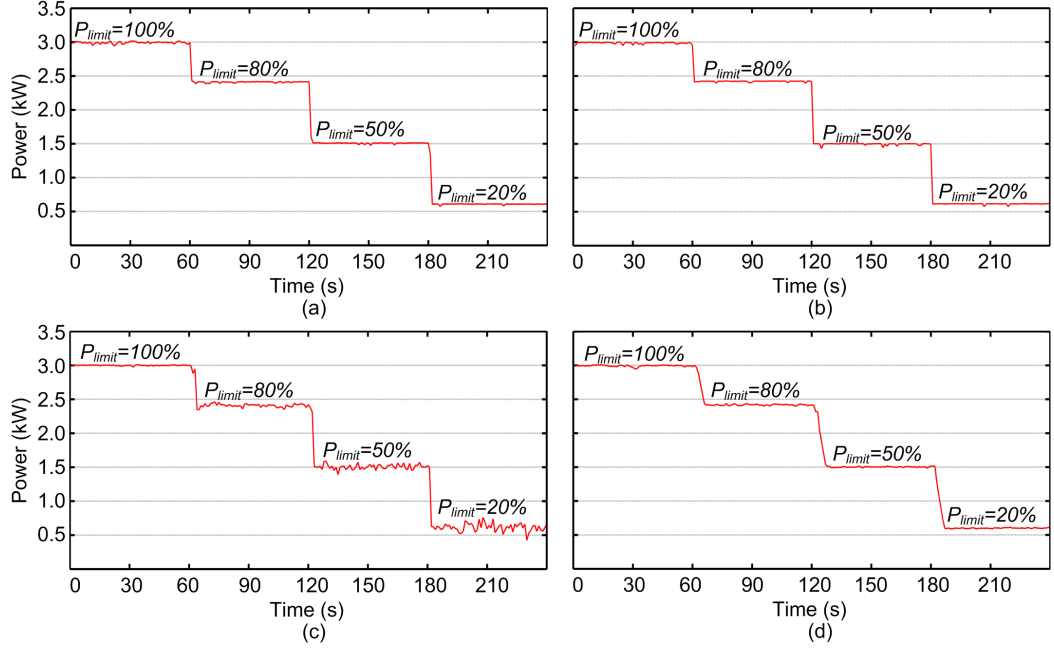


**Figure 4.17:** Experimental results of the CPG based on: (a) the power control (b) the current limit (c) the P&O at the right side of the MPP (d) the P&O at the left side of the MPP under a constant irradiance condition of  $1000 \text{ W/m}^2$ , where  $P_{limit}$  is chosen as 100 %, 80 %, 50 %, and 20 % of the rated power.

## B. Dynamic performances of the CPG algorithms

Two trapezoidal irradiance profiles with different slopes are used to emulate a slow- and fast-changing irradiance conditions. Considering the slow-changing irradiance condition shown in Fig. 4.18, all CPG algorithms have a smooth transition from MPPT to CPG operation and vice versa. One incident to be pointed out is the power losses in the I-CPG algorithm during the CPG to MPPT transition, when  $P_{limit} = 80\%$  and  $50\%$  of the rated power. This is due to the typical poor performance of the current-based MPPT controller under a decreasing irradiance, as discussed in Section 3.3.

The performances of the P-CPG and I-CPG algorithms are resembled when the PV system is tested with the fast-changing irradiance condition as is shown in Fig. 4.19. However, an overshoot occurs during the MPPT to CPG transition when the P&O-CPG algorithm is employed. There are also power losses in the P&O-CPG algorithm during the CPG to MPPT transition. This slow dynamic response is due to the perturbation behavior of the algorithm.

The trajectory of the operating point of the PV system in the P-V curve is also shown in Fig. 4.20, which shows how the operating points of the PV systems are moving. The  $P_{limit}$  is chosen at 80 % of the rated power and the PV system is tested under a slow-changing irradiance condition.

#### 4.5. Performance of the CPG Controllers

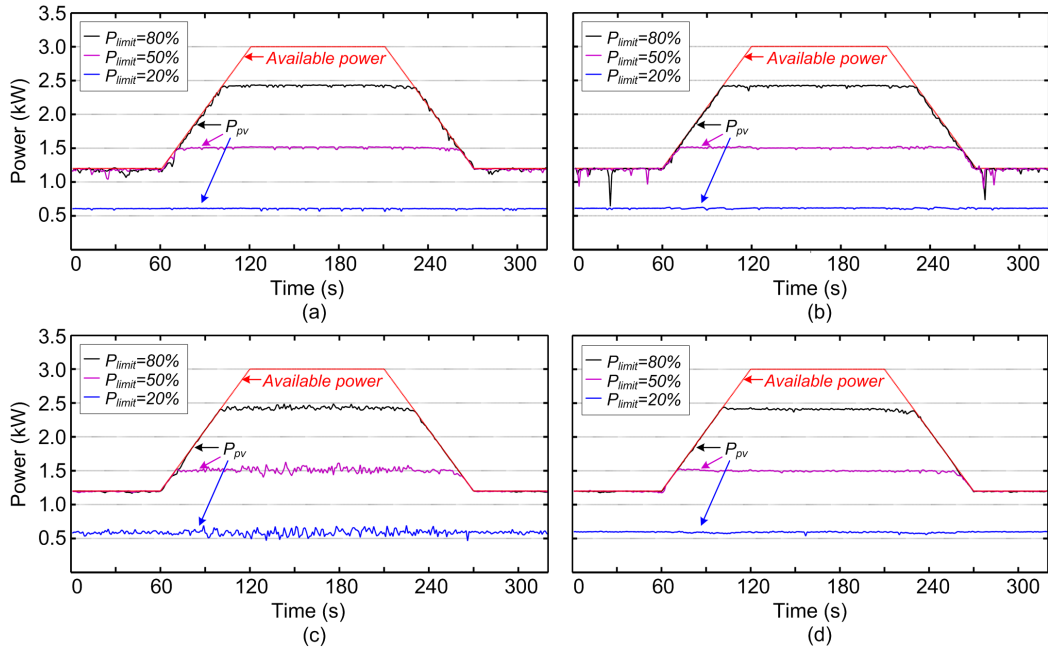


**Figure 4.18:** Experimental results of the CPG based on: (a) the power control (b) the current limit (c) the P&O at the right side of the MPP (d) the P&O at the left side of the MPP under a slow changing irradiance condition.

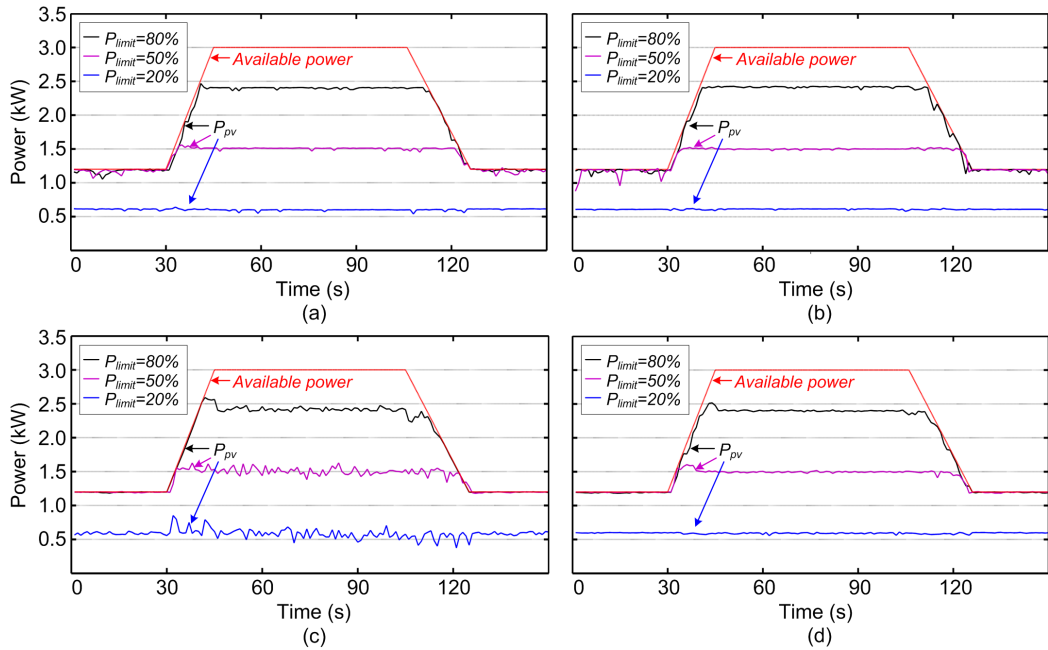


**Figure 4.19:** Experimental results of the CPG based on: (a) the power control (b) the current limit (c) the P&O at the right side of the MPP (d) the P&O at the left side of the MPP under a fast changing irradiance condition.

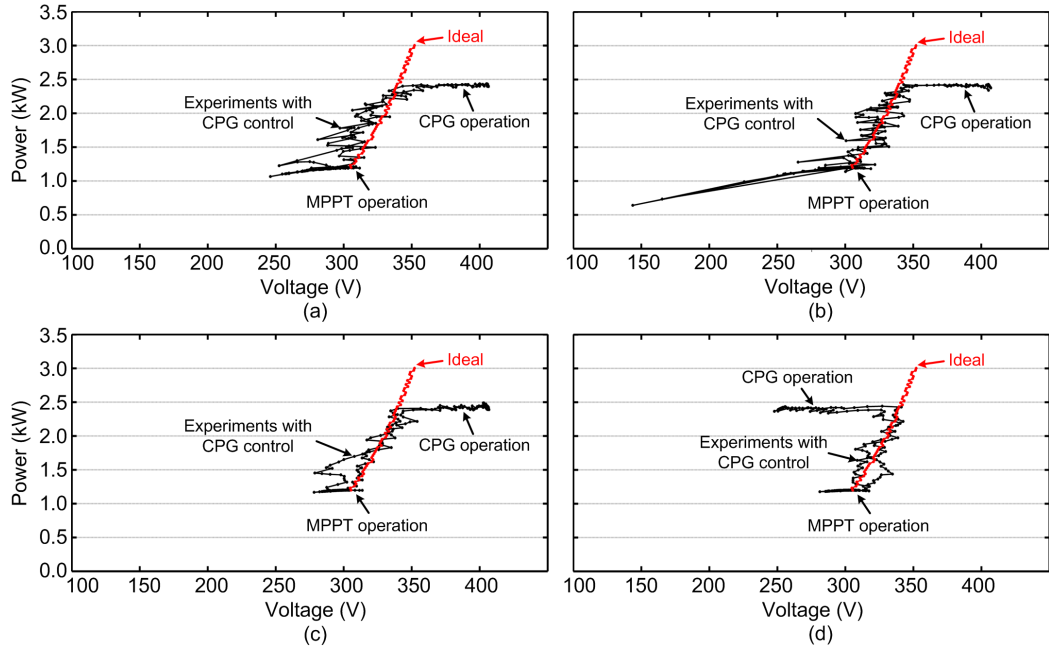


**Figure 4.20:** Trajectory of the operating point of the CPG based on: (a) the power control (b) the current limit (c) the P&O at the right side of the MPP (d) the P&O at the left side of the MPP under a slow changing irradiance condition, when  $P_{limit}$  is 2400 W.

### C. Performances of CPG algorithms under real irradiance profiles

The performances of the CPG algorithm are further investigated under real irradiance profiles. Similar to the experimental tests for the MPPT controller, two irradiance and temperature profiles are recorded from a clear and a cloudy days as shown in Fig. 3.15. The CPG algorithms are tested with two different values of  $P_{limit}$ : 80 % and 50 % of the rated power.

The results of the CPG algorithms under the clear day irradiance condition are shown in Figs. 4.21, 4.22, 4.23, and 4.24. Most of the CPG algorithms are feasible to limit the PV output power  $P_{pv}$  according to the power limit  $P_{limit}$ . Instability only occurs in the case of the I-CPG algorithm under a decreasing irradiance condition.

A cloudy irradiance profile is actually a severe condition for both the MPPT and CPG algorithms. The dynamic performance of the CPG algorithm is very challenged by the large and fast variations in the irradiance level during the test. A stable operation cannot be achieved by the I-CPG algorithm as can be seen in Fig. 4.26. The performance of the P-CPG algorithm is shown in Fig. 4.25. Here, it can be seen that the algorithm has a very fast dynamic response since no overshoot is observed. However, the performance of the P-CPG algorithm is diminished under a decreasing irradiance level, as can be seen from power losses when the irradiance level suddenly drops. Besides, the operating point of the PV system goes to the open-circuit condition due to the fact that the PV system is operating at the *CPP-b* far away from the

#### 4.5. Performance of the CPG Controllers

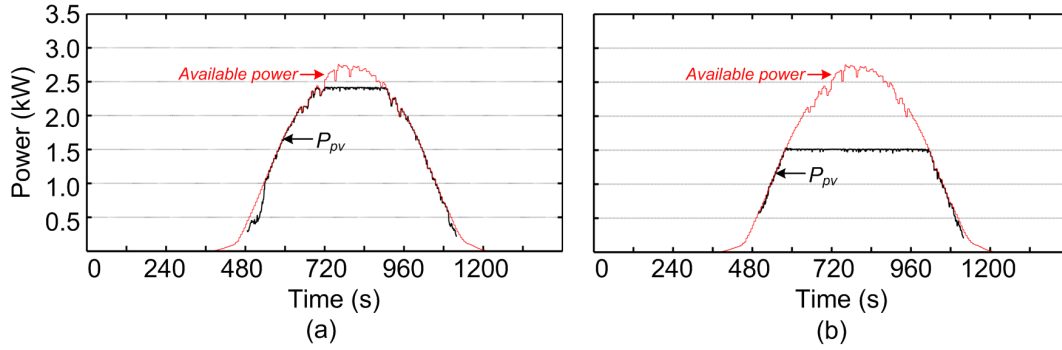


**Figure 4.21:** Experimental results of the CPG based on the power control under a clear day irradiance condition, where  $P_{limit}$  is chosen as: (a) 80 % and (b) 50 % of the rated power.

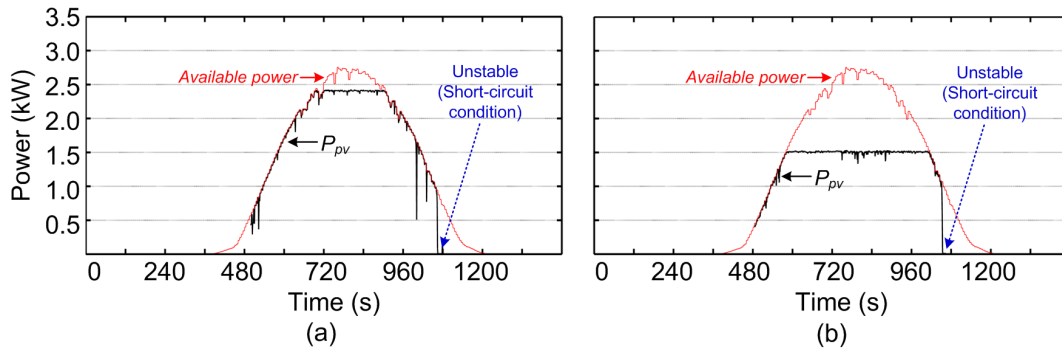


**Figure 4.22:** Experimental results of the CPG based on the current limit under a clear day irradiance condition, where  $P_{limit}$  is chosen as: (a) 80 % and (b) 50 % of the rated power.

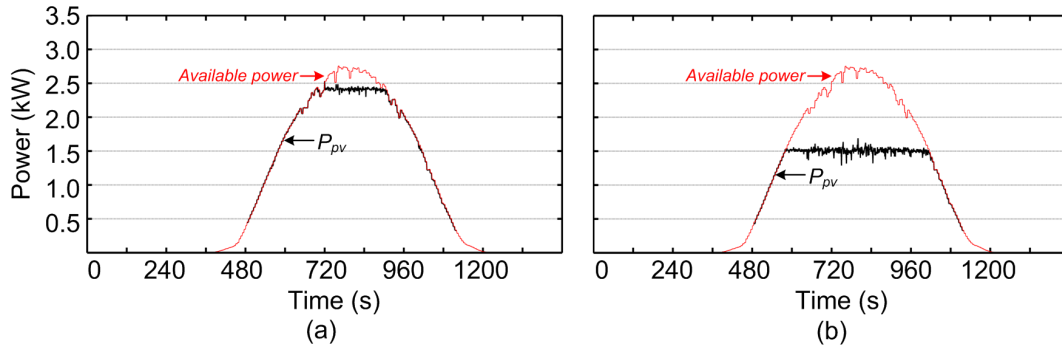


**Figure 4.23:** Experimental results of the CPG based on the perturb and observe at the *CPP-b* under a clear day irradiance condition, where  $P_{limit}$  is chosen as: (a) 80 % and (b) 50 % of the rated power.

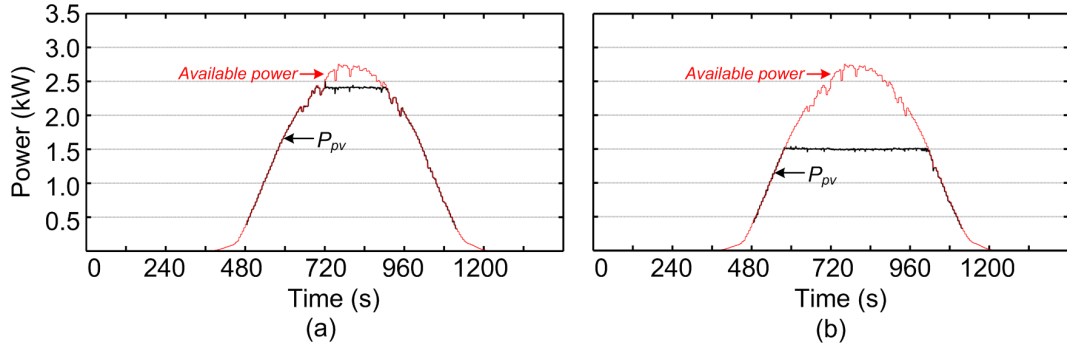


**Figure 4.24:** Experimental results of the CPG based on the perturb and observe at the **CPP-a** under a clear day irradiance condition, where  $P_{limit}$  is chosen as: (a) 80 % and (b) 50 % of the rated power.

MPP when  $P_{limit} = 50\%$  of the rated power, at  $t = 1000$  s in Fig. 4.25(b). Instability under a decreasing irradiance also occurs in the P&O-CPG algorithm when the PV system is operating at the **CPP-b**. In this case, the algorithm is more sensitive to the decrease in the irradiance compared to the P-CPG algorithm. The operating point of the PV system goes to the open-circuit condition when the irradiance suddenly decreases around  $t = 810$  s and  $780$  s when  $P_{limit}$  is 80 % and 50 % of the rated power, respectively.

It can be seen in Fig. 4.28 that the stable operation is only achievable when the P&O-CPG algorithm is chosen to operate at the **CPP-a**. The operating point of the PV system will never go to the open-circuit condition, regardless of the variations in the irradiance and the values of  $P_{limit}$ , which is the advantage of operating the PV system at **CPP-a** in the CPG operation. As a trade-off, the dynamic response of the CPG algorithm is restricted, resulting in several overshoots and power losses in the PV power  $P_{pv}$  when the irradiance suddenly changes.

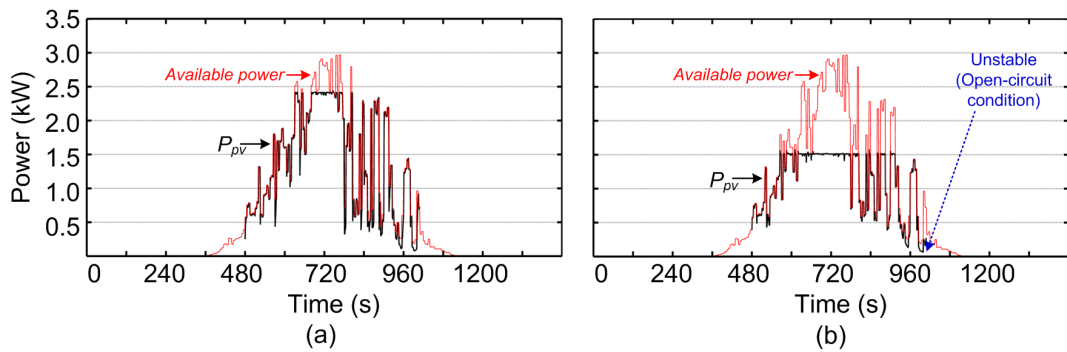


**Figure 4.25:** Experimental results of the CPG based on the power control under a cloudy day irradiance condition, where  $P_{limit}$  is chosen as: (a) 80 % and (b) 50 % of the rated power.

#### 4.5. Performance of the CPG Controllers

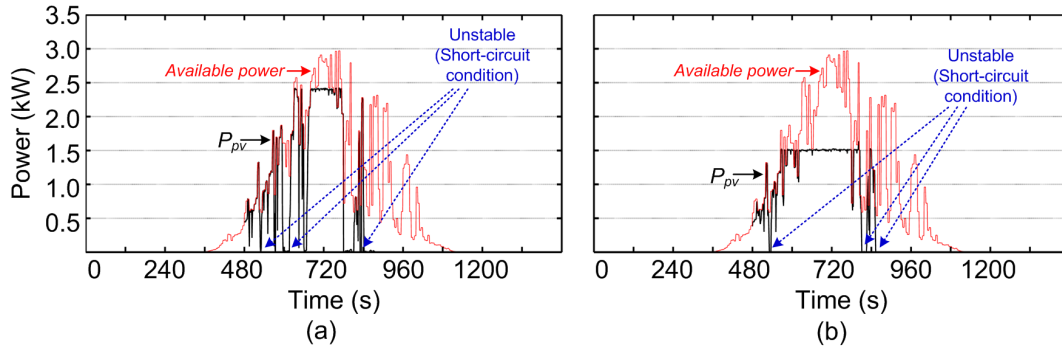


**Figure 4.26:** Experimental results of the CPG based on the current limit under a cloudy day irradiance condition, where  $P_{limit}$  is chosen as: (a) 80 % and (b) 50 % of the rated power.

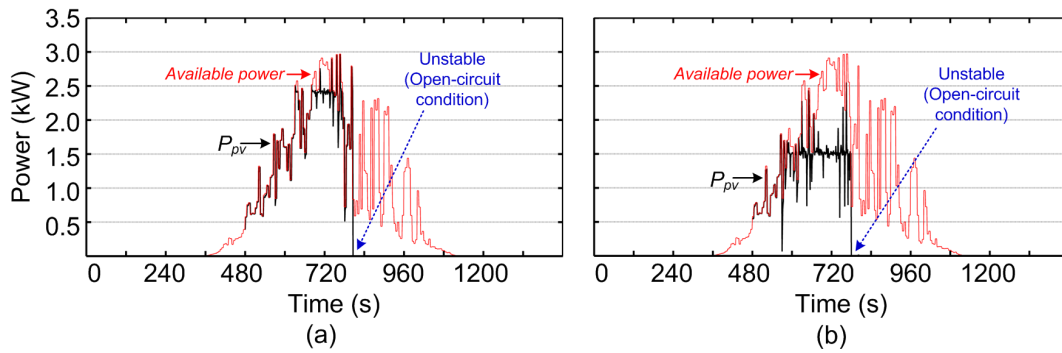


**Figure 4.27:** Experimental results of the CPG based on the perturb and observe at the *CPP-b* under a cloudy day irradiance condition, where  $P_{limit}$  is chosen as: (a) 80 % and (b) 50 % of the rated power.

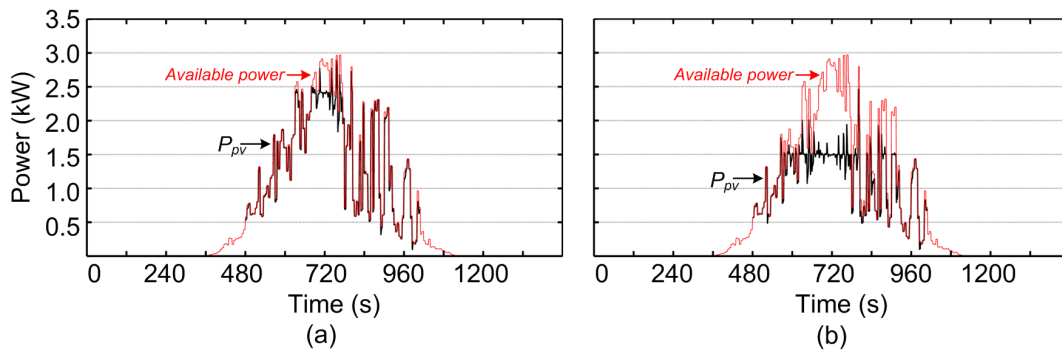


**Figure 4.28:** Experimental results of the CPG based on the perturb and observe at the *CPP-a* under a cloudy day irradiance condition, where  $P_{limit}$  is chosen as: (a) 80 % and (b) 50 % of the rated power.

According to the above results, the performances of the CPG algorithms have been observed under several operating conditions. One analytical way to measure the accuracy of the algorithm is by comparing the measured PV output power  $P_{pv,i}$  with the PV output power in the ideal operation  $P_{pv}$  according to Eq. (4.1). An average tracking error (in percentage) of the algorithm during the test can be calculated as

$$\text{Average tracking error \%} = \frac{\sum_{i=1}^n |P_{pv,i} - P_{pv}|}{\sum_{i=1}^n P_{pv}} \quad (4.4)$$

where  $P_{pv,i}$  is the measured PV output power in each sampling.

Fig. 4.29 shows the average tracking error of CPG algorithms which are calculated from the experimental results in Figs. 4.18, 4.19, 4.21-4.24 and 4.25-4.28 when  $P_{limit} = 80\%$  of the rated power. It can be seen from the average tracking error that the P&O-CPG algorithm has the worst tracking accuracy during the CPG operation, when the operating point is chosen at **CPP-b**. However, the overall tracking error of the P&O-CPG algorithm is less than both the P-CPG and I-CPG algorithms. This is mainly due to an accurate tracking performance during the MPPT operation of the voltage-based MPPT controller employed in the P&O-CPG algorithm. In contrast, the P-CPG algorithm has a very small tracking error during the CPG operation but an error during the MPPT operation is significant.

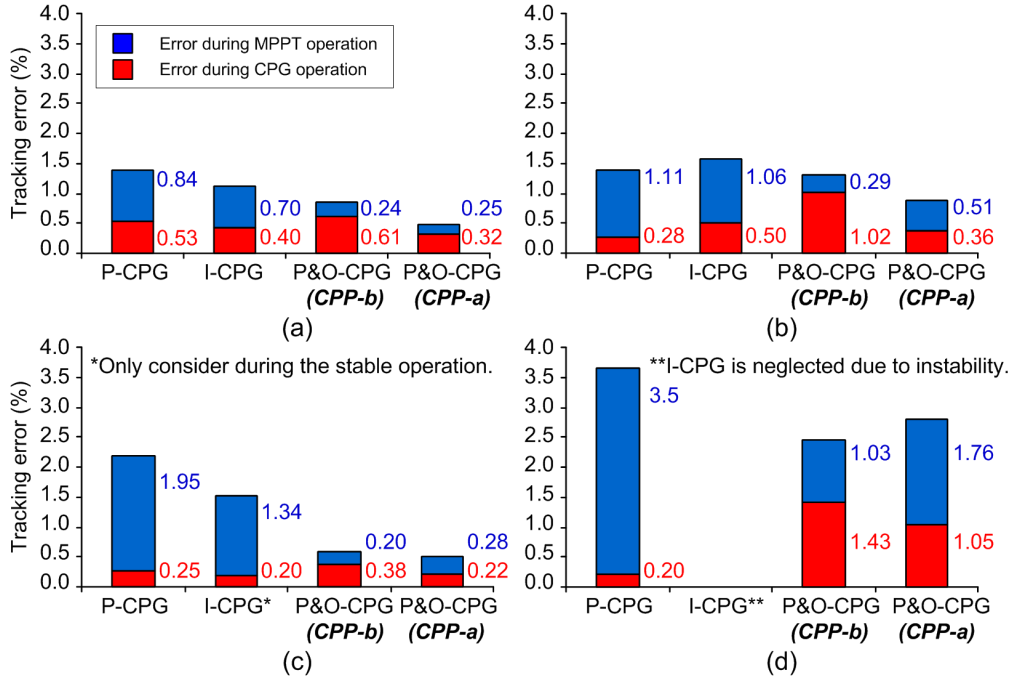


**Figure 4.29:** Average tracking error of the CPG algorithms under: (a) slow changing (b) fast changing (c) clear day and (d) cloudy day irradiance conditions.

## 4.6 Benchmarking of CPG methods

The simulation and experimental results confirm the feasibility of the three CPG algorithms presented in this project. The performances of the CPG algorithm have been investigated under several tested conditions. It is observed that the performance in the CPG operation of the PV system differs depending on the CPG algorithm in several aspects. Thus, it is also necessary to compare the performances of each algorithm in order to find the most suitable CPG algorithm to realize the CPG operation practically. A benchmarking of the CPG algorithms is then carried out based on several performance aspects which are:

### Dynamic responses

The dynamic responses are observed when an operating mode changes from MPPT to CPG and vice versa. The P-CPG and I-CPG algorithms have a very fast response with no overshoot during the MPPT to CPG transition. This is regardless of the irradiance profiles as it was examined with several different irradiance conditions in Section 4.5. An overshoot during MPPT to CPG transition occurs in the P&O-CPG algorithm. The overshoot amplitude gets larger when the P&O-CPG algorithm is chosen to operate the PV system at **CPP-a**.

When the operating mode changes from CPG to MPPT (i.e., the irradiance is decreasing), several CPG algorithms are suffered under a fast-decreasing in the irradiance level. The I-CPG algorithm, which relies on the current-based MPPT controller, has significant power losses and operating point tends to go to the short-circuit condition during the sudden decrease in the irradiance. The power losses in the P&O algorithm are not related to the MPPT controller but a slow response of the algorithm is observed due to the perturbation behavior.

### Steady-state responses

Under a steady-state CPG condition, P-CPG and I-CPG algorithms can track the CPP almost without significant oscillations in contrast to the case when the P&O-CPG algorithm is adopted. In fact, a large oscillation in  $P_{pv}$  only occurs when the operating point of the P&O-CPG algorithm is chosen at **CPP-b**, especially, at the low value of  $P_{limit}$ . This is actually in accordance with the analysis in Section 4.4.

### Stability

Stability is a very important aspect when comparing the CPG algorithms. It is desirable for the PV system to achieve a stable operation under both CPG and MPPT operating modes, despite of the environmental conditions. Nevertheless, instability can occur during a fast decreasing irradiance, as was observed in the simulation and experimental results.

Actually, the stability issues can be separated into two main reasons: 1) instability due to the MPPT controller, and 2) instability due to the CPG algorithm. Regarding

the MPPT controller, it was discussed in Section 3.3 that the current-based MPPT controller can introduce instability. If this incident occurs, the operating point of the PV system will go to the short-circuit condition, and the PV system will not be able to deliver power to the AC grid. This can be observed from the result of the I-CPG algorithm in Figs. 4.22(a) and (b). Another occurrence of the instability is due to the operating region of the CPG algorithm in the CPG operation. It was discussed in Section 4.4 that the operating point of the PV system has a chance to go into the open-circuit condition under a fast-decreasing irradiance condition, if the CPG algorithm chooses to operate at the **CPP-b**. This explains the instability in the P-CPG and P&O-CPG algorithms in Figs. 4.25 and 4.27.

To achieve a stable operation regardless of the irradiance conditions, the operating point of the PV system in the CPG operation should be chosen at the **CPP-a**. By operating the PV system at the **CPP-a**, the operating point will never go to the open-circuit condition due to the characteristic of the P-V curve. Moreover, instability due to the current-based MPPT controller can be avoided by using a voltage-based MPPT controller instead. Thus, among all CPG algorithms, a stable operation of the PV system can be ensured only if the P&O-CPG algorithm chooses to operate at the **CPP-a**.

### Possible operating regions

As it is illustrated in Fig. 4.7, there are two possible operating points (**CPPs**) that the PV system can operate to limit  $P_{pv}$  to a certain  $P_{limit}$ . However, not every CPG algorithms are capable of operating at both two **CPPs**. According to its assumption, the I-CPG algorithm can only operate at the region where the PV voltage  $v_{pv}$  is almost constant, at the right side of the MPP. A similar behavior is also observed in the power-based MPPT controller which is employed in the P-CPG algorithm. This implies that the PV system can only operate at **CPP-b** when the I-CPG or P-CPG algorithm is employed. Unlike the above two algorithms, the P&O-CPG is capable of operating the PV system at both **CPP-a** and **CPP-b**. This makes the P&O-CPG algorithm more flexible in terms of the operating region of the PV system in the CPG operation.

### Complexity

From the control structures presented in Section 4.4, the I-CPG algorithm has the simplest control structure, where only one additional current limiter is required. The calculation of  $i_{limit}$  is also simple by dividing the  $P_{limit}$  with the measured  $v_{pv}$ . The control structure of the P-CPG algorithm is more complicated, basically due to the power-based MPPT controller. In the case of the P&O-CPG algorithm, the modification needs to be done at the MPPT algorithm level as can be seen from the flow chart presented in Fig. 4.14. This makes the design of a P&O-CPG controller more complicated than the other two CPG algorithms.

## 4.7. Summary

Table 4.1 further summarizes the comparisons in terms of dynamic responses, steady-state performance, stability, and complexity.

**Table 4.1:** Benchmarking of Constant Power Generation algorithms

CPG based on:	Dynamic reponses		Steady-state reponses	Stability	Complexity
	MPPT $\rightarrow$ CPG	CPG $\rightarrow$ MPPT			
Power control	++	+	++	-	-
Current limit	+	--	+	--	++
Perturb and Observe ( <i>CPP-a</i> )	--	-	++	++	-
Perturb and Observe ( <i>CPP-b</i> )	-	-	--	-	-

Note: the more +, the better stability and less complexity.

## 4.7 Summary

Due to the intermittent power generation of the PV system, the power injected to the grid is fluctuated. The current requirement of the MPPT operation can introduce an overloading in the distribution system in a high penetration level of the grid-connected PV systems. One cost-effective solution to solve this problem is by modifying the MPPT algorithm at the PV inverter level to be able to limit the maximum feed-in power of the PV systems to a certain level. This power control strategy is referred to as a constant power generation (CPG).

In this chapter, the concept of the CPG operation is addressed. Some previous works related to the CPG algorithm have been discussed. The two main issues which can be improved are the stability of the CPG algorithm and the initialization of the controller during the change in the operating mode. According to the discussions, three selected CPG algorithms have been proposed: 1) P-CPG, 2) I-CPG, and 3) P&O-CPG. The concepts behind each CPG algorithms are discussed and the performances of the algorithms are investigated under several test conditions in this chapter.

In general, the dynamic performance of the CPG algorithm is challenged under a fast changing irradiance condition. During a fast decreasing irradiance condition, which is considered as the worst case scenario, instability can occur when the PV system operates at the *CPP-b*. This incidence has been witnessed in the experimental tests under a cloudy condition. Among all CPG algorithms, only the P&O-CPG algorithm, when the PV system operates at the *CPP-a*, can ensure a stable operation while the dynamic performance is limited. Thus, it is considered as the most suitable approach to realize the CPG operation practically.

## Chapter 5

# Design for High Performances P&O CPG Algorithm

In this chapter, the focus is on the design for high performances P&O-CPG algorithm. The problem regarding the dynamic performance of the P&O-CPG algorithm is discussed and analyzed. Solutions to minimize an overshoot during the MPPT to CPG transition and power losses during the CPG to MPPT transition are examined. Then, a design guideline to improve the dynamic performance of the P&O-CPG algorithm is provided.

### 5.1 Issues of the P&O CPG Method

Among the constant power generation algorithms, the CPG based on P&O algorithm is proven to have the most robust algorithm, when the operating point is chosen at **CPP-a** (i.e., at the left side of the MPP). The instability due to the decreased irradiance, which results in an open-circuit condition, can be avoided by operating the PV system at the left side of the MPP. This algorithm also employs a voltage-based MPPT controller, which has a stable and accurate tracking performance. Based on these advantages, the P&O-CPG algorithm, when the operating point is chosen at **CPP-a**, is considered to be the most suitable candidate to realize the CPG controller practically. From now on, the P&O-CPG algorithm will be regarded as the operating point is chosen at **CPP-a**, and will be referred to as the conventional P&O-CPG algorithm.

Although the conventional P&O-CPG algorithm offers a terrific steady-state performance, the dynamic performance of this CPG algorithm is not very satisfied, especially, under a fast changing irradiance condition, as was observed in the simulation and experimental results in the previous chapter. Specifically, an overshoot in the  $P_{pv}$  occurs during a fast increasing irradiance while power losses are observed during a fast decreasing irradiance. An example is shown in Fig. 5.1 where the algorithm is tested under a cloudy irradiance condition. As can be seen, the CPG condition is violated, when the irradiance level suddenly increases, resulting in an overshoot

## 5.1. Issues of the P&O CPG Method

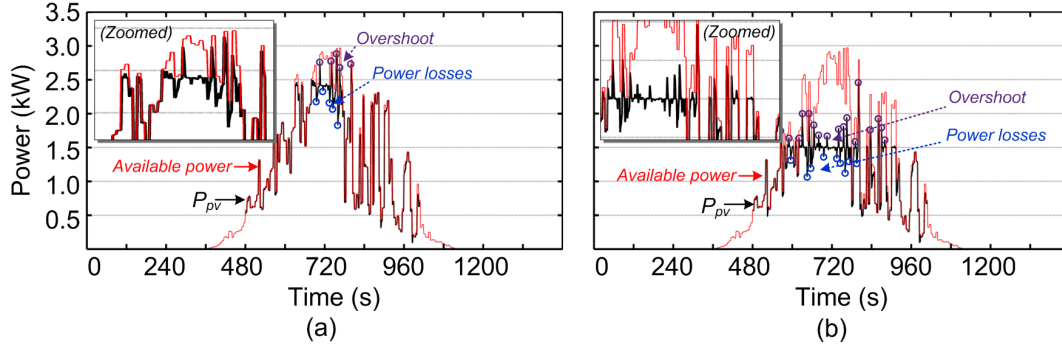


**Figure 5.1:** Experimental results of the CPG based on the perturb and observe algorithm (P&O-CPG) under a cloudy day irradiance condition, where the operating point of the PV system is chosen at the *CPP-a*.

of the PV power  $P_{pv}$  as highlighted in purple circles. Moreover, a constant power production cannot be maintained during a fast decreasing irradiance although the available power is still higher than the  $P_{limit}$  as it is highlighted in blue circles. This slow dynamic performance is due to the perturbation behavior of the algorithm. In order to achieve a satisfied performance under both dynamic and steady-state performances, this chapter is devoted to find a solution to improve the performance of the P&O-CPG algorithm.

### 5.1.1 Dynamic Behavior of the Conventional P&O-CPG Algorithm

In order to find a suitable solution to enhance the dynamic performance of the P&O-CPG algorithm, it is necessary to investigate the dynamic behavior of the conventional P&O-CPG algorithm in details. Let us assume a sudden change in the irradiance level from  $500 \text{ W/m}^2$  to  $1000 \text{ W/m}^2$  and vice versa. Considering the overshoot during the MPPT to CPG transition, the trajectory of the operating point during the MPPT to CPG transition is shown in Fig. 5.2(a). When the irradiance suddenly changes from  $500 \text{ W/m}^2$  to  $1000 \text{ W/m}^2$ , the PV voltage reference  $v_{pv}^*$  is not yet changed since it will be updated in the next iteration (e.g., next 100 ms in the case of 10 Hz updating frequency of the P&O-CPG algorithm). Therefore, the PV system is still operating at the same PV voltage  $v_{pv}$  while the P-V characteristic curve is now different due to the increased irradiance level. As a result, the PV power  $P_{pv}$  is basically lifted by the change in the irradiance as can be seen from the black arrow trajectory in Fig. 5.2(a). After one sampling period, the P&O-CPG algorithm will be able to detect that  $P_{pv} > P_{limit}$ . Hence, the PV system is entering into the CPG operation and the operating point is forced, through the P&O-CPG algorithm, to move towards the *CPP-a*.

Now let us assume that the PV system is operating in the CPG operation at the *CPP-a*, when the irradiance level is  $1000 \text{ W/m}^2$ . The irradiance level then suddenly decreases to  $500 \text{ W/m}^2$  as is shown in Fig. 5.2(b). Again, it will take one

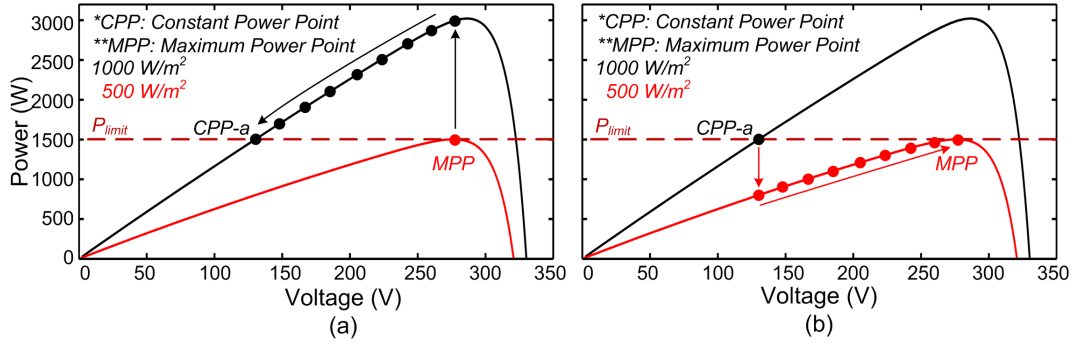


**Figure 5.2:** (a) Overshoot during MPPT to CPG transition when the irradiance level suddenly increases and (b) Power losses during the CPG to MPPT transition when the irradiance level suddenly drops.

iteration before the algorithm can detect that the operating mode should be changed to MPPT operation since  $P_{pv} \leq P_{limit}$ . Thus, at the first instance of the decrease in the irradiance level, the PV system will still operate at the same voltage  $v_{pv}^*$ . As a consequence, the PV power  $P_{pv}$  will suddenly drop according to the change in the P-V characteristic curve. This is shown by the red arrow trajectory in Fig. 5.2(b). After a number of iterations, the operating point of the PV system will be moved towards the MPP according to the normal MPPT operation.

According to the above discussions, the dynamic performances of the P&O-CPG algorithm during the operating transition have been explained in detail. Theoretically, the overshoot and power losses due to the sudden change in the irradiance level cannot be fully eliminated, since the controller will have to wait until the next sampling period to take an action. However, these undesirable occurrences can be minimized by increasing the tracking speed of the algorithm during the change in the operating mode. This will result in less iterations in order to achieve MPPT to CPG transition and vice versa. In order to do so, the design considerations should be taken into account and then the P&O-CPG algorithm can be modified accordingly.

## 5.2 Design for High Performance P&O CPG Method

To have a proper design guideline, it is very important to discuss the influence of the operating conditions, i.e., the speed of the change in the irradiance level, on the overshoot and power losses of the P&O-CPG algorithm. As was pointed out, the fast changing in the irradiance condition is the main cause of the poor dynamic performance of the P&O-CPG algorithm. In fact, the severity of the overshoot and the power losses increases as the changing speed of the irradiance increases. This circumstance can be illustrated by comparing the overshoot and power losses of the P&O-CPG algorithm under different changing speeds in the irradiance level. Fig. 5.3 shows the dynamic behavior of the P&O-CPG algorithm under a fast (from 500 W/m² to 1000 W/m²) and slow (from 500 W/m² to 700 W/m²) changing irradiance

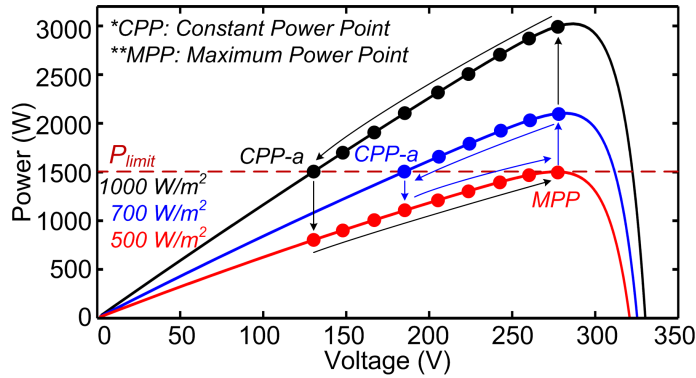


**Figure 5.3:** Dynamic behavior of the P&O-CPG algorithm during the MPPT to CPG transition and vice versa.

conditions. It is obvious from the trajectory of the operating point in the P-V characteristic curve that both the overshoot and power losses will increase as the changing speed of the irradiance level increases. Thus, under this condition, the algorithm should be modified in order to achieve a faster dynamic response.

### 5.2.1 Minimizing Overshoots during the MPPT to CPG Transition

Considering the overshoot during the MPPT to CPG transition, the main cause of this incident is that the algorithm cannot follow the change in the irradiance condition. Actually, this is similar to the typical problem in the P&O MPPT algorithm which was pointed out in Section 3.2. Thus, similar approaches can also be applied here in order to improve the dynamic performance of the P&O-CPG algorithm. One solution to achieve a fast tracking behavior is by increasing the step size of the perturbation. A large step size can reduce the required number of iterations of the algorithm in order to reach the reference value, i.e., **CPP-a**. In order to avoid the large oscillation during the steady-state, the step size modification should be applied only when the algorithm detects a fast increase in the irradiance condition.

Thus, the first step is to detect the fast increase condition in the irradiance when the operating mode changes from MPPT to CPG. The change in the operating mode can easily be detected by comparing the  $P_{pv}$  with the  $P_{limit}$ . When the measured power  $P_{pv}$  exceeds  $P_{limit}$ , the MPPT to CPG transition is detected. Once the CPG operation is detected, the speed of the change in the irradiance can be measured from the difference between  $P_{pv}$  and  $P_{limit}$  during the MPPT to CPG transition. The value of  $(P_{pv} - P_{limit})$  will be larger under a fast changing irradiance condition. A criterion to detect a fast changing irradiance condition is shown in Eq. (5.1).

$$\text{Irradiance condition} = \begin{cases} \text{Fast increasing, when } P_{pv,n} - P_{limit} > \varepsilon_{inc} \\ \text{Normal operation, when } P_{pv,n} - P_{limit} \leq \varepsilon_{inc} \end{cases} \quad (5.1)$$

where  $P_{pv,n}$  is the measured PV power at the present sampling,  $\varepsilon_{inc}$  is the criterion to determine a fast increasing irradiance condition. The value of  $\varepsilon_{inc}$  should be large

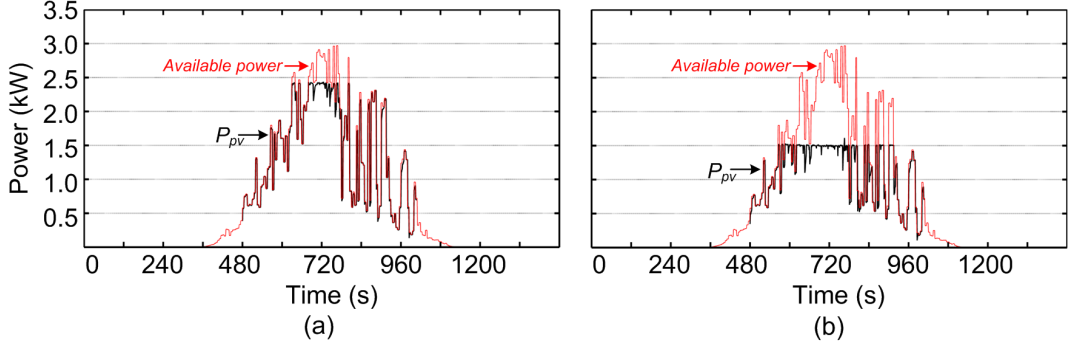


**Figure 5.4:** Experimental results of the CPG based on the perturb and observe with an adaptive step size under a cloudy day irradiance condition, where  $P_{limit}$  is chosen as: (a) 80 % and (b) 50 % of the rated power.

enough to avoid the wrong detection due to the steady-state oscillation from the perturbation under the normal CPG operation.

When a fast changing irradiance condition is detected, the faster the irradiance changes, the larger step size should be used. It is suggested to use an adaptive step size where the large step size is used at the beginning and the step size is eventually being reduced as the operating point is moving closer to the **CPP-a**. Actually, the distance between the present operating point of the PV system and the target **CPP-a** can easily be measured by continuously monitoring the difference between the PV output power and the  $P_{limit}$ . If the value of  $(P_{pv,n} - P_{limit})$  is large, then the operating point is still far away from the **CPP-a**. The difference in the  $P_{pv,n}$  and the  $P_{limit}$  will be reduced continuously as the operating point is getting closer to the **CPP-a**. Based on this observation, the calculation of the  $(P_{pv,n} - P_{limit})$  should be used as a weight function to the modified step size. The proposed adaptive step size during a fast increasing irradiance condition can be calculated as

$$v_{pv}^* = v_{pv,n} - \left[ (P_{pv,n} - P_{limit}) \frac{P_{limit}}{P_{mp} \cdot K} \right] \cdot STEP \quad (5.2)$$

where  $v_{pv}^*$  is the reference output voltage of the PV arrays,  $v_{pv,n}$  and  $P_{pv,n}$  are the measured output voltage and power of the PV array at the present sampling, respectively.  $P_{mp}$  is the rated power of the PV arrays.  $STEP$  is the original step size of the P&O-CPG algorithm. The term  $P_{limit}/P_{mp}$  is introduced to alleviate the dependency of the step size in the level of  $P_{limit}$ . For example, the term  $(P_{pv} - P_{limit})$  when the  $P_{limit} = 50\%$  of the rated power can be 10 times larger than the case when the  $P_{limit} = 80\%$  of the rated power, which is not preferable. Therefore, the calculation of  $(P_{pv} - P_{limit})$  should be scaled with the percentage of the power limit according to the rated power in order to avoid the use of too large step size at a low value of  $P_{limit}$ .  $K$  is a constant which can be used to tune the speed of the algorithm. A large value of  $K$  will result in a smooth increase in the step size,

while the tracking speed is compromised. A small value of  $K$  can challenge the boost converter controller since the value of the voltage reference  $v_{pv}^*$  will experience a large jump at the initial steps.

The dynamic performances of the P&O-CPG algorithm during the MPPT to CPG transition have been significantly improved by introducing the adaptive step size. Overshoots are minimized as it can be compared from the previous and the improved results in Figs. 5.1 and 5.4, respectively. Therefore, the next step is to improve the performance during the CPG to MPPT transition in order to minimize the power losses.

### 5.2.2 Minimizing Power Losses during the CPG to MPPT Transition

It is more complicated to apply the idea of the adaptive step size when the irradiance suddenly drops and the operating mode changes from CPG to MPPT, since the distance between the present operating point of the PV system and the target MPP cannot easily be measured. In fact, the MPP cannot be located unless an advance detection technique is employed, which will result in a much more complicated algorithm.

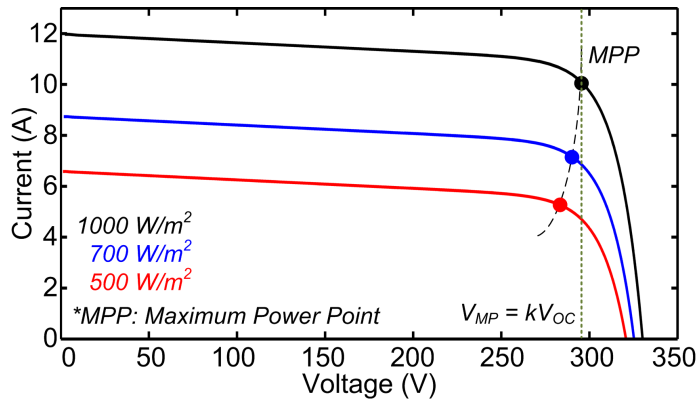


**Figure 5.5:** I-V characteristic curve of the PV arrays, where the voltage at the MPP is almost constant especially at a higher irradiance level [41], [48].

An alternative solution is to use a constant voltage strategy to force the operating point of the PV system to be close to the MPP when the irradiance suddenly drops and the operating mode changes from CPG to MPPT. Due to the characteristic of the PV arrays, the voltage at the MPP is almost constant and can be approximated as 71-78 % of the open circuit voltage  $V_{OC}$  [41], as can be seen from Fig. 5.5. Thus, when a fast decrease in the irradiance condition is detected during the CPG to MPPT transition, the PV voltage reference  $v_{pv}^*$  can be calculated as

$$v_{pv}^* = k \cdot V_{OC}, \text{ where } 0.71 \leq k < 0.78. \quad (5.3)$$

By doing so, the operating point can be instantaneously moved close to the MPP in one perturbation, resulting in a significant reduction in the number of iterations until the operating point reaches the MPP. This approach is quite simple but effective, which is very suitable to be implemented.

Similar to the modification during MPPT to CPG transition, the algorithm should first detect the change in the irradiance level as well as the change in the operating mode from CPG to MPPT. If the irradiance suddenly drops but the operating mode is still be the MPPT, the controller should let the MPPT algorithm tracks the operating point in the normal manner. This is due to the fact that the present operating point of the PV system does not change much under the sudden drop in the irradiance level if the PV system keeps operating in the MPPT operation compared to when the PV system is initially operating in the CPG operating mode. Fig. 5.6 further illustrates the trajectory of the PV system in the two cases mentioned above.

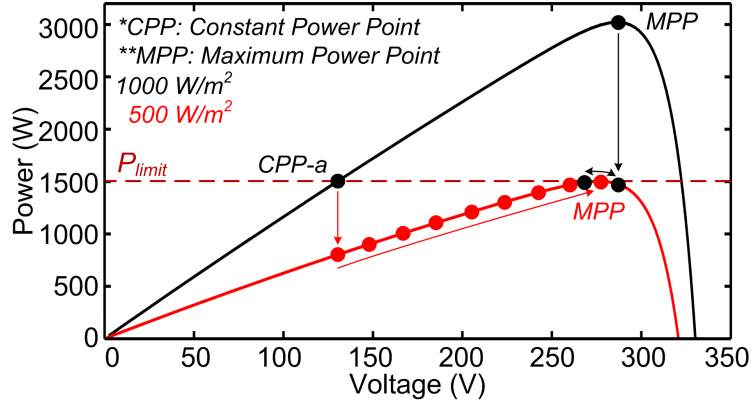


**Figure 5.6:** Comparison between the trajectory of (red) the CPG to MPPT transition and (black) normal MPPT operation under a fast decreasing irradiance condition.

Actually, the fast decreasing irradiance condition can be detected by comparing the PV power  $P_{pv}$  from the previous sampling,  $P_{pv,n-1}$ , with the present sampling,  $P_{pv,n}$ , as is shown in Eq. (5.4). If the  $(P_{pv,n-1} - P_{pv,n})$  is larger than a certain value,  $\varepsilon_{dec}$ , it can be assumed that the fast decreasing irradiance condition is detected. The change in the operating mode can also be detected by comparing the power  $P_{pv,n-1}$  with the power limit  $P_{limit}$ . If the value of the  $P_{pv,n-1}$  is close to  $P_{limit}$ , it can be assumed that the PV system was operating in the CPG operating mode in the previous sampling as is shown in Eq. (5.5).

$$\text{Irradiance condition} = \begin{cases} \text{Fast decreasing, when} & P_{pv,n-1} - P_{pv,n} > \varepsilon_{dec} \\ \text{Normal operation, when} & P_{pv,n-1} - P_{pv,n} \leq \varepsilon_{dec} \end{cases} \quad (5.4)$$

$$\text{Previous operating mode} = \begin{cases} \text{CPG, when} & |P_{limit} - P_{pv,n-1}| < \varepsilon_{ss} \\ \text{MPPT, when} & |P_{limit} - P_{pv,n-1}| \geq \varepsilon_{ss} \end{cases} \quad (5.5)$$

## 5.2. Design for High Performance P&O CPG Method

where  $\varepsilon_{dec}$  and  $\varepsilon_{ss}$  are criterions to determine the fast decreasing irradiance condition and the CPG operating mode, respectively. The value of  $\varepsilon_{ss}$  should be slightly larger than the oscillation during the steady-state operation of the P&O-CPG algorithm (e.g., 1-2 % of the rated power of the PV system).

A flow chart of the improved P&O-CPG algorithm during the operating transitions including the detection of fast changing irradiance is shown in Fig. 5.7. As can be seen from the flow chart, an adaptive step size is used when the fast increasing irradiance condition is detected during the MPPT to CPG transition. Moreover, when the fast decreasing irradiance condition is detected during the CPG to MPPT transition, a constant voltage strategy should be applied.

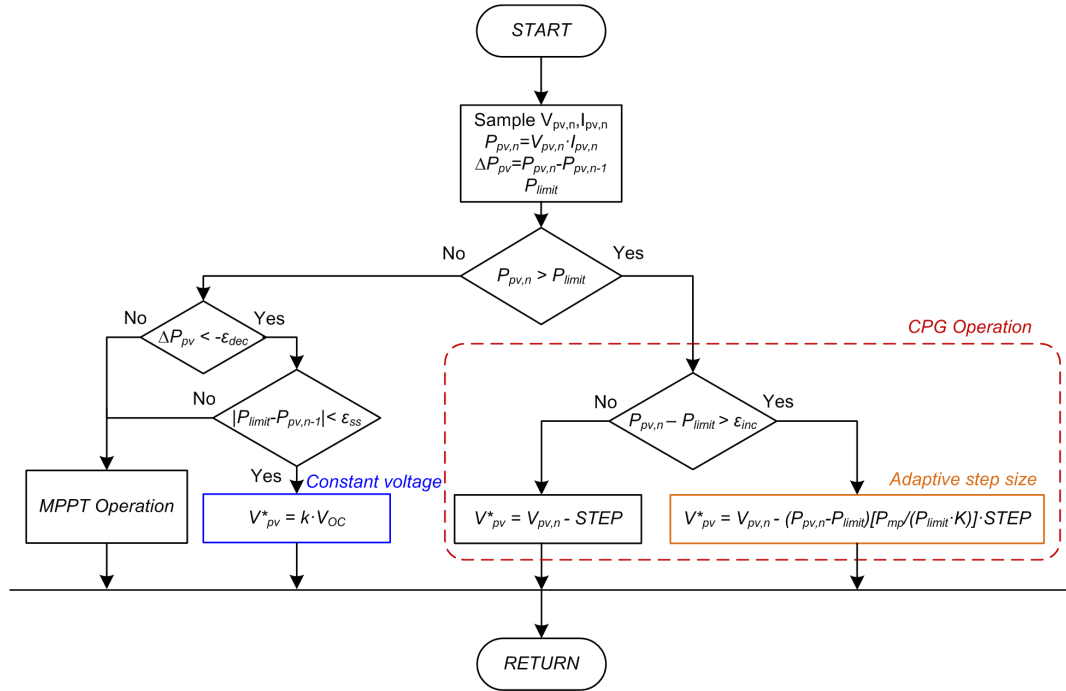


**Figure 5.7:** Flow chart of the modified P&O-CPG algorithm where both adaptive step size and constant voltage strategy are employed.

### 5.2.3 Design Guideline and the Performance of the Modified P&O-CPG algorithm

Solutions to improve the dynamic performance of the P&O-CPG algorithm have been discussed. One important part is the detection of the operating condition, e.g., fast increasing or decreasing irradiance condition, the MPPT to CPG or CPG to MPPT transitions. Once the condition is detected, a proper action can be assigned as can be seen from the functional diagram in Fig. 5.8. In brief, the reference value of the PV voltage  $v_{pv}^*$  can be determined by using the following equation

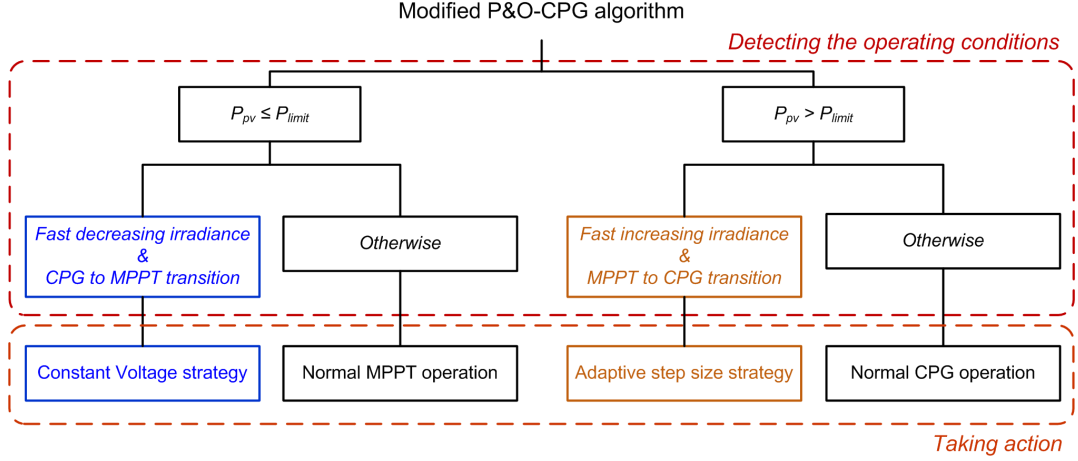


**Figure 5.8:** Functional diagram of the modified P&O-CPG algorithm.

$$v_{pv}^* = \begin{cases} v_{MPPT}^*, & \text{Normal MPPT operation} \\ k \cdot V_{OC}, & \text{Constant voltage strategy} \\ v_{pv,n} - STEP, & \text{Normal CPG operation} \\ v_{pv,n} - \left[ (P_{pv,n} - P_{limit}) \frac{P_{limit}}{P_{mp} \cdot K} \right] \cdot STEP, & \text{Adaptive step size strategy} \end{cases}$$

Parameters of the modified P&O-CPG algorithm are given in Table 5.1. The performances of the modified P&O-CPG algorithm shown in Fig. 5.9 are compared with the conventional P&O-CPG method shown in Fig. 5.1. As can be seen from the experimental results under cloudy conditions, overshoots and power losses are significantly reduced, while a stable operation is still maintained. The algorithm also has a selective behavior to only react when the fast irradiance condition is detected. This can be seen from the performance under clear irradiance conditions in Fig. 5.10, which is similar to the conventional P&O-CPG algorithm. Table 5.2 summarizes a benchmarking of the CPG algorithm including the modified high performance P&O-CPG algorithm. The modified P&O-CPG algorithm has a superior performance in several aspects compared to the other CPG algorithms. Nevertheless, the complexity of the algorithm increases due to the use of the adaptive step size and the detection of the operating condition.

**Table 5.1:** Designed parameters of the modified P&O-CPG algorithm.

Adaptive step size	$K = 10$
Constant voltage strategy	$k = 0.715$
Fast increase detection	$\varepsilon_{inc} = 50$
Fast decrease detection	$\varepsilon_{dec} = 100$
Previous operating mode detection	$\varepsilon_{ss} = 30$

## 5.2. Design for High Performance P&O CPG Method

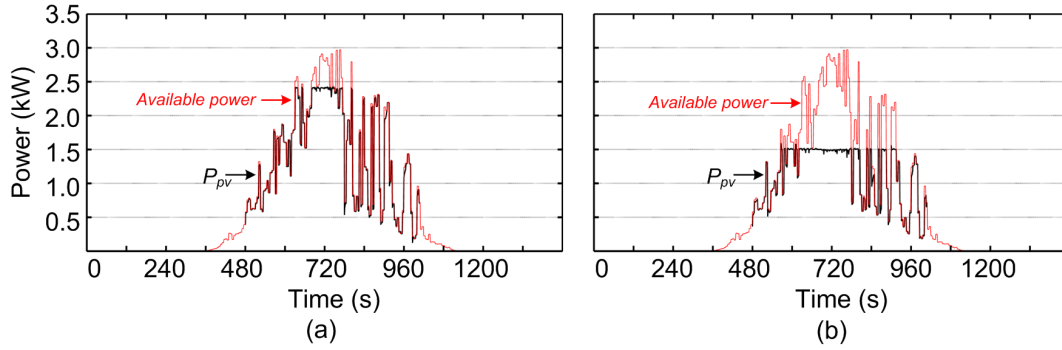


**Figure 5.9:** Experimental results of the modified CPG based on the perturb and observe under a cloudy day irradiance condition, where  $P_{limit}$  is chosen as: (a) 80 % and (b) 50 % of the rated power.

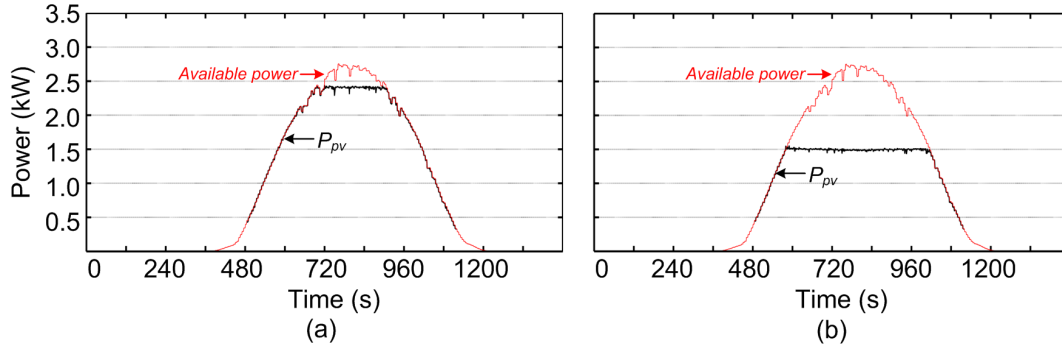


**Figure 5.10:** Experimental results of the modified CPG based on the perturb and observe under a clear day irradiance condition, where  $P_{limit}$  is chosen as: (a) 80 % and (b) 50 % of the rated power.

**Table 5.2:** Benchmarking of Constant Power Generation algorithms

CPG based on:	Dynamic reponses		Steady-state reponses	Stability	Complexity
	MPPT $\rightarrow$ CPG	CPG $\rightarrow$ MPPT			
Power control	++	+	++	-	-
Current limit	+	--	+	--	++
Perturb and Observe (CPP-a)	--	-	++	++	-
Perturb and Observe (CPP-b)	-	-	--	-	-
Perturb and Observe (Modified)	+	+	++	++	--

Note: the more +, the better stability and less complexity.

### 5.3 Summary

Although the P&O-CPG algorithm offers a robust operation, and is considered as the most suitable algorithm to realize the CPG operation, an improvement in the dynamic performance is required in order to achieve a high performance CPG operation. Problems regarding the dynamic performance of the P&O-CPG algorithm have been analyzed. An overshoot can occur during the MPPT to CPG transition under a fast increasing irradiance condition. The proposed solution is to employ an adaptive step size when the above condition is detected. This can ensure the use of a large step size at the initial step and a smaller step size when the operating point is reaching the *CPP*. Considering the power losses, this incidence occurs during the CPG to MPPT transition under a fast decreasing irradiance condition. Here, the constant voltage MPPT strategy is employed to improve the performance of the algorithm. By doing so, the required number of iterations can be significantly reduced and the power losses are minimized.

In brief, there are two main processes in the modified high performance P&O-CPG algorithm. First, the operating condition should be detected. If the PV system is operating under an extreme condition, which can lead to the overshoot or power losses, the algorithm should be modified according to the functional diagram in Fig. 5.8. The performances of the modified P&O-CPG algorithm are presented. Under a cloudy condition, the overshoot and power losses are significantly improved compared to the conventional P&O-CPG algorithm. However, the satisfied performance, as was achieved with the conventional P&O-CPG algorithm, is attained under a clear irradiance condition. The modified P&O-CPG algorithm is then include in the benchmarking of the CPG algorithms at the end of the chapter.

# Chapter 6

## Conclusion

In this chapter, the summary of the thesis is provided. The main contribution of the project is pointed out and future work initiated by this project is also discussed.

### Summary

Several studies have been done in this thesis. In Chapter 1, the background of the PV systems was discussed, where the focus is on the grid-connected applications. According to the high growth rate of the grid-connected PV systems in the recent years, it is expected that more intermittent power will be injected to the grid, which may rise a challenge to the system operator. Specifically, an overloading may occur during the peak power production since the PV systems are currently required to deliver the maximum available power to the grid at all time in most countries. In order to solve this problem in a cost-effective way, an advanced power control strategy which can limit the maximum feed-in power from the PV system is required. Thus, the main focus of this thesis has been on developing a grid-friendly power control strategy in single-phase grid-connected PV systems by means of a Constant Power Generation (CPG) operation.

In this project, the two-stage grid-connected PV system has been employed since it offers a wide range of operation. Accordingly, the boost converter and Full-Bridge (FB) inverter are modeled in Chapter 2. The control systems, mainly for the PV inverter, have also been discussed. The performance of the developed two-stage single-phase PV system and its control systems have been verified experimentally.

Chapter 3 focuses on the MPPT operation, which is a currently requirement of the PV systems in most countries. The MPPT algorithm is realized by a Perturb and Observe (P&O) algorithm due to its simple structure. Typically, the boost converter is controlled by its input voltage or current during the MPPT operation. However, another control structure based on the input power of the boost converter has also been presented since it is suitable for a power control strategy. A design guideline regarding the step size and the sampling rate of the MPPT controllers has been provided. The designed MPPT controllers are examined with several different

test conditions. It is observed that the voltage-based MPPT controller has the most robust and accurate tracking performance. Care should be taken when the current-based MPPT controller is employed since it can introduce instability during a fast decreasing irradiance condition.

The main contribution of this thesis has been presented in Chapter 4. First, active power control strategies are discussed where the focus is on the constant power generation. The CPG operation was introduced with the aim to prevent an overloading issue in grid-connected PV systems. One cost-effective approach to realize the CPG control is by modifying the MPPT algorithm. Several active power control methods similar to the CPG operation have been reviewed. Two similar drawbacks of most presented methods are: 1) a limited operating region (at the right side of the MPP), and 2) a complicated control structure to activate the controller under different operating mode. Therefore, this thesis has presented three CPG algorithms to realize the CPG operation: 1) CPG based on the power control (P-CPG), 2) CPG based on the current limit (I-CPG), and 3) CPG based on the Perturb and Observe algorithm (P&O-CPG). It should be noted that some of the above CPG algorithms can be considered as an improvement of the prior-art work. The performances of the CPG algorithms have been examined in both the simulation and experiment under several test conditions. A benchmarking of the CPG algorithms is provided in terms of steady-state performance, dynamics, complexity, and stability. It has been revealed that the P&O-CPG is the most suitable algorithm to realize the CPG operation practically due to the robustness of the algorithm and a satisfactory steady-state performance.

However, the perturbation behavior of the P&O-CPG algorithm results in a slow dynamic performance. In order to achieve a high performance CPG operation, an improvement in the algorithm is required, which is the main content in Chapter 5. The issues regarding the dynamic performance of the P&O-CPG algorithm thus have been investigated. According to the analysis, poor dynamic performances occur due to a fast changing irradiance condition, which results in overshoots and power losses. As a consequence, the P&O-CPG algorithm has been modified. An adaptive step size is adopted when the irradiance level increases rapidly during MPPT to CPG transition. Another modification is the use of a constant voltage strategy under a fast decreasing irradiance during the CPG to MPPT transition. The improved performance of the modified P&O-CPG algorithm has been compared with the previous results from the conventional P&O-CPG algorithm. It has been demonstrated that the overshoots and power losses are minimized while a satisfactory steady-state performance is still maintained. Nevertheless, the complexity of the algorithm increases due to use of the adaptive step size and the detection of the operating condition.

## **Future work**

The work carried out in this project can also lead to other possibilities which have not yet been investigated:

### ***Implementation with other MPPT algorithms***

So far, only the P&O MPPT algorithm is considered due to its simple structure. However, the performance of the MPPT can be improved by introducing more advanced P&O algorithms (e.g., variable step sizes, adaptive step sizes) or other MPPT algorithms (e.g., incremental conductance method, ripple correlation). The improvement in the MPPT algorithm will directly improve the performance of the CPG algorithms as well, e.g., during the transitions of the operation.

### ***Other active power control strategies***

As has been mentioned in Chapter 4, the CPG operation is actually one of the active power control strategies in the wind turbine power system. It is also possible that some other active power control strategies will be required in the near future (e.g., power ramp constraint for the frequency support function) for the PV systems. Thus, a further investigation to apply the power control strategies presented in this thesis to enable more functionality of the PV system is also interesting.

### ***Analyze the additional effects of the CPG control strategies***

Although the main aim of the CPG operation is to prevent an overloading issue, the limitation of the feed-in power may also introduce other effects to the PV system. For example, the utilization of the PV inverter can be improved since the rated power of the inverter is decided by the power limit not the maximum power of the PV system. This may improve the other aspects such as reliability of the overall system, which will require more investigation.

### ***Apply the control strategy in three-phase PV systems***

The concept presented in this thesis can also be applied to the three-phase grid-connected PV systems with a higher power rating. Some modifications may be required in terms of the control strategy. For instance, reactive power control may also be included since its effectiveness increases with the lower R/X ratio.

### ***Investigate the CPG operation under a partial shading condition***

Under a partial-shading condition, the P-V characteristic curve of the PV arrays is different from what has been used in this thesis. More than one local maximum power points can occur according to the shading condition. It is also necessary to first investigate if the proposed solution in this thesis can be applied under this condition. Otherwise, some modifications are required.

# Bibliography

- [1] EPIA, “Global market outlook for photovoltaics 2014–2018,” *EPIA Report*, 2014. [Online]. Available: <http://www.epia.org/news/publications/global-market-outlook-for-photovoltaics-2014-2018/>
- [2] F. R. of Germany, “National renewable energy action plan in accordance with directive 2009/28/ec on the promotion of the use of energy from renewable sources,” 2010.
- [3] Energinet.dk, “Strategy plan 2012.”
- [4] A. Zervos, “Renewables 2013 global status report,” *Renewable Energy Policy Network for the 21st Century. Paris, France*, 2013.
- [5] H. Wirth and K. Schneider, “Recent facts about photovoltaics in germany,” *Report from Fraunhofer Institute for Solar Energy Systems, Germany*, 2013.
- [6] I. Wilhelm, S. Teske, and G. Massonet, “Solar photovoltaic electricity empowering the world,” *Solar Gen*, vol. 6, pp. 17–28, 2011.
- [7] Y. Yang, H. Wang, F. Blaabjerg, and T. Kerekes, “A hybrid power control concept for pv inverters with reduced thermal loading,” *Power Electronics, IEEE Transactions on*, vol. 29, no. 12, pp. 6271–6275, Dec 2014.
- [8] Y. Yang, “Advanced control strategies to enable a more wide-scale adoption of single-phase photovoltaic systems,” Ph.D. dissertation, Department of Energy Technology, Aalborg University, 2014.
- [9] Y. Yang, P. Enjeti, F. Blaabjerg, and H. Wang, “Suggested grid code modifications to ensure wide-scale adoption of photovoltaic energy in distributed power generation systems,” in *Industry Applications Society Annual Meeting, 2013 IEEE*, Oct 2013, pp. 1–8.
- [10] EPIA, “Connecting the sun: Solar photovoltaics on the road to large-scale grid integration,” *Sept*, 2012. [Online]. Available: <http://www.epia.org/news/publications/>
- [11] *German Federal Law: Renewable Energy Sources Act (Gesetz für den Vorrang Erneuerbarer Energien) BGBl*, Std., July 2014.

## Bibliography

- [12] T. Stetz, F. Marten, and M. Braun, “Improved low voltage grid-integration of photovoltaic systems in germany,” *Sustainable Energy, IEEE Transactions on*, vol. 4, no. 2, pp. 534–542, April 2013.
- [13] T. Orłowska-Kowalska, F. Blaabjerg, and J. Rodriguez, *Advanced and Intelligent Control in Power Electronics and Drives*, 1st ed., ser. 530. Springer International Publishing, 2014.
- [14] T. Kerekes, “Analysis and modeling of transformerless photovoltaic inverter systems,” Ph.D. dissertation, Institut for Energiteknik, Aalborg Universitet, 2009.
- [15] R. Teodorescu, M. Liserre, and P. Rodriguez, *Grid converters for photovoltaic and wind power systems*. John Wiley & Sons, 2011, vol. 29.
- [16] D. Maxwell, “Parts of northern ireland’s electricity grid overloaded,” *BBC News NI*, 2013. [Online]. Available: <http://www.bbc.com/news/uk-northern-ireland-24921411>
- [17] Y. Yang, F. Blaabjerg, and H. Wang, “Constant power generation of photovoltaic systems considering the distributed grid capacity,” in *Applied Power Electronics Conference and Exposition (APEC), 2014 Twenty-Ninth Annual IEEE*, March 2014, pp. 379–385.
- [18] M. R. Patel, *Wind and solar power systems: design, analysis, and operation*. CRC press, 2005.
- [19] M. Villalva, J. Gazoli, and E. Filho, “Comprehensive approach to modeling and simulation of photovoltaic arrays,” *Power Electronics, IEEE Transactions on*, vol. 24, no. 5, pp. 1198–1208, May 2009.
- [20] BPSolar. (2003) Bp 365, 65 watt photovoltaic module. Online. [Online]. Available: <http://www.solarpanelstore.com/pdf/bp-365.pdf>
- [21] F. Blaabjerg, R. Teodorescu, M. Liserre, and A. Timbus, “Overview of control and grid synchronization for distributed power generation systems,” *Industrial Electronics, IEEE Transactions on*, vol. 53, no. 5, pp. 1398–1409, Oct 2006.
- [22] R. W. Erickson and D. Maksimovic, *Fundamentals of power electronics*. Springer Science & Business Media, 2001.
- [23] C. L. Phillips and R. D. Habor, *Feedback control systems*. Simon & Schuster, 1995.
- [24] A. Reznik, M. Simoes, A. Al-Durra, and S. Muyeen, “Lcl filter design and performance analysis for grid-interconnected systems,” *Industry Applications, IEEE Transactions on*, vol. 50, no. 2, pp. 1225–1232, March 2014.

- [25] M. Liserre, F. Blaabjerg, and S. Hansen, "Design and control of an lcl-filter based three-phase active rectifier," in *Industry Applications Conference, 2001. Thirty-Sixth IAS Annual Meeting. Conference Record of the 2001 IEEE*, vol. 1, Sept 2001, pp. 299–307 vol.1.
- [26] Y. Yang, K. Zhou, H. Wang, F. Blaabjerg, D. Wang, and B. Zhang, "Frequency adaptive selective harmonic control for grid-connected inverters," *Power Electronics, IEEE Transactions on*, vol. 30, no. 7, pp. 3912–3924, July 2015.
- [27] K. Zhou, K.-S. Low, Y. Wang, F.-L. Luo, B. Zhang, and Y. Wang, "Zero-phase odd-harmonic repetitive controller for a single-phase pwm inverter," *Power Electronics, IEEE Transactions on*, vol. 21, no. 1, pp. 193–201, Jan 2006.
- [28] S. Jiang, D. Cao, Y. Li, J. Liu, and F. Z. Peng, "Low-thd, fast-transient, and cost-effective synchronous-frame repetitive controller for three-phase ups inverters," *Power Electronics, IEEE Transactions on*, vol. 27, no. 6, pp. 2994–3005, June 2012.
- [29] Y. Wang, D. Wang, B. Zhang, and K. Zhou, "Fractional delay based repetitive control with application to pwm dc/ac converters," in *Control Applications, 2007. CCA 2007. IEEE International Conference on*, Oct 2007, pp. 928–933.
- [30] Y. Yang and F. Blaabjerg, "Synchronization in single-phase grid-connected photovoltaic systems under grid faults," in *Power Electronics for Distributed Generation Systems (PEDG), 2012 3rd IEEE International Symposium on*, June 2012, pp. 476–482.
- [31] A. Nagliero, R. Mastromauro, M. Liserre, and A. Dell'Aquila, "Monitoring and synchronization techniques for single-phase pv systems," in *Power Electronics Electrical Drives Automation and Motion (SPEEDAM), 2010 International Symposium on*, June 2010, pp. 1404–1409.
- [32] M. Elgendy, B. Zahawi, and D. Atkinson, "Assessment of perturb and observe mppt algorithm implementation techniques for pv pumping applications," *Sustainable Energy, IEEE Transactions on*, vol. 3, no. 1, pp. 21–33, Jan 2012.
- [33] N. Femia, G. Petrone, G. Spagnuolo, and M. Vitelli, "Optimizing sampling rate of p&o mppt technique," in *Power Electronics Specialists Conference, 2004. PESC 04. 2004 IEEE 35th Annual*, vol. 3, June 2004, pp. 1945–1949 Vol.3.
- [34] W. Cao, Y. Ma, J. Wang, L. Yang, J. Wang, F. Wang, and L. Tolbert, "Two-stage pv inverter system emulator in converter based power grid emulation system," in *Energy Conversion Congress and Exposition (ECCE), 2013 IEEE*, Sept 2013, pp. 4518–4525.
- [35] W. Xiao and W. Dunford, "A modified adaptive hill climbing mppt method for photovoltaic power systems," in *Power Electronics Specialists Conference, 2004. PESC 04. 2004 IEEE 35th Annual*, vol. 3, June 2004, pp. 1957–1963 Vol.3.

## Bibliography

- [36] C. Hua, J. Lin, and C. Shen, "Implementation of a dsp-controlled photovoltaic system with peak power tracking," *Industrial Electronics, IEEE Transactions on*, vol. 45, no. 1, pp. 99–107, Feb 1998.
- [37] E. Koutroulis, K. Kalaitzakis, and N. Voulgaris, "Development of a microcontroller-based, photovoltaic maximum power point tracking control system," *Power Electronics, IEEE Transactions on*, vol. 16, no. 1, pp. 46–54, Jan 2001.
- [38] S. Kollimalla and M. Mishra, "Variable perturbation size adaptive p&o mppt algorithm for sudden changes in irradiance," *Sustainable Energy, IEEE Transactions on*, vol. 5, no. 3, pp. 718–728, July 2014.
- [39] A. Al-Diab and C. Sourkounis, "Variable step size p&o mppt algorithm for pv systems," in *Optimization of Electrical and Electronic Equipment (OPTIM), 2010 12th International Conference on*, May 2010, pp. 1097–1102.
- [40] D. Hohm and M. Ropp, "Comparative study of maximum power point tracking algorithms using an experimental, programmable, maximum power point tracking test bed," in *Photovoltaic Specialists Conference, 2000. Conference Record of the Twenty-Eighth IEEE*, 2000, pp. 1699–1702.
- [41] T. Eswam and P. Chapman, "Comparison of photovoltaic array maximum power point tracking techniques," *Energy Conversion, IEEE Transactions on*, vol. 22, no. 2, pp. 439–449, June 2007.
- [42] K. Hussein, I. Muta, T. Hoshino, and M. Osakada, "Maximum photovoltaic power tracking: an algorithm for rapidly changing atmospheric conditions," *Generation, Transmission and Distribution, IEE Proceedings-*, vol. 142, no. 1, pp. 59–64, Jan 1995.
- [43] Y. Yang and F. Blaabjerg, "A modified p&o mppt algorithm for single-phase pv systems based on deadbeat control," in *Power Electronics, Machines and Drives (PEMD 2012), 6th IET International Conference on*, March 2012, pp. 1–5.
- [44] D. Sera, T. Kerekes, R. Teodorescu, and F. Blaabjerg, "Improved mppt algorithms for rapidly changing environmental conditions," in *Power Electronics and Motion Control Conference, 2006. EPE-PEMC 2006. 12th International*, Aug 2006, pp. 1614–1619.
- [45] N. Femia, G. Petrone, G. Spagnuolo, and M. Vitelli, *Power electronics and control techniques for maximum energy harvesting in photovoltaic systems*. CRC press, 2012.
- [46] M. Rosu-Hamzescu and S. Oprea, "Practical guide to implementing solar panel mppt algorithms," *Microchip Technology Inc*, 2013.

- [47] R. Bründlinger, N. Henze, H. Häberlin, B. Burger, A. Bergmann, and F. Baumgartner, “pren 50530—the new european standard for performance characterisation of pv inverters,” in *Proc. 24th European Photovoltaic Solar Energy Conf*, 2009, pp. 3105–3109.
- [48] H. Schmidt, B. Burger, U. Bussemas, and S. Elies, “How fast does an mpp tracker really need to be?” in *24th European Photovoltaic Solar Energy Conference, 21-25 September 2009, Hamburg, Germany*.
- [49] H.-J. Jung, K.-S. Ha, B.-M. Song, J.-S. Lai, D. seok Hyun, and R. young Kim, “Low frequency current reduction using a quasi-notch filter operated in two-stage dc-dc-ac grid-connected systems,” in *Energy Conversion Congress and Exposition (ECCE), 2011 IEEE*, Sept 2011, pp. 2746–2750.
- [50] Energinet.dk, “Technical regulation 3.2.5 for wind power plants with a power output greater than 11 kw,” Technical report, Tech. Rep., 2010.
- [51] M. Thomson and D. Infield, “Impact of widespread photovoltaics generation on distribution systems,” *Renewable Power Generation, IET*, vol. 1, no. 1, pp. 33–40, March 2007.
- [52] R. Wandhare and V. Agarwal, “Precise active and reactive power control of the pv-dgs integrated with weak grid to increase pv penetration,” in *Photovoltaic Specialist Conference (PVSC), 2014 IEEE 40th*, June 2014, pp. 3150–3155.
- [53] A. Urtasun, P. Sanchis, and L. Marroyo, “Limiting the power generated by a photovoltaic system,” in *Systems, Signals Devices (SSD), 2013 10th International Multi-Conference on*, March 2013, pp. 1–6.
- [54] C. Rosa, D. Vinikov, E. Romero-Cadaval, V. Pires, and J. Martins, “Low-power home pv systems with mppt and pc control modes,” in *Compatibility and Power Electronics (CPE), 2013 8th International Conference on*, June 2013, pp. 58–62.
- [55] T. Caldognetto, S. Buso, and P. Mattavelli, “Digital controller development methodology based on real-time simulations with view fpgac hardware-software toolset,” *Electronics*, vol. 17, no. 2, pp. 110–117, 2013.
- [56] C. Sepulveda, J. Munoz, J. Espinoza, M. Figueroa, and C. Baier, “Fpga v/s dsp performance comparison for a vsc-based statcom control application,” *Industrial Informatics, IEEE Transactions on*, vol. 9, no. 3, pp. 1351–1360, Aug 2013.
- [57] N. Instruments, “Ni labview high-performance fpga developer’s guide,” 2014.
- [58] ——. Ni single-board rio general purpose inverter controller (gpic). [Online]. Available: <http://www.ni.com/singleboard/gpic/>

## Appendix A

# Hardware Implementation of LabVIEW-FPGA

In the field of the digital controller for power electronics, two different platforms are typically used based on [55], [56]: 1) Digital Signal Processors (DSP) or Microcontrollers and 2) Field-Programmable Gate Arrays (FPGA). In general, FPGAs can achieve a faster computation speed due to the parallel computation structure [57]. However, the resources of the FPGAs are usually limited compared to the DSPs. Moreover, the debugging procedure of the FPGA can be troublesome and requires knowledge of a hardware-level language. This makes the DSPs usually preferable in the applications that do not strictly require the fast and parallel operation [56].

In order to combine the advantages of these two platforms, the NI Single-Board RIO General Purpose Inverter Controller (GPIC) includes both FPGA and DSP (referred as Real-Time) module in the same digital controller [55], [58]. It also provides peripheral Input/Output (I/O) ports compatible for controlling power converters. Both FPGA and Real-Time (RT) modules are programmed through the LabVIEW program, which offers a graphical programming approach, making it easy to be im-

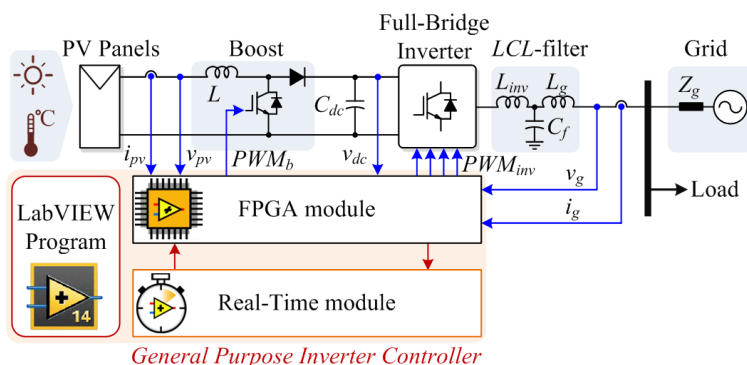


**Figure A.1:** System configuration of a two-stage single-phase PV system developed with the General Purpose Inverter Controller (GPIC).

plemented. Due to these advantages, the two-stage single-phase PV system has been developed with the GPIC in the implementation as shown in Fig. A.1. A brief guideline for programming the GPIC according to the control structure in this particular system is discussed in the following as well as the implementations of commonly used controllers.

## A.1 Control Structure of Two-Stage Single-Phase PV System in GPIC

The GPIC provides a combination of the FPGA- and RT-module which can work independently from each other. A fast speed computation can be achieved in the FPGA-module while more resources and tools are available in the RT-module. Typically, it is recommended to develop controllers that require a fast and strict execution time in the FPGA-module. The RT-module can be used for developing the controllers with a slower computation speed, and also for monitoring system. Therefore, it is necessary to design a proper control structure in order to best utilizing the resources and performances of the GPIC.

According to the control structure in Section 2.4, the two-stage single-phase PV systems consist of several controllers. Regarding the computation speed, the MPP-T/CPG controller requires a much slower sampling rate compared to the rest of the controllers. The required sampling rate of the controller is in the range of 0.5-20 Hz which is suitable to be developed in the RT-module. According to this, the development platform for each controller can be assigned as shown in Table A.1.

**Table A.1:** Development platform of control systems.

<i>Controller functionality</i>	<i>Platform</i>
Measurements PWM generator Phase Lock Loop Boost controller Current controller DC-link controller	FPGA module
MPPT CPG	Real-Time module

In the FPGA programming, the controller is basically executed in a loop manner. The sampling rate or the execution time of the controller is defined by the loop rate. Thus, the controller with different sampling rate is usually developed in a different control loop. The control structure in the FPGA-module is shown in Fig. A.2. It is worth mentioning that the controller can be further optimized according to the development guide [57].

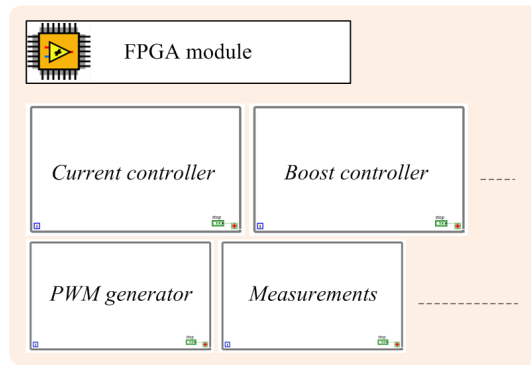


Figure A.2: Suggested control structure in the FPGA-module.

## A.2 Controller Design in LabVIEW-FPGA Environment

Although the LabVIEW-FPGA offers a graphical programming platform, the implementation of the controllers usually needs to be built up from discrete blocks. A certain understanding of the digital control in a hardware-level operation is required. The purpose of this section is to provide some examples for designing controllers employed in the two-stage grid-connected PV systems.

### A.2.1 Proportional Integral (PI) controller

Actually, the control structure of the PI controller in Fig. A.3 is quite simple. A proportional gain  $k_p$  and an integral gain  $k_i$  need to be multiplied with an input error and its cumulative value, respectively. The digital integrator is realized by a Backward-Euler method where the sampling rate is obtained from the loop rate of the main While Loop.

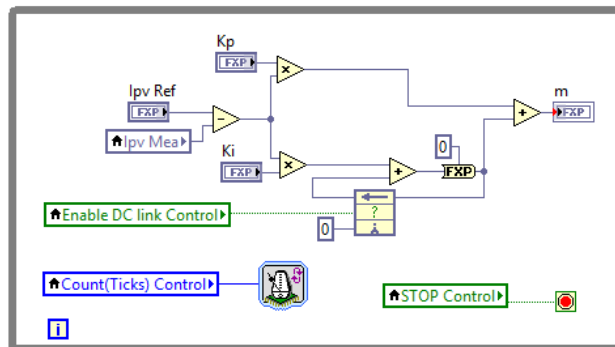
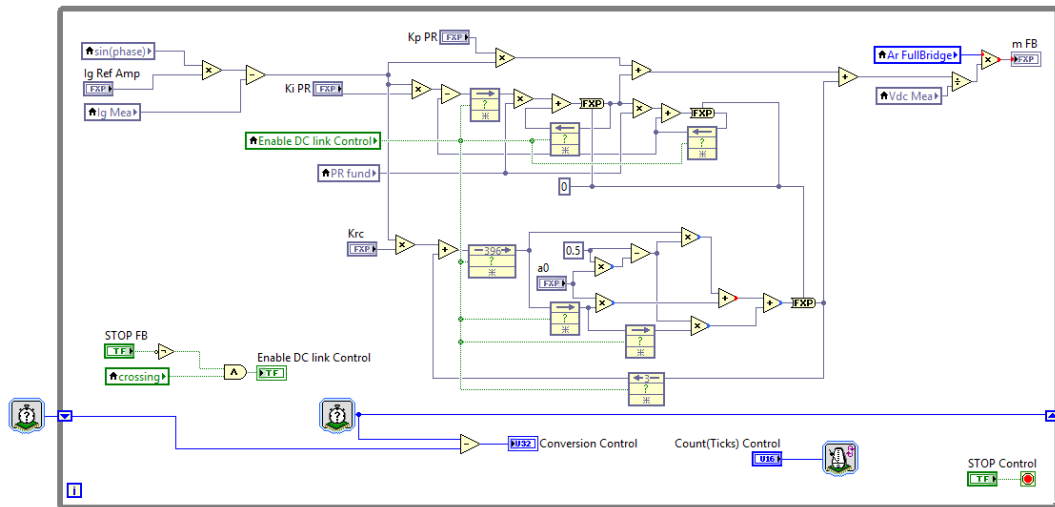


Figure A.3: Implementation of proportional integral controller in the FPGA-module.



**Figure A.4:** Implementation of proportional resonant controller and repetitive controller in FPGA-module.

### A.2.2 Proportional Resonant (PR) and Repetitive Controller (RC)

PR controllers are more difficult to be implemented compared to the PI controller. This is due to the double integrators and several feedback loops. Regarding the two integrators, a Forward-Euler and a Backward-Euler method are used to implement the first and the second integrators, respectively. The implementation of a PR controller in the LabVIEW-FPGA is shown in Fig. A.4. Harmonic compensators by means of a RC controller can be added in parallel with the PR controller. The controller is realized by a certain amount of discrete delays.